



**university of  
 groningen**

**faculty of science  
 and engineering**

**University of Groningen  
 Kapteyn Astronomical Institute**

# **A coevolution study for the most extreme star factories and most active black holes**

**Master's Thesis**

Master of Science in Astronomy  
 at University of Groningen under the supervision of  
 Dr. Lingyu Wang

**Ismail Eissa (s4073886)**

July 17, 2024

## Abstract

We study the co-evolution between host galaxies and their central supermassive black hole (SMBH) with an unprecedented large sample of SDSS type-1 quasars which are also detected by the far-infrared (FIR) SPIRE instrument on *Herschel*. This subsample of optical quasars, newly identified as ‘cold quasars’, provide a unique opportunity to study systems for which both star-formation activity and active galactic nucleus (AGN) activity are at the most extreme. We aim to construct the cosmic star formation history (CSFH) and black hole accretion rate density (BHARD) within the same systems using IR and X-ray luminosity functions, respectively. Thanks to the well-established FIR to radio correlation, we make use of the high angular resolution of the radio observations from telescopes such as LOFAR, Meerkat and VLA to cross-match the *Herschel* sources with the SDSS quasar catalog. Our sample spans over a wide range of redshifts ( $0 < z < 5$ ) and is spread over 9 extragalactic fields (Boötes, ELAIS-N1, GAMA-09, GAMA-12, GAMA-15, HATLAS-NGP, Lockman, Stripe-82 and XMM-LSS). We analyse the scaling relation between stellar mass and star-formation rate (SFR). This is done by assembling an extensive multi-wavelength catalog (from X-ray to radio wavelengths) and individually modelling the spectral energy distributions (SED) to derive physical properties on the accreting SMBH and its host galaxy. We show that 22% of the quasars are hosted by ‘starburst’ (SB) galaxies while normal star-forming galaxies account for the rest of our sample. We acquired black hole masses for our sample from single-epoch broad-line emission measurements (Wu & Shen, 2022). Compared to local studies, our sample seems to have significantly more massive black holes, suggesting the predating of black hole growth compared to their host galaxies. We observe a positive correlation between BHAR and SFR with a slope that flattens as the redshift increases. The SFR and BHAR values derived for our sample expand the empirical range of previous studies. Finally, the derived BHARD shows low density compared to the CSFH at high redshifts. However, as redshift decreases, the BHARD gradually increases until it peaks at  $z \sim 1$ , which is later than the peak of our CSFH ( $z = 1.5 - 2$ ). We do not find direct evidence of AGN feedback affecting the star formation activity.

# Contents

<b>Abstract</b>	<b>2</b>
	<b>Page</b>
<b>Acknowledgements</b>	<b>4</b>
<b>1 Introduction</b>	<b>5</b>
1.1 Coevolution of star formation and black holes	5
1.2 AGN feedback	7
1.3 Quasars	10
1.4 This study	13
<b>2 Data</b>	<b>15</b>
2.1 Multi-wavelength data	15
2.1.1 <i>Herschel</i>	15
2.1.2 Radio	16
2.1.3 SDSS	18
2.1.4 Ancillary data	19
2.2 Catalog cross-matching	19
2.3 Final quasar sample	24
<b>3 Methods</b>	<b>28</b>
3.1 CIGALE SED fitting	28
3.2 Luminosity function fitting	37
3.2.1 Total IR LF	37
3.2.2 X-ray LF	40
<b>4 Results</b>	<b>43</b>
4.1 Star formation activity	43
4.2 The role of BH in SFR growth	47
4.2.1 sSFR-sBHAR relation with redshift	47
4.2.2 $M_* - M_{\text{BH}}$ relation	48
4.2.3 SFR-BHAR evolution	50
4.2.4 BHAR/SFR ratio against the stellar mass	52
4.3 LF fitting	53
4.4 SFRD and BHARD across cosmic time	56
<b>5 Discussion and Conclusion</b>	<b>61</b>
<b>Appendices</b>	<b>63</b>
A Separation distribution	63
B Bolometric correction factor	64
C Main sequence fitting	64
D SFR-BHAR fitting parameters	64

## Acknowledgments

This project represented a challenge to me on so many different levels and I could not be more grateful for all the people who helped me complete it.

I would like to thank my supervisor, Dr. Lingyu Wang for her guidance and professionalism that taught me many things during my thesis. I will always be thankful for her continuous support throughout the ups and downs during a year of hard work.

I also need to thank Antonio La Marca, who helped me numerous times in setting up CIGALE and clearing any doubts I had about anything. I also appreciated his flexibility in scheduling meetings despite them being sometimes sudden or late.

Thanks to Pratika Dayal for reading my thesis as a second examiner.

Last but not the least, I would like to thank my family and friends, who, without a doubt, provided me with the best support possible.

# 1 Introduction

A Hierarchical model is thought to be the base of galaxy formation (White & Rees, 1978). The currently accepted cosmological model,  $\Lambda$  cold dark matter ( $\Lambda$ CDM), is established on self-interacting dark matter influencing the distribution of the baryonic matter. The fully pressurized baryonic content is then able to counter the gravitational force of dark matter, creating small density fluctuations across what is known as the ‘cosmic web’ (Weygaert & Bond, 2008). Large structures of the cosmic web consist of dense interconnected filaments that show hierarchical trends (Sheth, 2004). Such a trend is based on low mass dark matter haloes existing in high-density regions that merge into bigger systems, creating the massive systems we observe today (e.g. Carlberg and Couchman, 1989; Gawiser, 2005). The assembly of these massive systems is thought to be accompanied with a top-down star formation sequence, also known as ‘downsizing’ (Cowie et al., 1996; Silk J. et al., 2014). Downsizing is where massive galaxies exhibit high star formation rates early in the cosmic epoch, but slows down as the redshift decreases. On the other hand, the star formation rates of lower mass galaxies are less extreme but remain consistent over time. This phenomenon have been observed before (e.g. Heavens et al., 2004), and is believed to explain the red sequence of galaxies (Firmani & Avila-Reese, 2010). We highlight that downsizing could vary depending on the local environment of the galaxies (Peng et al., 2010).

According to De Lucia and Blaizot (2007), 50% of the stars in massive galaxies have already been formed by  $z \sim 5$  through ‘in-situ’ star formation. This means that during the ongoing mergers (Pillepich et al., 2015) stars formed 8 Gyr ago (Qu et al., 2017), and became the old stellar populations we see in massive galaxies with high  $\alpha$  enhancement due to core-collapse supernovae (Thomas et al., 2019). It is complex to generalize evolution cases for galaxies due to different conditions (Cimatti et al., 2019) (i.e. gravitational interactions, kinematics and feedback). For example, some mergers have shown to pump molecular gas into central regions of the galaxy (Larson et al., 2016; Violino et al., 2018), enhancing the environment with star-forming regions (Saintonge et al., 2012), in addition to triggering the black hole into its active accretion stage, known as ‘active galactic nuclei’ (AGN) (Hopkins et al., 2008). Such environments with rapid star formation are thought to decrease the gas depletion timescale compared to non-interacting galaxies (Michiyama et al., 2016). As a result, a significant amount of the galaxy population has shown to be already quenched by  $z \sim 2$  (Daddi et al., 2005; Strazzullo et al., 2016; Deshmukh et al., 2018), and for some cases at higher redshifts (Carnall et al., 2023; Kakimoto et al., 2024). In the case of low redshift galaxies, gas exhaustion could indeed be a viable theory for their quenching. For high redshift galaxies with star formation suppressed, however, the decline in stellar growth has been attributed to the AGN (Neistein et al., 2006).

## 1.1 Coevolution of star formation and black holes

The mutual evolution between a supermassive black hole (SMBH) and its host galaxy has been supported by multiple observational studies (for a recent review, see Harrison and Ramos Almeida, 2024). Properties such as galaxy velocity dispersion ( $\sigma$ ), bulge mass and bulge luminosity have shown to correlate with the black hole mass ( $M_{\text{BH}}$ ) (e.g. Ferrarese and Merritt, 2000; Marconi and Hunt, 2003; Häring and Rix, 2004; Kormendy and Ho, 2013). We show the established  $M_{\text{BH}} - \sigma$  scaling relation in Figure 1, which also holds as we go to higher redshifts ( $4 < z < 7$ ) (Maiolino et al., 2023). The velocity dispersion is fundamentally dependent on the gravitational potential well of the galaxy center for which the mass of the black hole is a proxy. For the  $M_{\text{BH}}$ - bulge mass relation however, recent ob-

servations by the *James Webb Space Telescope* (JWST) show a large deviation ( $> 3\sigma$ ) from the local relation at high redshift (e.g. Harikane et al., 2023; Maiolino et al., 2023; Übler et al., 2023). This indicates there exist overmassive black holes where their  $M_{\text{BH}}$  roughly reach  $\sim 30\%$  of the host galaxy mass (Kokorev et al., 2023), and not just  $\sim 0.1\%$  as derived in the local relation (Reines & Volonteri, 2015). Such masses are thought to develop through different seeding distributions depending on the progenitor’s mass. For instance, ‘metal-free’ Population III (Pop III) stars, that remain undetected to this day which might have formed at  $z = 20 - 30$  (Bromm & Larson, 2004), are thought to be light seed mass progenitors for primordial black holes. Their masses could reach ( $\lesssim 10^3 M_{\odot}$ ) due to their inefficient cooling (Stacy et al., 2016). However, several works consider Pop III stars to be possible progenitors only if the succeeding black hole crosses an Eddington-limited accretion, meaning that the SMBH has to accrete at ‘super-Eddington’<sup>1</sup> rates (Pezzulli et al., 2016). Kawaguchi et al. (2020) showed the possibility for a black hole to sustain such intense mass inflows for 10 Myr.

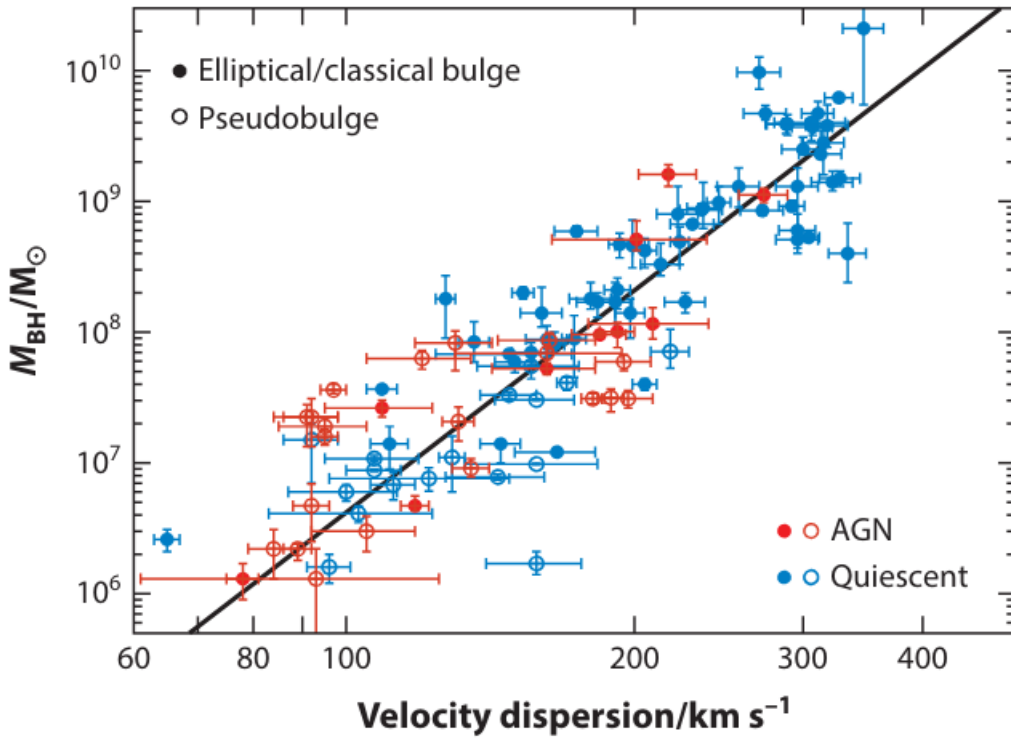


**Figure 1:** The  $M_{\text{BH}} - \sigma$  local relation for pseudobulge and elliptical galaxies. The solid black line derived by McConnell and Ma (2013). Image credit: Heckman and Best, 2014

Heavy seed ( $10^5 M_{\odot}$ ) progenitors for black holes could be supermassive stars. These stars could form in gas clouds that retain their mass and avoid fragmentation. Such conditions could be achieved if the environment lacks  $\text{H}_2$ , which aids cooling (Omukai, 2001; Inayoshi et al., 2014; Tanaka & Li, 2014). A further possible scenario for black hole formation could arise from intermediate seeds ( $10^3 M_{\odot}$ ) which are runaway mergers of stellar remnants in dense clusters, where their environment is required to have a  $\text{H}_2$  cooling deficiency. Conditions to suppress  $\text{H}_2$  formation and cooling are rare but proved to be possible through background Ultraviolet radiation (Dijkstra et al., 2014; Visbal et al., 2014). A Semi-analytical model by Sassano et al., 2021 showed that heavy seeds have the largest contribution

<sup>1</sup>Eddington luminosity ( $L_{\text{Edd}} = 1.2 \times 10^{38} (M/M_{\odot})$ ) defines the maximum luminosity possible while the black hole is still in hydrostatic equilibrium. Super-Eddington would hence surpass that limit.

towards forming SMBH at  $z \sim 6$ . However, all the aforementioned scenarios are thought to be compatible with each other in contributing to SMBH formation. The initial conditions of the environment are assumed to dictate the evolution of primordial black holes (Sassano et al., 2021). None of these formation mechanisms have been directly observed yet, though the recent increase in detections of SMBH at high redshifts by JWST is helping to constrain the seeding models further (Pacucci & Loeb, 2024).

## 1.2 AGN feedback

After a progenitor collapses, a black hole is formed, which starts accreting the surrounding gas and dust. The infalling material, due to mass-energy conservation, emits radiation (Capelo et al., 2023). By comparing the illuminated light with the accreted mass, AGNs showed to have a radiative efficiency ( $\epsilon$ ) of 0.1 (Soltan, 1982; Small & Blandford, 1992), which could go even lower for black holes in a super-Eddington state with thin accretion disk models (e.g. Li et al., 2005). This would allow a light seed progenitor to become a SMBH within 1 Gyr (Madau et al., 2014).

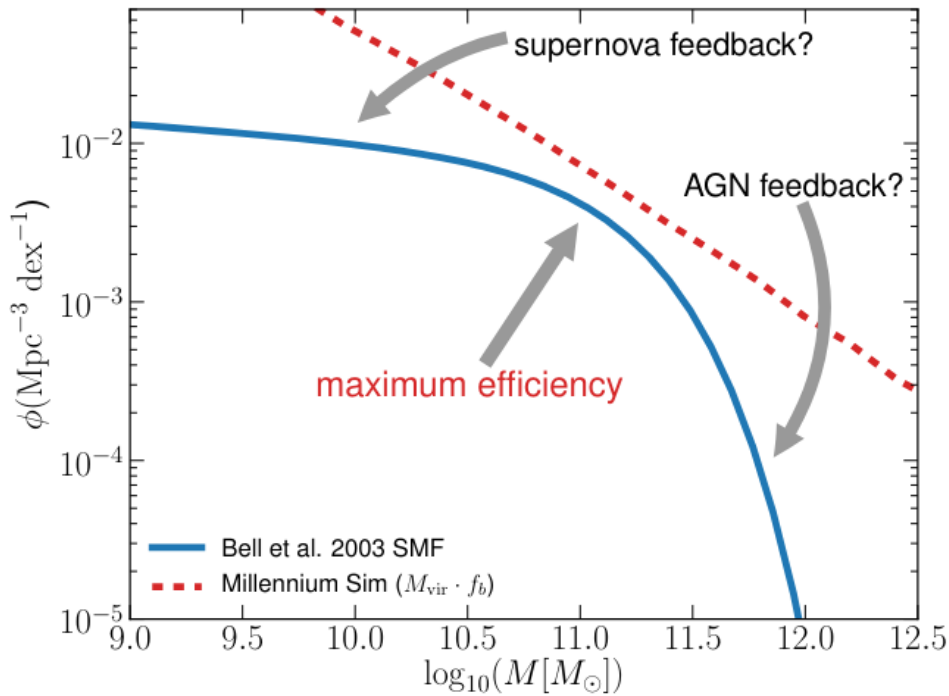


**Figure 2:** A plot to demonstrate the discrepancy between the observed SMF (blue solid line) and the halo mass functions (red dashed line). The difference is due to unaccounted major feedback processes, AGN suppresses the galaxy growth at the massive-end slope while supernovae affect the low-end slope. The smallest distance (the ) between both functions represents the highest efficiency for the galaxies. Image credit: Mutch et al., 2013.

The emitted radiation as a result of accreting material holds a crucial role in regulating the star formation of the host galaxy, known as a ‘feedback’ process (Di Matteo et al., 2005; Van De Voort et al., 2011). Feedback is thought to be essential in understanding the assembly and evolution of galaxies. To elaborate further, we display Figure 2 from Mutch et al. (2013). If the dark matter halo entirely

collapses and is directly transformed to baryonic matter, the mass distribution of galaxies would follow the red dashed line. This is clearly not the case, since what we observe is the blue solid line. The largest differences lie at the low- and massive-ends of the stellar mass function (SMF), while at the ‘knee’ of the observed trend, galaxies seem to become the most efficient as they lie close to the halo mass function. Efforts to connect the inconsistencies implemented cooling timescales for the collapsed baryonic matter in the halo (Benson et al., 2003). This indeed, shrinks the difference between observations and the model, but still, the model produces many more small and massive galaxies. Massive galaxies especially experience fast cooling rates, since high density gas cools much quicker (Balogh et al., 2001), leading to overproduction of massive galaxies, also known as the ‘overcooling’ problem (Dekel & Silk, 1986; Kauffmann et al., 1993). Moreover, Benson et al. (2003) attempted to add photoionization to quench the production of low-mass galaxies. Photoionization from the first-ever galaxies is thought to suppress the growth of low-mass galaxies (Barkana & Loeb, 2001; Dawoodbhoy et al., 2018). However, this was not sufficient to match the low mass-end of the slope. When Benson et al. (2003) applied a disk-heating feature for star-forming galaxies, it produced a reasonable trend for the low mass-end slope, but it required a very efficient gas heating by the radiation.

At the end stage of the stellar evolution, stars run out of fusion energy to sustain themselves against their own gravity, resulting in a supernova (core-collapse) event. The energy injected into the surroundings are believed to suppress star formation and therefore fix the discrepancy for the low mass-end galaxy distribution (Croton et al., 2016). Supernovae are thought to only affect low stellar mass ( $M_*$ ) galaxies ( $M_* < 10^{9.5} M_\odot$ ), because their potential well is relatively shallow (Pontzen et al., 2017; Henriques et al., 2019). All of the aforementioned mechanisms were applied to solve the discrepancy in the low mass regime of galaxy population. To suppress the growth of massive galaxies however, AGN feedback is thought to be the sole mechanism to have enough energy to solve the overcooling problem (Donnari et al., 2021; Scharré et al., 2024).

The exact physics of the AGN feedback is not entirely understood, though studies have indicated the existence of two modes for feedback. The ‘radiative/quasar’ feedback, which occurs for SMBH with high accretion rates, and are hence radiatively efficient (e.g. Combes, 2017), shown as the right panel in Figure 3. The dominant mechanism of the feedback are radiation pressured wide-angle outflows that could scale up to a few kpc (Revalski et al., 2018). Which in some cases is accompanied by relativistic jets (Husemann et al., 2014). This type of feedback is powerful enough to ionize the surroundings, including the interstellar medium (ISM), located a few kpc away from the SMBH. The outflows could also extend much further outside of the galaxy (Davies et al., 2020). Such huge scales could also be present in ‘radio/kinetic’ feedback (left panel of Figure 3), which is the weaker form of AGN activity and is associated with AGNs of low accretion rates (e.g. giant elliptical galaxies and low luminosity AGN) (Machacek et al., 2006; Nulsen et al., 2009). Observations of this feedback mode are based on the largely extended (hundreds of kpc) collimated jets due to the momentum energy transferred (radiatively inefficient) (McNamara & Nulsen, 2012; Blandford et al., 2019). These radio jets have been observed to be dominated with a helical-shaped magnetic field, carrying the momentum of the gas parallel to the jets (Gabuzda et al., 2004; Avachat et al., 2014).

Baron and Netzer, 2019 found that AGNs with winds have excess mid-IR emission compared to AGNs that do not have detectable winds, indicating an extra dust component. This is also supported by X-ray observations that attributed the spectral absorption in the outflows to high dust column densities (Lee et al., 2001). Furthermore, the presence of molecular (Aalto et al., 2015; Stone et al., 2016), neutral and ionized gas have been detected in the quasar mode outflows (Liu et al., 2013; Caz-

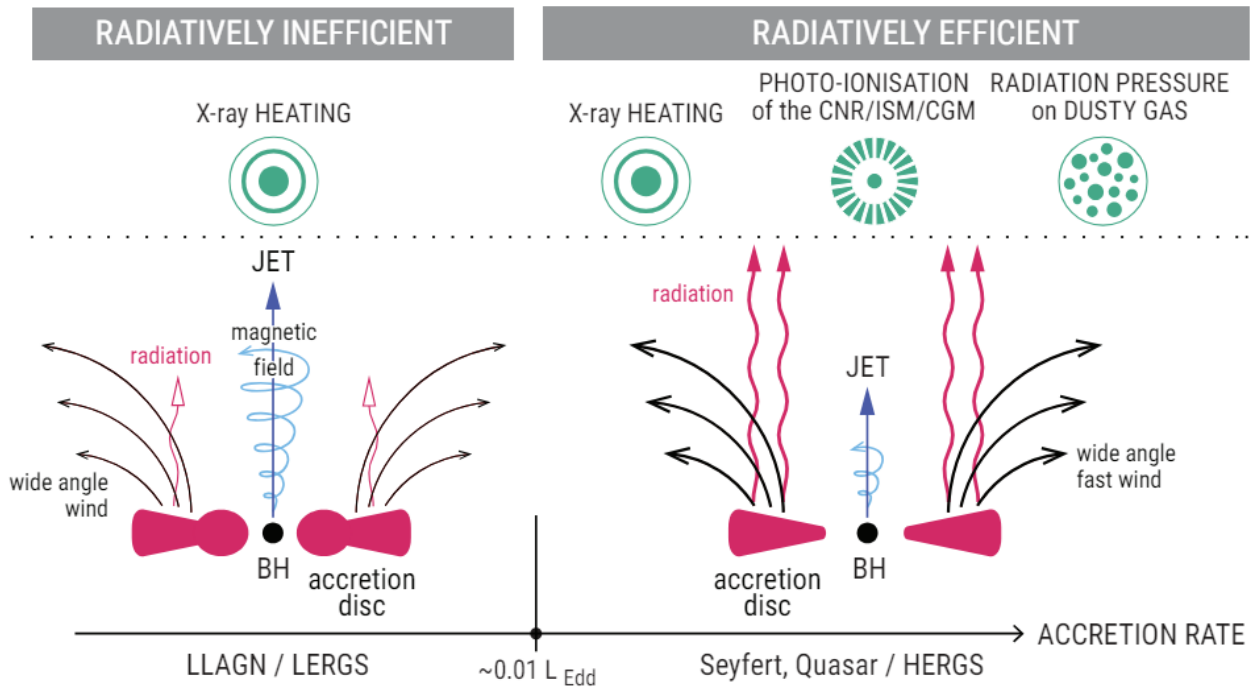


**Figure 3:** A sketch diagram to illustrate the difference between the kinetic (left) and the quasar (right) modes of feedback. Image credit: Harrison and Ramos Almeida, 2024

zoli et al., 2016), adding complexity to the puzzle of their origin. This multiphase outflow, however, hinted at the possibility of in-situ formation for the molecular gas. That is, the swept away gas by the AGN created clumps of cold gas after  $\sim 1$  Myr (e.g. Thompson et al., 2016; González-Alfonso et al., 2017; Richings and Faucher-Giguère, 2018). The entrainment of hot, warm and cold gas all together by an AGN outflow is also another possible scenario, but several studies suspect the inability of the gas cloud to withstand the strong AGN wind (Brüggen & Scannapieco, 2016; D. Zhang et al., 2017). It is a challenge to conclude the origin of these multiphase outflows since not many studies have conducted such work (Cicone et al., 2018). The physics of the outflows as we currently understand it are based on the ‘inner wind’ model (King & Pounds, 2003). The AGN drives radiation-pressured winds with a speed of  $0.1c$  into the surrounding ISM, which typically lies tens of kpc away from the central region. A shock is created as soon as the outflow interacts with the ambient ISM, decelerating the inner wind itself (Faucher-Giguère & Quataert, 2012). Simulations done by Costa et al. (2014) showed that outflows are expected to be energy-driven to support observational results for multiphase outflows. Energy-driven outflows are thermally stable to conserve the inner wind energy and maintain the expanding shell front. As the shell expands, it loses energy, enabling the gas to cool down and entrain itself with cold gas.

Besides their origin, the front shocked shell of the outflows could heat up the ISM by injecting kinetic energy into it, which is thought to hold back the cooling of molecular gas. These shocks have a typical velocity of  $1000 \text{ km s}^{-1}$ , allowing them to be detected in X-ray wavelengths as they interact with the ISM (Raga et al., 2002). Complemented with radio observations (Morganti, 2017), X-ray images show shocked hot gas at a scale of hundreds of kpc that is overlapped by lobes of radio emission (Fornasini et al., 2022). This observation implies the suppression of star formation due to gas heating, which had been observed before (e.g. Wylezalek and Zakamska, 2016; Vayner et al., 2017), and

is considered ‘preventative’ feedback, where the star formation activity is delayed, but not entirely quenched. Another form of negative feedback is the ‘ejective feedback’. Powerful outflows expel the surrounding gas outwards. This is common in galaxies containing AGNs, where there is a significant reduction in the molecular gas depletion timescale (Brusa et al., 2018). In addition, ejective feedback is suspected to only affect the central region of the galaxy. Ellison et al. (2021) computed the CO molecular gas fraction in the central region to be two times less than the general star-forming galaxies.

On the other hand, quasar mode feedback could also enhance the star formation activity of a galaxy. The outflows could compress the neighboring molecular gas, which could facilitate the gravitational collapse of a cloud (Silk, 2013). For example, Cresci et al. (2015) detected a young stellar population in a gas clump coexisting with ionized [O III] outflows. Bessiere and Ramos Almeida, 2022 did a spatial distribution analysis on a type 2 quasar, Mrk 34, to find a young stellar population by the outflow edges, suggesting enhancement of star formation. In addition, Shin et al. (2019) found both types of feedback in one system. Enhanced star formation was detected in the outflows at kpc scales, while gas in outer regions is further expelled by the AGN radiation pressure. Such findings, however, do not necessarily draw a clear conclusion about the feedback effect. It could simply be caused by efficient inflow, where both the SMBH and the galaxy could simultaneously accrete material, resulting in a positive correlation while not relating to one another (Peng, 2007; Hirschmann et al., 2010). Positive feedback could also arise from within the galactic outflows. Maiolino et al. (2017) studied a nearby merger which contained high density molecular gas in the outflows themselves, emission line ratios revealed in-situ star formation.

Radio mode feedback is thought to have similar quenching mechanisms (i.e. heating molecular gas or expelling the gas outside of the galaxy) as the quasar mode but for low accretion rate galaxies (Croton et al., 2006; Fabian, 2012; Gürkan et al., 2015). It can also trigger star formation within radio jets, provided the environment is cool and has a high gas density (Kalfountzou et al., 2014). An observational study done by Kalfountzou et al. (2017) compared the star formation rate (SFR) in radio-quiet quasars (RQQs) and radio-loud quasars (RLQs). They found RQQs to have enhanced SFR compared to RLQs, suggesting a threshold for radio jets power where they switch from inducing to suppressing the star formation activity.

### 1.3 Quasars

AGNs can be of different types (e.g. blazars, seyferts or quasars), but this variation is thought to solely depend on the viewing angle of the central region with respect to us (see Figure 4). A unification model was developed and divided AGNs into two main classes based on their orientation with respect to the observer (Antonucci, 1993; Urry & Padovani, 1995). To illustrate, AGNs with face-on orientation exhibit visible broad emission lines and are hence categorized as type 1, while type 2 AGNs only have narrow lines due to their edge-on alignment. Broad lines originate from fast rotating ( $\text{FWHM} > 1000 \text{ km s}^{-1}$ ) ionized gas being located deep inside the gravitational well of the SMBH in the so-called broad line region (BLR). In a less dense region lies the narrow line region (NLR) where it extends a few pc beyond the toroidal-shaped torus and is about ten times the size of the BLR (Suganuma et al., 2006; Peterson et al., 2013). It is however currently debated whether different types of AGN are indeed just a difference in inclination or if they are inherently different evolutionary stages of an AGN. For example, Malkan et al. (1998) challenged the unification model by measuring excessive dust absorption for Seyfert 2 galaxies compared to Seyfert 1, showing a morphological difference between both galaxies. Moreover, Almeida et al. (2011) reported a structural difference in the tori of

Seyfert 1 and Seyfert 2 galaxies where the latter contained more clumps of dusty clouds, indicating a dependence of the AGN type on its surrounding structure.

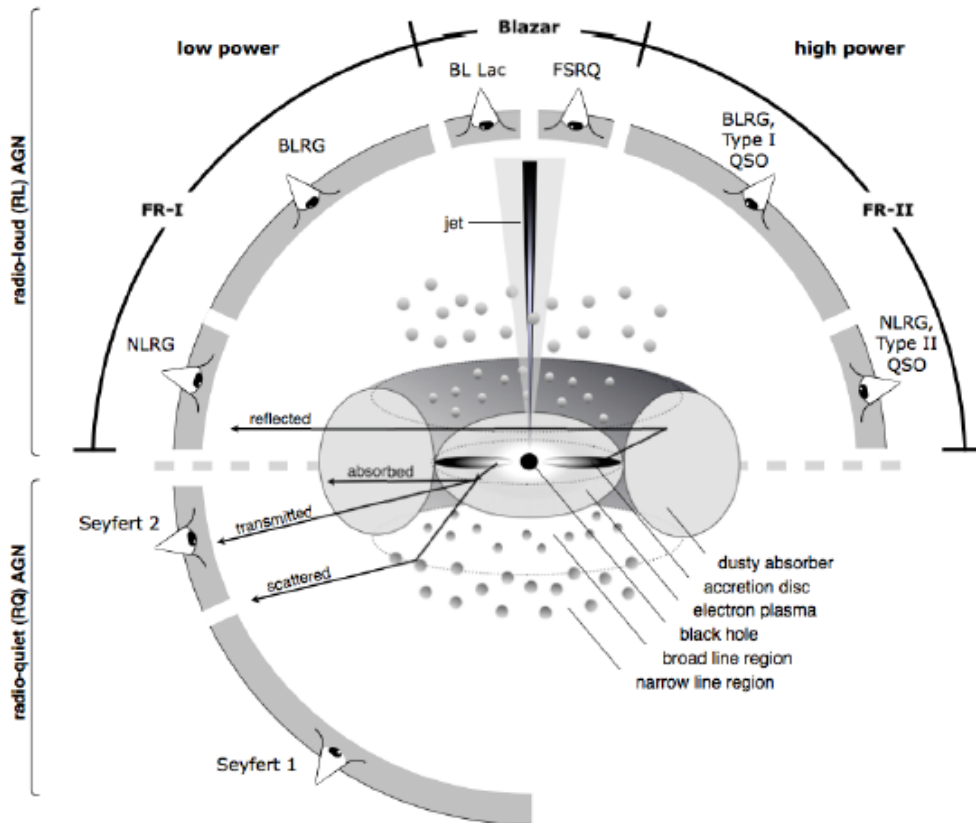


**Figure 4:** A sketch of the unification model to showcase the crucial role of inclination and its effect in displaying different types of AGNs. Image credit: Beckmann and Shrader, 2012.

Quasars are considered the most luminous evolutionary stage of the AGN paradigm, lasting for 1 Myr – 1 Gyr (La Plante & Trac, 2016). Their origin is thought to be two gas-rich major mergers (Hopkins et al., 2006). The merger funnels in gas and dust, causing complete obscuration of the galaxy while extreme star formation and SMBH accretion occur. It is thought that the intense accretion halts  $\sim 1.5$  Gyr after the merging event (Rodríguez Montero et al., 2019), when the radiative mode feedback is activated and blows out the shrouding dust (Wylezalek & Zakamska, 2016), causing the galaxy to be optically visible. The quasar exhausts the gas supply and eventually becomes an elliptical galaxy. Several works have suggested the Ultraluminous Infrared Galaxies (ULIRGS; Sanders and Mirabel, 1996) to be the stage prior to type 1 AGN, where extreme SFR occurs due to the gas availability from the gas rich merger. For example, Villar-Martín et al. (2013) and Humphrey et al. (2015) used the CO(1–0) line to study an optically detected merger system where they found a large unsettled (40%) reservoir of molecular gas to be located in the outer regions while the luminous ( $> 10^{12} L_{\odot}$ ) infrared center contained the remaining gas. They suggest the distant gas reservoir will eventually fall back into the galaxy and assist the SFR of the galaxy.

The findings above suggest that an AGN evolution paradigm might indeed be the origin for quasars.

An open question that remains, however is the aspect of coevolution between the AGN and their host galaxy. A main reason for the different conclusions derived, could be due to observational bias. For instance, AGN studies using X-ray surveys are popular, since the AGN X-ray luminosity outshines that of its host galaxy. Nonetheless, X-ray emission is vulnerable to absorption in Compton-thick regions ( $> 10^{24} \text{ cm}^{-2}$ ), which makes it hard to deduce the true X-ray emission of the AGN (Brandt & Alexander, 2015; Azadi et al., 2017). For reference, it is estimated that  $\sim 20\%$  of the AGN population is Compton thick (Gilli et al., 2007; Tasnim Ananna et al., 2019). In addition to the obscured X-ray emission, their observations usually include a luminosity threshold which ends up excluding AGNs in low mass galaxies, that are rare and much more efficient than the ones in massive galaxies (Mendez et al., 2013). Recent work therefore include X-ray stacking analysis for non-detected galaxies (e.g. Ito et al., 2022).

Depending on the tracer used, SFR measurements can also introduce biases. One of the most common SFR tracer used locally is the recombination emission line  $\text{H}\alpha$  ( $6563 \text{ \AA}$ ), as it directly tracks the ionized hydrogen from high mass stars (Kennicutt, 1983). Studies should correct for the AGN radiation that can also contribute to  $\text{H}\alpha$  emission by also ionizing their surroundings (Stern & Laor, 2012). As  $\text{H}\alpha$  line gets redshifted outside of the optical range at  $z \sim 0.5$ , other SFR proxies can be used. The  $24 \mu\text{m}$  MIR emission can trace the re-emitted stellar UV radiation by dust. The wavelength of the  $24 \mu\text{m}$  allows for low dust contamination because it lies beyond the peak emission of polycyclic aromatic hydrocarbons (PAHs) at  $8 \mu\text{m}$  (Lu et al., 2014; Figueira et al., 2022). Other tracers can also be used, but the derived SFR might contain large uncertainties. For example, [OII] line ( $372.2 \text{ nm}$ ) can also track ionized stellar emission, but it is highly attenuated by dust in addition to the strong dependence on metallicity. Calibrating for metallicity could introduce some uncertainties, depending on the emission line ratio used (Figueira et al., 2022). Infrared (IR) dust emission ( $8 \mu\text{m}$ ) originating from the reprocessed O and early-type B ultraviolet (UV) emission may be biased toward old stellar population (Kennicutt, 1998; Kouroumpatzakis et al., 2020). Furthermore, IR monochromatic can underestimate SFR measurements in low-metallicity galaxies (e.g. Boquien et al., 2015).

Moreover, AGN contamination can cause the SFR to be overestimated in the IR by heating the dust residing in the NLR (Fritz et al., 2006). The dust heating by AGN is thought to peak at  $20 - 40 \mu\text{m}$  (Roebuck et al., 2016). In some rare cases, the far-IR (FIR) wavelength regime can be dominated if the AGN is completely covered in dust. Such Compton thick envelopes are thought to exist only for host dust-obscured galaxies (Tsai et al., 2015; Ricci et al., 2017). As a result of these limitations, hybrid SFR estimators (e.g.  $24 \mu\text{m}$  with  $\text{H}\alpha$  or  $8 \mu\text{m}$  with [O II]) (Calzetti et al., 2000; R. C. Kennicutt et al., 2009) are used to trace the unobscured UV light in addition to measuring re-emitted UV light by dust.

## 1.4 This study

The aim of this thesis is to investigate the coevolution aspect of galaxies by studying the same galaxy population across a wide range of redshifts. Our primary goal is to derive the accretion histories of black holes and their host galaxies within the same systems. Due to observational constraints, most studies typically measure either the star formation rate density (SFRD) or the black hole accretion rate density (BHARD), rarely both simultaneously. For example, Harikane et al. (2022) and (Magnelli et al., 2013) derived the SFRD for their galaxies using UV and IR luminosity functions, respectively while Ueda et al., 2014 computed only the BHARD using X-ray luminosity functions. Combining both accretion histories together, Madau and Dickinson (2014) showed a joint peak between the (SFRD) and (BHARD) at  $z \sim 2$ , as illustrated in Figure 5. Their SFRD is derived from 13 different studies that used UV or IR to trace the SFR. Furthermore, the overlaid BHARD fits (blue, red and green) are based on various observational studies, the one derived from Aird et al. (2010) (green) had X-ray selected AGNs, while Delvecchio et al. (2015) (blue) contained IR detected galaxies and Shankar et al. (2009) (red) constructed an AGN model mainly based on X-ray observations.

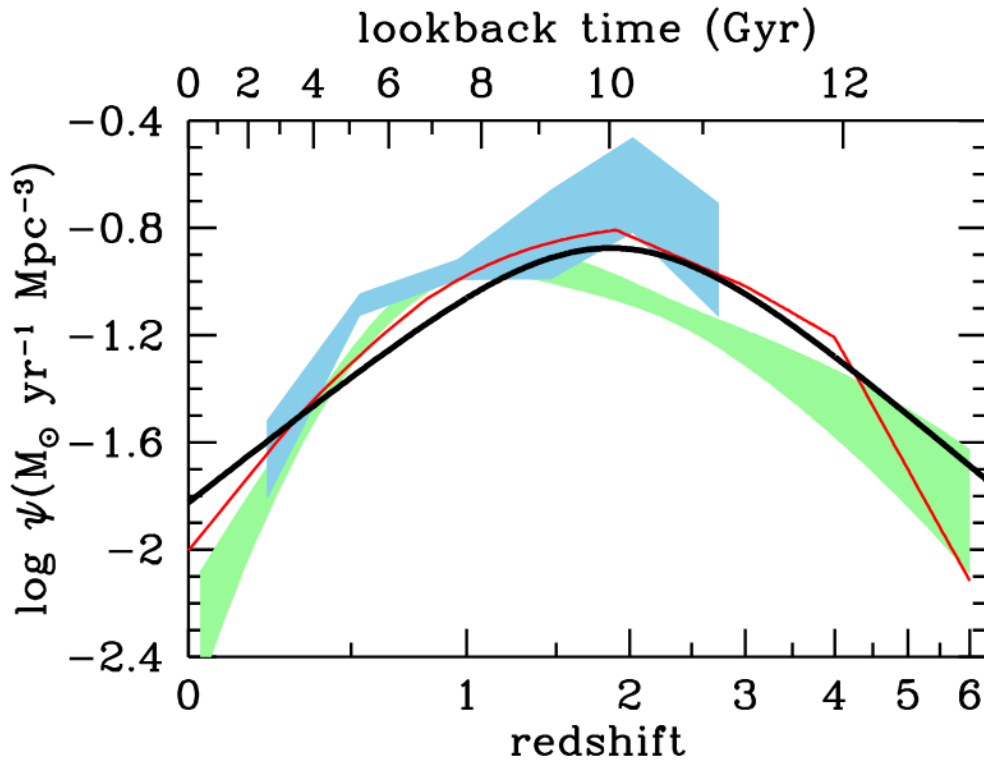


**Figure 5:** The best fit SFRD derived from 13 different catalogs show in the black solid line. The red, green and blue trends are BHARD derived from Shankar et al. (2009), Aird et al. (2010) and Delvecchio et al. (2014), respectively. Both aspects share a peak at  $z \sim 2$  but then fall off till our current cosmic epoch. Image credit; Madau and Dickinson (2014).

Our approach towards simultaneously studying the SMBH and SFR aspects for the same galaxies depends on the characteristics of their emission. First, this thesis will only focus on optical quasars. These typically dominate the optical and UV spectra (Kuźmicz et al., 2021), hence the ideal wavelength range to study AGN activity. As already mentioned above, the AGN contribution in the FIR

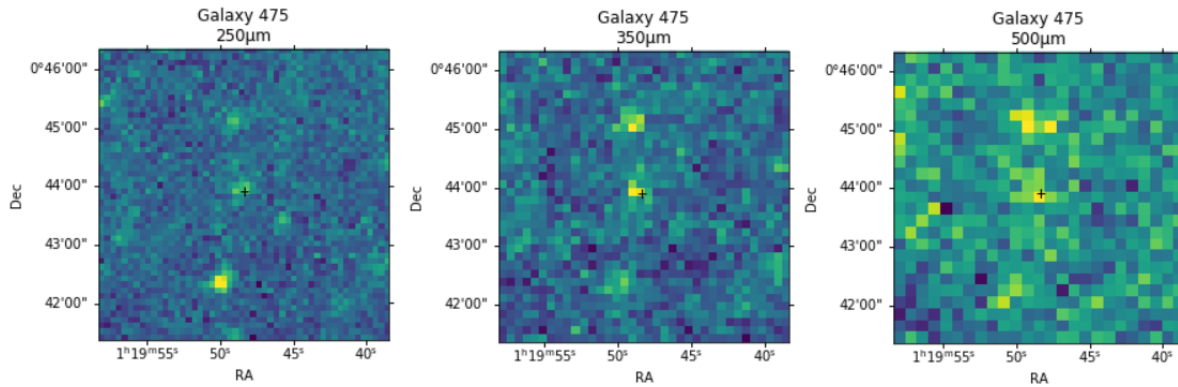


**Figure 6:** *Herschel* images at 250, 350 and 500  $\mu\text{m}$  for a cold quasar included in Kirkpatrick et al. (2020) study. The black cross is their X-ray counterpart position.

regime is thought to be negligible (Mullaney et al., 2011). We therefore use the FIR emission to trace star formation activity in the host galaxy. Optical quasars with a FIR counterpart have been studied before (e.g. Stacey et al., 2010; Ivison et al., 2019) and more recently by Kirkpatrick et al., 2020, Coleman et al., 2022 and Mintz et al., 2024. It was Kirkpatrick et al., 2020 who suggested the name ‘cold quasars’ for such objects, due to their bright FIR (cold dust) emission. A major limitation to this study however, is the poor angular resolution of FIR observations.

We display an image for one of the galaxies included in the cold quasar study by Kirkpatrick et al. (2020) in the 250, 350 and 500  $\mu\text{m}$  FIR bands. One can see that these observations lack the resolving power. To tackle the issue, we use deep and wide radio surveys, which have a much better angular resolution than FIR observations. We use the high resolution of radio observations to help us better locate the galaxies in the FIR bands. This was previously not possible as deep radio surveys in the northern sky have only become available recently.

Our study focuses on the redshift range of  $z = 0 - 5$ . Considering this wide redshift range, we aim to study the star formation activity by fitting spectral energy distributions (SED) to our galaxies. The SEDs will also allow us to investigate the galaxies physical properties as well as the growth of their central engines.

In Section 2, we discuss the catalog assembly process and the fields involved in this study. Next we demonstrate in Section 3 our approach in deriving the physical properties of the galaxies and the limitation. We also illustrate our approach in fitting luminosity functions out our data. We explain the results in Section 4, where we not only investigate coevolution aspects, but also take a closer look at the general properties of what is considered to be a subsample of optical quasars. We conclude this thesis with a general discussion about the results in Section 5 and summarize the key findings that our analysis and discussion seem to suggest.

## 2 Data

In this section, we discuss the construction of our multi-wavelength catalog for type-1 quasars with a FIR counterpart. As mentioned before, an important aspect to optimize the SED fitting process is to collect panchromatic data sets. Our multi-wavelength catalog span from X-ray to radio wavelengths. We note that the fields used in our study are selected based on the availability of their radio data. Our study includes nine fields, where, most of them are located in the northern sky. The fields are Lockman-Hole (Lockman), Boötes, European Large Area ISO Survey-North 1 (ELAIS-N1; Oliver et al., 2000), GAMA fields (GAMA-09, GAMA-12 and GAMA-15) (Driver et al., 2011), XMM-Newton Large Scale Structure field (XMM-LSS), Herschel Stripe 82 field (Stripe-82; Viero et al., 2014) and *Herschel* Astrophysical Terahertz Large Area Survey (HATLAS-NGP; Eales et al., 2010) which is the largest field used in this study, spanning an area over 660 deg<sup>2</sup>. After showcasing the catalogs used in this study, we discuss our cross-matching process, we analyse the final sample acquired and compare it to the general population of optical quasars.

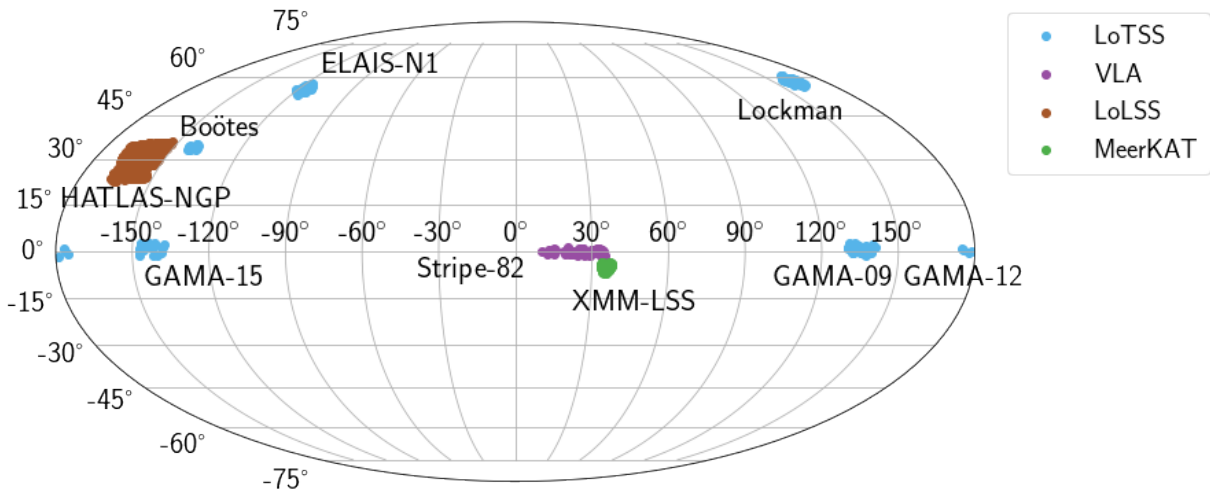


**Figure 7:** A mollweide projection of right ascension (RA) and declination (Dec) for the quasars used in this study in their respective field as a function of their main radio survey. Lockman, Boötes, ELAIS-N1, and GAMA fields are part of the deep field radio observations done by LOFAR. The radio data for the largest field in our study, HATLAS-NGP, was derived from wide field LOFAR observations. For Stripe-82 and XMM-LSS, we used deep radio survey observations done with the VLA and MeerKAT, respectively. For details about the radio surveys, check [Section 2.1.2](#).

### 2.1 Multi-wavelength data

#### 2.1.1 *Herschel*

We make use of the *Herschel* Spectral and Photometric Imaging Receiver (SPIRE) instrument which is part of the Multi-tiered Extragalactic Survey (HerMES) that provided a large survey area of 1270 deg<sup>2</sup> (Pilbratt et al., 2010). This project is a branch of the *Herschel* Extragalactic Legacy Project (HELP), which contains data products of mid-infrared (MIR) from the Spitzer Multiband Image Photometer (MIPS; Rieke et al., 2004) operating at 24  $\mu$ m in addition to far-infrared instrument *Herschel* Photoconductor Array Camera and Spectrometer (PACS; Poglitsch et al., 2010) that is centered at 70, 100

and  $160 \mu\text{m}$ .

The SPIRE instrument on board of the *Herschel* observatory has a FWHM of  $18.1''$ ,  $24.9''$  and  $36.6''$  for wavelengths of  $250$ ,  $350$  and  $500 \mu\text{m}$ , respectively. The extragalactic confusion noise levels are  $5.8$ ,  $6.3$  and  $6.8 \text{ mJy beam}^{-1}$  for  $250$ ,  $350$  and  $500$  microns, respectively. The large beam sizes of SPIRE lead to source confusion. We therefore use the blind SPIRE catalog (dmu22<sup>2</sup>) (Shirley et al., 2021), which is based on extracting sources from SPIRE images using matched filtered maps. Match filtered maps compute flux density peaks for source-confused images (Chapin et al., 2011). A peak is selected, provided they have a 85% completeness level in every SPIRE band (Chapin et al., 2011). The completeness is computed as  $1 - \frac{N_{\text{spurious}}}{N_{\text{real}}}$ , where  $N_{\text{real}}$  is true count of flux density peaks and  $N_{\text{spurious}}$  represent the peaks of fluctuation noise in the image. The accurate centers for each source are then determined by computing Pearson correlation coefficient on each sub-pixel in their initial detection position for all three bands. A best-fit flux density from the largest correlation is then assigned as the new position. The flux densities are then determined using the Bayesian probabilistic deblender XID+ (Hurley et al., 2017), where they used the blinded source catalog as the prior. For the sources used in this study, we apply the 85% completeness limit computed from the match filtered maps as a threshold. We use the  $250 \mu\text{m}$  flux density limit of each field. The limits are  $18$ ,  $19$ ,  $20$ , and  $20 \text{ mJy}$  for XMM, GAMA fields, Stripe-82 and HATLAS-NGP, respectively. The fields ELAIS-N1, Lockman and Boötes and had their respective flux limits of  $35$ ,  $40$ ,  $45 \text{ mJy}$  taken from Wang et al. (2021), which corresponded to a low false identification rate ( $\sim 5\%$ ).

### 2.1.2 Radio

Radio surveys are essential in this study for several reasons. Besides their high resolution and depth, the well established correlation between radio and FIR emission is significant. Bright radio sources tend to also have intense FIR emission. This is because young stars emit excess UV radiation, which gets reprocessed by the surrounding dust into IR wavelengths (Charlot & Fall, 2000). The radio emission originates from dying massive stars, which emit cosmic rays that interact with the galactic magnetic field, resulting in radio synchrotron emission (Klessen & Glover, 2016). The far-infrared radio correlation (FIRC) holds for the local Universe but several works argued that it evolves with redshift (Calistro Rivera et al., 2017; Molnár et al., 2018), while others suspect this evolution may be due to observational biases such as AGN contamination or other physical processes boosting the radio emission (M. J. Jarvis et al., 2010; Bourne et al., 2011; Read et al., 2018). The FIRC allows us to utilize high angular resolution used to detect radio sources to thus locate their FIR counterpart. We show in Figure 8 the remarkable difference in resolution between SPIRE  $250 \mu\text{m}$  and Low-Frequency Array (LOFAR; Van Haarlem et al., 2013)  $150 \text{ MHz}$ . For the FIR image, it is impossible to conclude how many sources visibly exist in the image. This demonstrates the importance of the radio data to conduct this project which otherwise would have an observational bias. This is crucial for our cross-matching process. We use the cross-matched objects between radio and *Herschel* to then search for their optical counterpart, as demonstrated in Figure 9.

Due to its vast sky survey area, high spatial resolution and its wide low frequency, LOFAR is the main source of radio data in this study. The LOFAR Two Meter Sky Survey (LoTSS) currently operating at  $120 - 168 \text{ MHz}$  is targeting a spatial resolution of  $6''$  while maintaining noise levels of  $\lesssim 100 \mu\text{m beam}^{-1}$  and aims to eventually reach sensitivity of  $10 \mu\text{m beam}^{-1}$  (Shimwell et al., 2017;

<sup>2</sup>[https://github.com/H-E-L-P/dmu\\_products/tree/master/dmu22](https://github.com/H-E-L-P/dmu_products/tree/master/dmu22)

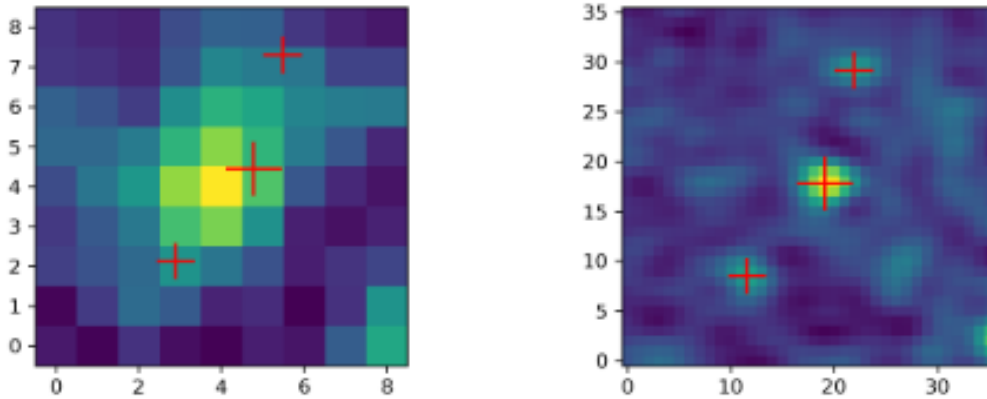


**Figure 8:** *Left panel:* The SPIRE 250  $\mu\text{m}$  image. *Right panel:* LOFAR 150 MHz image. These images were obtained from Wang et al. (2021) where the red plus signs indicate the position of LOFAR sources.

Shimwell et al., 2019). The survey running on high-band antenna (HBA) is set to cover the entire northern sky and has already observed six of our fields. Producing reliable images at such low frequencies is extremely challenging due to direction dependent effects (DDE), which causes radio waves fluctuations on interferometers. Calibration of DDE is major since it can sharpen the angular resolution of an observation by a factor of 4 – 5 (e.g. Weeren et al., 2016). The origin of DDE is due to the free electrons by the Earth’s ionosphere scattering off weak electric fields that ultimately scatter radio radiation on the radio interferometers (Ratcliffe, 1956; Albert et al., 2020). Smirnov and Tasse (2015) and Tasse et al. (2018) were able to synthesize thermal noise limited maps to counteract the DDE while maintaining the high efficiency of the HBA. The resulting root mean square noise levels were 20, 23 and 30  $\mu\text{Jy beam}^{-1}$  for ELAIS-N1, Lockman and Boötes, respectively. The GAMA fields, observed with confusion levels of  $\lesssim 170 \mu\text{Jy beam}^{-1}$  were part of the eROSITA Final Equatorial-Depth Survey (eFEDS). We note that for the GAMA fields, which lie in the equatorial region, suffer a much lower sensitivity due to the shorter baseline. Because of their low declination on the sky with respect to us, a projection effect occurs that affects their sensitivity (Weeren et al., 2016). For Boötes, we complemented the low frequency data with 1.4 GHz observations by the Westerbork Synthesis Radio Telescope (WSRT). The observations achieved a resolution of  $13'' \times 27''$  and had a sensitivity of  $28 \mu\text{Jy beam}^{-1}$ .

The other fields involved in our study have not been observed by LoTSS. However, HATLAS-NGP was part of another LOFAR survey, which is The LOFAR LBA Sky Survey (LoLSS), running at the frequency range of 42 – 66 MHz. The low band antenna (LBA) survey aims to map the northern sky with an angular resolution of  $15''$  (De Gasperin et al., 2021). The first data release by De Gasperin et al. (2023) covers  $650 \text{ deg}^2$  with 42463 detections in the HETDEX spring field Hill et al. (2008), which includes HATLAS-NGP. The field was observed with a median rms noise of  $1.55 \mu\text{Jy beam}^{-1}$ .

Stripe-82 radio counterpart was acquired through a Very Long Array (VLA) survey which spanned over  $92 \text{ deg}^2$  (Hodge et al., 2011). The survey was done in the L-band (20 cm or 1.4 GHz) with a remarkable  $1.8''$  angular resolution. The Stripe-82 VLA radio catalog contains 17969 detections with median rms noise levels of  $52 \mu\text{Jy beam}^{-1}$ . As the field lies on the celestial equator (check Figure 7), and due to the nature of the VLA interferometers distribution, the observation was also subject to antenna shadowing (Heywood et al., 2021). The low elevation of the observation tilts the radio dishes

downwards where the antennas could partially block the pointing of the antennas behind.

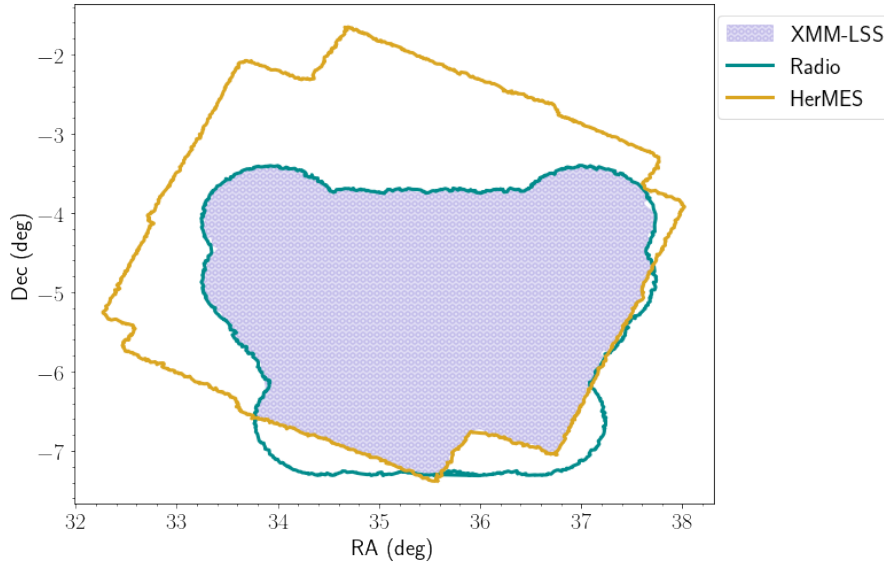


**Figure 9:** The survey footprints of the FIR and radio data, where the shaded overlapping region is where the *Herschel*-detected quasars are. The footprints of the other surveys are available in [Figure 12](#).

At an exceptionally high sensitivity of  $1.5 \mu\text{Jy beam}^{-1}$ , the XMM-LSS field was observed by the MeerKAT telescope as part of The MeerKAT International GHz Tiered Extragalactic Exploration (MIGHTEE; M. Jarvis et al., 2018) survey. The survey is mainly carried out in the L-band (1284 MHz) to track HI through environments of cold gas. This will allow us to look for quenching evidence in addition to mapping the neutral hydrogen density through galaxies (M. Jarvis et al., 2018). The data is observed at angular resolution of  $\sim 8.2''$  (Heywood et al., 2022).

### 2.1.3 SDSS

As mentioned in [Subsection 1.3](#), quasars have their BLR exposed, meaning that they are optically visible, and to capitalize on that, we make use of the largest optical quasar survey. We use the newly added Data Release 16 quasar catalog (DR16Q) as part of SDSS (Lyke et al., 2020). The SDSS quasar observations have been going for 20 years (Schneider et al., 2010), with the latest being the extended Baryon Oscillation Spectroscopic Survey (eBOSS; Dawson et al., 2016) which have resulted in a massive expansion of the quasars catalog. The eBOSS latest catalog, DR16Q, contains 750,414 quasars that are spread over a wide range of redshifts ( $0 < z \lesssim 7$ ). The eBOSS had its spectroscopic data taken by the Baryon Oscillation Spectroscopic Survey (BOSS; Dawson et al., 2013) spectrograph mounted on the 2.5 m Sloan Telescope (Gunn et al., 2006), with a spectral of resolution  $\lambda/\Delta\lambda \approx 2000$  (Smee et al., 2013). The DR16Q imaging data contains photometric data in  $u$ ,  $g$ ,  $r$ ,  $i$  and  $z$  bands and covers a massive area of  $9,376 \text{ deg}^2$ .

### 2.1.4 Ancillary data

The importance of ancillary data lies in their contribution towards modeling an SED that accurately reflects the true emission of the galaxy. Firstly, we use the Wide-field Infrared Survey Explorer (WISE; Wright et al., 2010), which has mapped the entire sky with a higher sensitivity than all previous IR sky surveys. The WISE flight system had a 40 cm telescope equipped with four MIR bands, W1, W2, W3 and W4, centered at 3.4, 4.6, 12 and 22  $\mu\text{m}$ , respectively. The angular resolution achieved was 6.1", 6.4", 6.5" and 12.0" for W1, W2, W3 and W4. The  $5\sigma$  sensitivity of the observations were 0.08, 0.11, 1 and 6 mJy.

The Galaxy Evolution Explorer (GALEX; Martin et al., 2005) is crucial for constraining the UV wavelength range of our SEDs. The telescope provides photometric data for 65 million sources over a sky area coverage of 21,435 deg<sup>2</sup>. The All-sky imaging survey (AIS) catalog contains far-UV (FUV) and near-UV (NUV) photometric bands centered at 1539 Å and 2316 Å, respectively (Morrissey et al., 2007). Bianchi, Efremova, et al. (2011) only included sources within 0.5° off the center of the 1.2° field of view to avoid instrumental artifacts and acquire more accurate photometry. The FWHM of the FUV and NUV are 4.2" and 5.3", respectively. The AIS managed to reach  $5\sigma$  noise levels of 19.9 mag (FUV) and 20.8 mag (NUV). We make use of the fifth data release for GALEX released by Bianchi, Herald, et al. (2011).

X-ray catalogs are the highest frequency data we use in this study. We use the European Photon Imaging Camera (EPIC) on board of the XMM-Newton observatory (XMM; Jansen et al., 2001) for its full photon band (0.2 – 12 keV) data. The newest XMM data release (4XMM-DR13) which covered 1328 deg<sup>2</sup> of sky area, contains 656,997 unique sources in almost a million detections (Webb et al., 2020). Additional X-ray data for the GAMA-09 was acquired through the newly launched extended ROentgen Survey with an Imaging Telescope Array (eROSITA; Predehl et al., 2021). Their wide field and spatial resolution are on par with XMM. We obtained soft band (0.2-2.3 keV) X-ray data for the GAMA-09 field as part of the eROSITA Early Data Release<sup>3</sup>.

## 2.2 Catalog cross-matching

We make use of the FIRC by cross-matching the FIR *Herschel* data with the radio catalogs with a matching radius of 18", corresponding to the beam size of the 250  $\mu\text{m}$  SPIRE photometer (Griffin et al., 2010). The Tool for OPERations on Catalogues And Tables (TOPCAT; Taylor, 2005) cross-matching resulted in ‘unique’ and ‘multiple’ matches. A *Herschel* source which had multiple radio sources cross-matched to them as their ‘true counterpart’, are identified as multiple matches. On the other hand, *Herschel* sources with only one matched radio counterpart are considered unique matches. The large beam sizes of sub-millimetre (sub-mm) dishes and FIR photometers complicate source detections in their band. Early optical and NIR observations revealed existence of multiple counterparts in single sub-mm sources (Dunlop et al., 2004). Sub-mm observations by the Atacama Large Millimeter/submillimeter Array (ALMA; Wootten and Thompson, 2009) at 870  $\mu\text{m}$  revealed a multiplicity rate of 30% for 28 SDSS quasars (Hatziminaoglou et al., 2018). Depending on the study, multiplicity rates can significantly vary. For example, A hyperluminous IR galaxies (HLIRGS) study by Wang et al. (2021) found a multiplicity rate of 15 – 30% while Trakhtenbrot et al. (2017) found sub-mm galaxy counterparts in 3 out of the 6 quasars they studied. Scudder et al. (2016) suspects  $\sim 95\%$  of their galaxy sample to have more than two counterparts. The multiplicity rate of our study

<sup>3</sup><https://erosita.mpe.mpg.de/edr/eROSITAObservations/Catalogues/>

is shown in Figure 10 as a function of survey depths (field on top is the deepest). The multiplicity plot of the FIR wavelength is based on the 250  $\mu\text{m}$  SPIRE band. We note that the offset FIR depth among Lockman, XMM-LSS, ELAIS-N1 and Boötes is 0.72 mJy (see Table 1). As the observation depth increases, the multiplicity rate of the field increases. The multiplicity rate ranked by radio depths share the same trend. The multiplicity plot for the radio data is based on the LoTSS 150 MHz survey. Thus, we converted the depths of MIGHTEE 1.284 GHz, VLA 1.4 GHz and LoLSS 54 MHz surveys assuming a spectral index value of  $\alpha = 0.7$  ( $S_\nu \propto \nu^\alpha$ ; Smolčić et al., 2017; De Gasperin et al., 2021) and we list the frequency-corrected depths in Table 1. Two fields had a significant amount of their FIR sources contain two or more radio counterparts. The multiple matches in XMM-LSS and ELAIS-N1 accounted for 60% and 45% of their total *Herschel* sources, respectively. On the other hand, GAMA fields, Stripe-82 and HATLAS-NGP are much shallower in depth and their multiplicity rates did not exceed  $\sim 20\%$ . A higher multiplicity rate in deep radio observations could translate as an observational bias. Wang et al. (2021) derived the flux ratio between LOFAR deep fields and 250  $\mu\text{m}$  SPIRE observations where they concluded the ability of LoTSS to detected sources that are 3 – 4 times fainter than the applied 250  $\mu\text{m}$  flux limit. This suggests that fields with shallower FIR depth may show similar multiplicity rates, provided deeper radio data.

We suspect there might be a physical interpretation towards the high multiplicity rates in radio deep fields. It could be due to the environment surrounding our quasars. As quasars are thought to be progenitors for local elliptical galaxies. A recent large-scale structure study by Poudel et al. (2017) revealed the fraction of elliptical galaxies in the central region of cosmic web filaments to be the highest. We propose it could hence be the dense environment of the filaments that causes high multiplicity rates in the fields with deep observations.



**Figure 10:** Unique and multiple matches ranked by the observation depth (highest depths at top), *left panel:* Multiplicity as observed by the SPIRE instrument at 250 microns. Lockman, XMM-LSS, ELAIS-N1 and Boötes have very similar FIR depths. *Right panel:* Multiplicity ranked as a function of radio observations depths of LoTSS, LoLSS, MIGHTEE and VLA mentioned in Section 2.1.2. We display the quantitative depths for both FIR and radio data for all fields in Table 1.

Sources with multiple matches were discarded, making our sample much smaller. We only make use of unique matches in this study. We apply a separation radius of  $6''$  to the unique matches. This limit

was used by Wang et al. (2021) to derive low ( $\sim 5\%$ ) false identification rates in Lockman, Boötes and ELAIS-N1. This radius eliminates any *Herschel* sources with their radio counterpart situated more than  $6''$  away. The number of sources remaining after applying the separation radius above are displayed for each field in Table 2 under the column ‘ $6''$  Matching Radius’.

Moreover, we plot in Figure 11 the distribution in positional separation between *Herschel* sources and their matched radio component for all nine fields combined. We note that the separation distribution is similar for all fields except GAMA-12, where it is more evenly distributed between  $2''$  and  $6''$  (see Figure A.1). In Figure 11, the separation peaks at  $\sim 2.2''$ , which matches the positional offset of SPIRE observations Smith et al., 2011; Bourne et al., 2014. LOFAR on the other hand, has a negligible positional error ( $0.2''$ ) compared to *Herschel* Williams et al., 2019.

Once the *Herschel*-radio unique matches were assembled, shown as the shaded region in Figure 9. We used the radio data positional coordinates to cross-match our galaxies with DR16Q using a matching radius of  $2''$ . This resulted in 731 optical quasars having a *Herschel* counterpart, which is 1% of the SDSS population in the fields used in this study. For adding the ancillary data, we also cross-matched their catalogs with the radio counterparts using a matching radius of  $2''$ . WISE is the ancillary data catalog with the most matches in our sample, they complemented 93% of our data sample. Moreover, 40% of our quasars had GALEX matches. The XMM contributed its data to 19% (139/721) of our population, with XMM-LSS containing the most matched sources (81). With eROSITA, we found 11 sources matches for the GAMA-09 field. The WSRT data were matched with 5(45%) sources from Boötes. We display the distribution of galaxies and their ancillary data across all fields in Table 2.

Field	Radio sensitivity ( $\mu\text{Jy beam}^{-1}$ )	SPIRE 250 $\mu\text{m}$ depth (mJy)
XMM-LSS	9.25	2.53
ELAIS-N1	22.9	3.15
LH	23	2.32
Boötes	30	3.25
Stripe-82	52	7.33
GAMA-15	170	5.11
GAMA-12	170	5.08
GAMA-09	170	5.20
HATLAS-NGP	1550	5.17

**Table 1:** Sensitivity of the radio data and the SPIRE 250  $\mu\text{m}$  instrument. The radio observations depth of XMM-LSS, Stripe-82, HATLAS-NGP were corrected to the central frequency of 144 MHz, corresponding to the LoTSS.

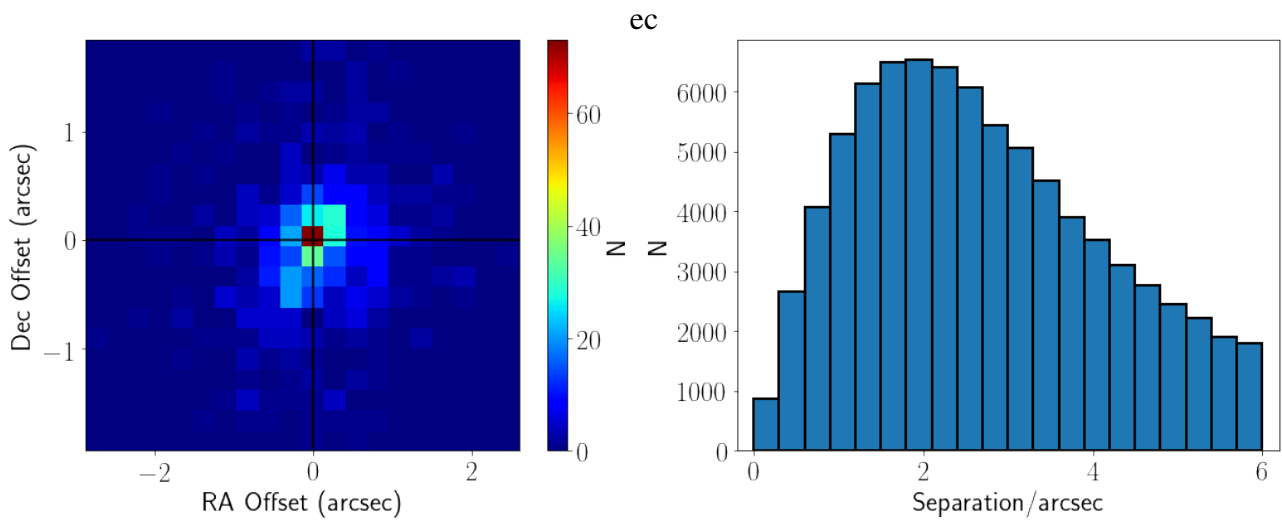


**Figure 11:** *Left panel:* Positional offsets in RA and D between radio sources and their matched SDSS sources, with a cross-matching radius limit of  $2''$ . *Right panel:* Distribution of positional separation between *Herschel* and their unique radio counterparts, which peaks at  $2.2''$ . This plot combines separation from all nine fields, where they share the same trend except for GAMA-12. We show the separation distribution for each field individually in [Figure A.1](#).

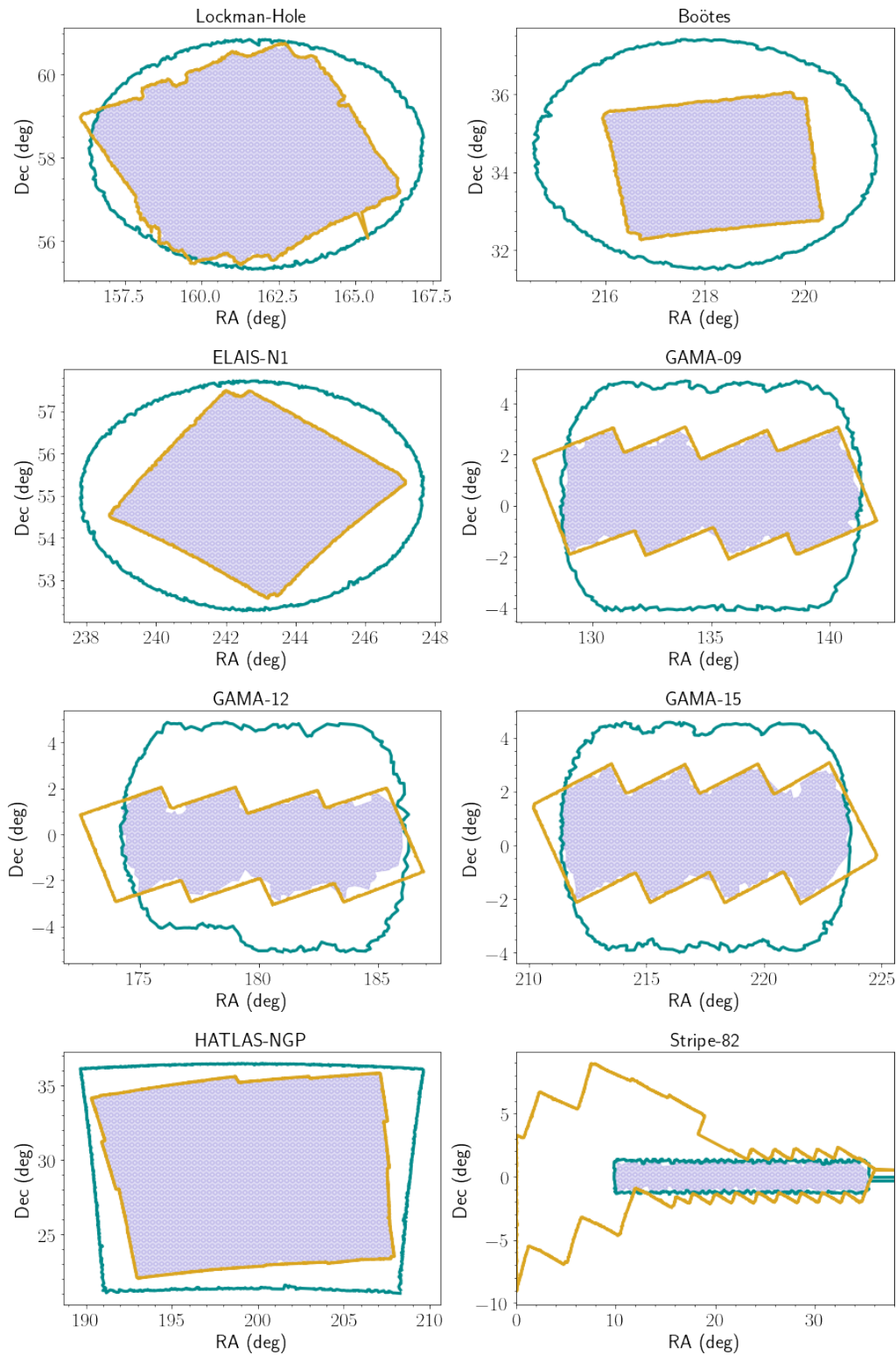


**Figure 12:** Survey footprints of all fields used in this study excluding XMM-LSS which was shown in Figure 9. The yellow line represents the *Herschel* sky coverage and the cyan line is the radio data sky coverage. The shaded region is the overlapping region where cross-matched objects were found, check Subsection 2.2 for details.

### 2.3 Final quasar sample

Our final sample of objects span a large range of redshifts ( $0 < z \lesssim 7$ ). From [Figure 13](#), one can see our galaxy population concentrated at  $z \leq 3$ , which matches the peak duration of quasar activity (Hewitt & Burbidge, 1993; Richards et al., 2006). Moreover, there is only a few (8) objects located at  $z > 4$ , where our most distant galaxy is situated at  $z = 6.7$ . However, we expect the redshift range of our study to shrink due to galaxies with unreliable SED fits.

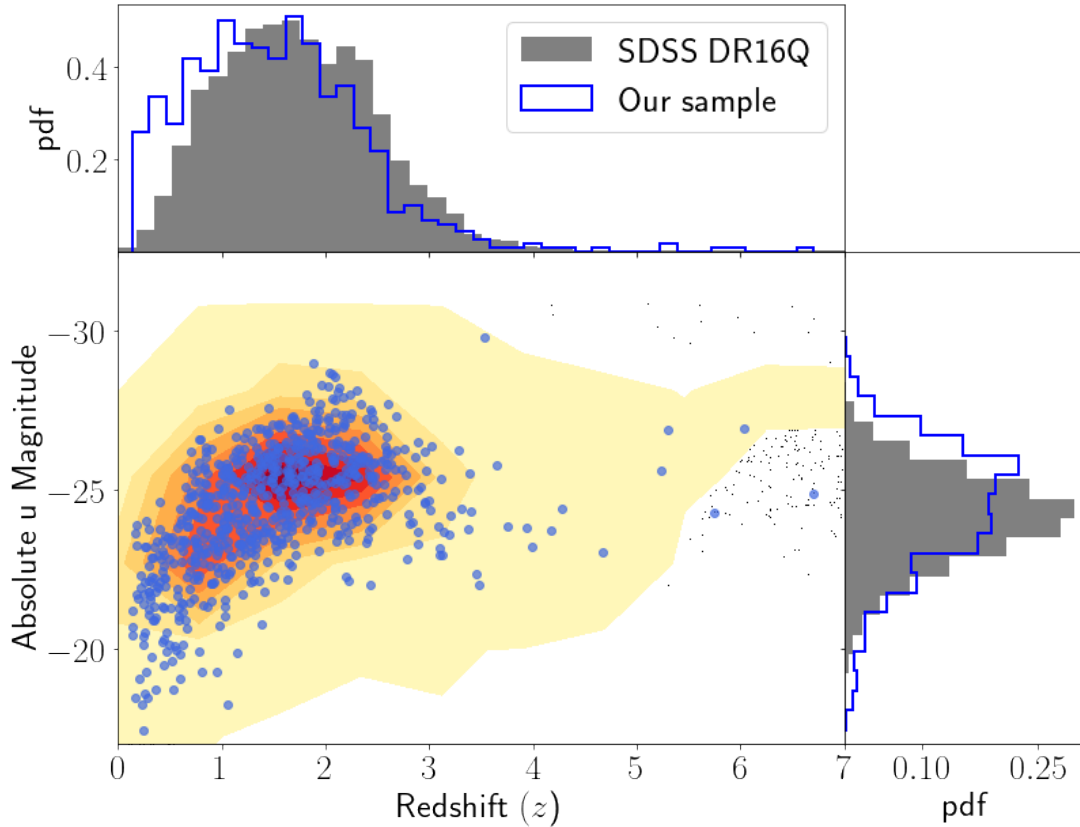


**Figure 13:** A contour plot of the SDSS parent catalog (DR16Q) u-band absolute magnitude distribution as a function of redshift, overlaid with our galaxy sample (blue dots). Our galaxies mostly lie at  $z \leq 3$  and are slightly dimmer in the u-band. The small black points at high redshifts are due to the scattering of the contour. The normalized histograms show the redshift and u-band absolute magnitude of our sample compared to DR16Q.

We are interested in comparing the optical and IR emission of our sample to the general optical quasar population. We can already see in [Figure 13](#) our sample shifting towards dimmer absolute u magnitudes compared to the parent SDSS catalog. One of the possible interpretations for such a feature could be due to dust obscuring the blue light in our cold quasars sample. We also compare the reddening by plotting a color-color diagram of  $g - r$  against  $r - i$  in [Figure 14](#). We can see the blueness of the DR16Q catalog is shifted leftwards compared to our sample. In addition, the median  $g - r$  for DR16Q is 0.17 while for ours it was only a bit higher, 0.2. The distribution itself however, displays our sample to be residing in the redder regime of the plot, while also being less blue than the majority of the SDSS quasars. Such a distribution shows our quasar sample to be slightly redder than the general unobscured quasar population.

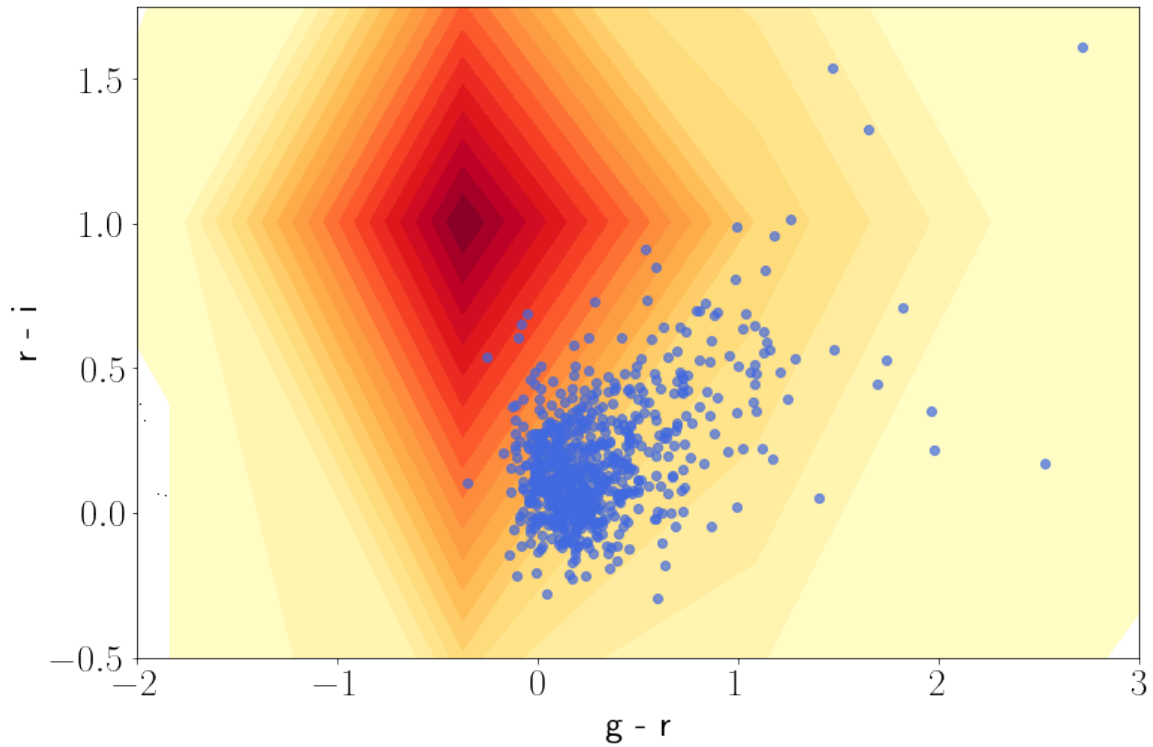


**Figure 14:**  $g - r$  versus  $r - i$  color-color diagram. The heat contour is the DR16Q catalog while the scattered blue points are the quasars in this study. There is a slight reddening in our quasars compared to the parent sample.

Kirkpatrick et al. (2020) compared the MIR emission of their cold quasars sample with SDSS quasars within the same fields. They found their cold quasars to fall below a certain slope, which is the solid line displayed in Figure 15. They conclude that cold quasars are, on average redder in the MIR than most optical quasars. We note that below their established relation, 40% of unobscured quasars were also located. When applying our sample on this relation, 74% (538/731) of our sample lie below the line. While this could indicate most of our sample are classified as cold quasars, the slope derived by Kirkpatrick et al. (2020) is clearly not a strict threshold.

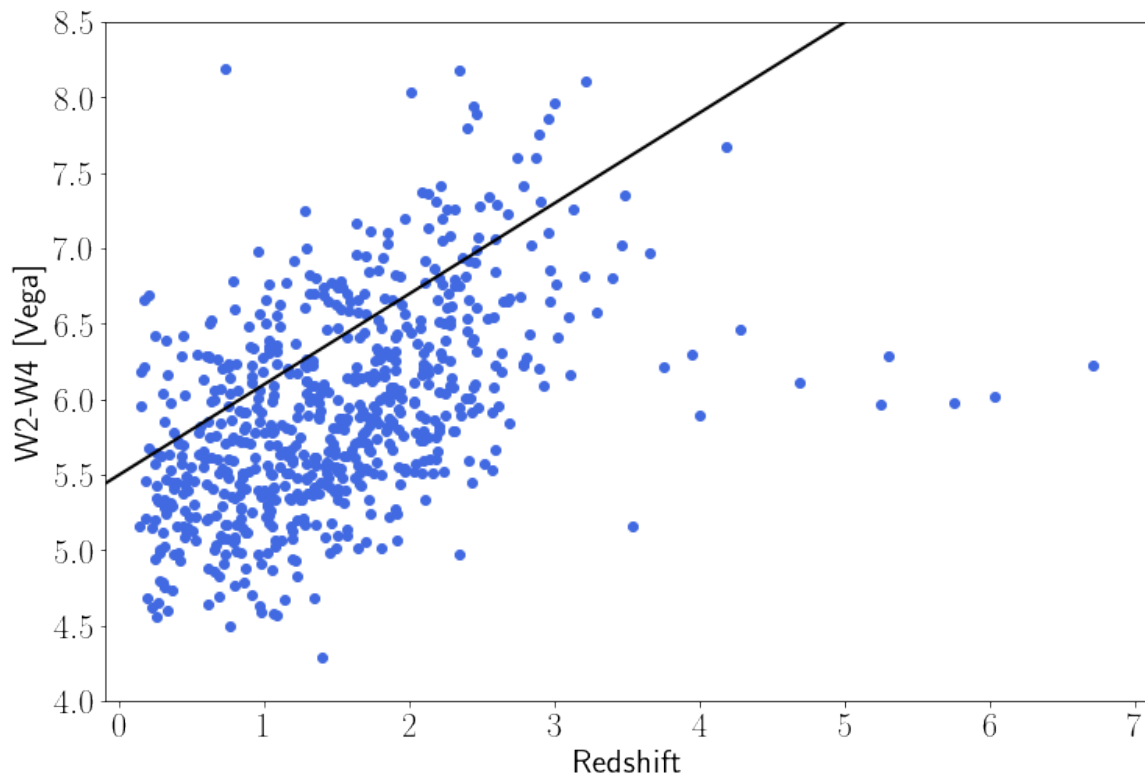


**Figure 15:**  $W2-W4$  as a function of redshift. The black line slope is expressed as  $W2 - W4 = 0.6z + 5.5$ , and was derived by Kirkpatrick et al. (2020) to show all their quasars lying below it. In our case, 74% of the quasars lie below the slope.

<b>Field</b>	Area <sup>a</sup> (deg <sup>2</sup> )	S <sub>250,μm</sub> <sup>limit</sup> (mJy)	<i>Herschel</i> -LOFAR <sup>b</sup>	6'' Matching Radius	SDSS	WISE <sup>c</sup>	XMM <sup>c</sup>	WSRT <sup>c</sup>	GALEX <sup>c</sup>	eROSITA <sup>c</sup>
Lockman-Hole	20.1	40	3641(1069)	3498	37	37	2(37)	–	9(37)	–
Boötes	12.5	45	1599(566)	1539	11	8(11)	0(37)	5(11)	4(11)	–
Elais-N1	14.7	35	3503(2899)	3359	43	30(43)	2(43)	–	15(43)	–
GAMA-09	48.3	19	4166(404)	2862	36	34(36)	7(36)	–	12(36)	11(36)
GAMA-12	32	19	1706(208)	1005	8	8	0(8)	–	2(8)	–
GAMA-15	45.1	19	3140(329)	2119	22	21(22)	2(22)	–	9(22)	–
HATLAS-NGP	178.9	20	59938(12280)	46899	419	399(419)	32(419)	–	194(419)	–
<b>Field</b>	Area <sup>a</sup> (deg <sup>2</sup> )		<i>Herschel</i> -VLA <sup>b</sup>	6'' Matching Radius	SDSS	WISE <sup>c</sup>	XMM <sup>c</sup>		GALEX <sup>c</sup>	
HATLAS-Stripe-82	36.2	20	1460(403)	983	53	49(53)	13(53)	22(53)		
<b>Field</b>	Area <sup>a</sup> (deg <sup>2</sup> )		<i>Herschel</i> -MIGHTEE <sup>b</sup>	6'' Matching Radius	SDSS	WISE <sup>c</sup>	XMM <sup>c</sup>		GALEX <sup>c</sup>	
XMM-LSS	15	18	11095(16917)	10296	102	91(102)	81(102)	29(102)		
Total SDSS objects					731					

**Table 2:** An overview of the cross-matching process and number of matches found for each field for each of the multi-wavelength catalogs

*a:* The area is overlapped between radio and SPIRE data, as demonstrated in [Figure 9](#)

*b:* The number in brackets shows the number of *Herschel* sources that had multiple radio matches

*c:* The number in brackets indicate the total number of SDSS compared to the number of objects matched in the corresponding catalog.

### 3 Methods

In this part of the thesis, we will discuss our SED fitting process in [Subsection 3.1](#), including the model we use, the validation of our SEDs and their analysis. We also illustrate our approach at constructing luminosity functions to study the BHARD and SFRD in [Subsection 3.2](#).

#### 3.1 CIGALE SED fitting

As already mentioned in [Section 1.3](#), studying the SFR of a galaxy by applying a conversion factor to one of the SFR tracers is a frequently used method. Depending on the calibration model used on the tracer, different measurements could be derived. In our case, we use SED fitting. The usage of SED analysis requires a panchromatic wavelength coverage to be able to accurately assess the galaxy properties, which is why the inclusion of ancillary data is vital.

The library we use is Code Investigating GALaxy Emission (CIGALE; Burgarella et al., 2005; Noll et al., 2009; Boquien et al., 2019), which is a python-oriented SED fitting and modelling tool that allows us to derive physical properties (e.g.  $M_*$  and bolometric luminosity,  $L_{bol}$ ). The improvement of CIGALE code over the years has made it possible to fit fluxes from X-ray to radio wavelengths (Yang et al., 2020; Yang et al., 2022).

For setting up the CIGALE SED fitting, we demonstrate here the models we use in addition to the parameters we select from Boquien et al. (2019). Firstly, to establish the general stellar environment for our sample, we assume a ‘delayed’ star-formation history (SFH) model. This model is given as:

$$\text{SFR}(t) \propto \frac{t}{\tau^2} \times \exp(-t/\tau) \text{ for } 0 \leq t \leq t_o. \quad (1)$$

The  $t$  is the age of the galaxy itself, and  $t_o$  is the age of the occurring star formation. This model is based on having a linear increase in the star formation activity, until it peaks at  $t = \tau$ . After that peak, the star formation activity for the population exponentially decreases. This model is logical to apply on our sample, as quasars are expected to be active star formation factories (Willott et al., 2007). We adopt the single stellar population model (SSP) of Bruzual and Charlot (2003) with solar metallicity. As already established before, a significant amount of the stellar emission is re-emitted in the IR by dust. Boquien et al. (2019) discussed the complexity in assembling a template of attenuation curves due to the dust structure depending on the host galaxy itself (for recent a review see Salim and Narayanan, 2020). They therefore provided us with two models to adjust the attenuation curve template to, and we chose Calzetti et al. (2000) flexible model complemented with Leitherer et al. (2002). This is starburst attenuation curve is equipped with a Lyman break feature, where galactic neutral hydrogen absorbs the ionizing UV radiation, affecting the emission spectra (Gonzalez Delgado et al., 1998). It is also important to account for the dust emission which causes the attenuation in the first place. For that, we use the model of Draine et al. (2014). They derived the surface density of dust for our most nearby galaxy, Andromeda. Their dust emission model is split into two parts depending on the spatial location. The model shows the stellar bulge to account for dust heating in the central regions. In the outer regions, star-forming regions cause an increase in reprocessed dust emission. The aforementioned modules govern the stellar emission component of the SED.

For modelling the AGN, an update to CIGALE by Yang et al. (2020) and Yang et al. (2022) was implemented to add X-ray and radio wavelengths to the SED fitting range in addition to adding new

AGN modules to the template. Previously in CIGALE, Fritz et al. (2006) was the only AGN template available. Their template assumed a smooth structure for the dusty torus. However, it is thought that thick clumps in the torus are needed to avoid dust dissipation by AGN radiation (Krolik & Begelman, 1988; García-Bernete et al., 2022). Therefore, CIGALE added the SKIRTOR model (Stalevski et al., 2016), which assumes significant dust clumpiness in addition to a non-uniform AGN disk emission. Our sample consists of *Herschel*-detected SDSS quasars. Being an SDSS quasar automatically classifies the object to be optically visible with respect to the observer. We therefore select the viewing angle of  $30^\circ$ , which is what is recommended by CIGALE for type-1 AGN. We note that the  $30^\circ$  model adds a polar dust extinction of  $E(B - V) = 0.1$ . The approach by CIGALE focused on connecting the X-ray with other wavelengths in the SED. Firstly, the X-ray flux is then fitted as :

$$f_{\nu} \propto E^{-\Gamma+1} \exp(-E/E_{\text{cut}}) \quad (2)$$

Where  $\Gamma$  is the photon index which describes the power-law X-ray spectrum and  $E_{\text{cut}}$  represents the threshold where the X-ray contribution falls off. This cut-off term, for a spatially resolved central region, could help locate where the dense gas (Comptonizing region) responsible for absorption lies (Malizia et al., 2014). Secondly, CIGALE uses  $\alpha_{\text{ox}} - L_{\nu,2500\text{\AA}}$  relation to link the X-ray emission (2 keV) to the intrinsic UV luminosity ( $L_{\nu,2500\text{\AA}}$ ) (Steffen et al., 2006; Just et al., 2007; Lusso & Risaliti, 2017). The  $\alpha_{\text{ox}}$  is the power-law term given as

$$\alpha_{\text{ox}} = -0.3838 \log \frac{L_{\nu,2500\text{\AA}}}{L_{\nu,2\text{keV}}}, \quad (3)$$

and CIGALE allows the user to vary  $\alpha_{\text{ox}}$ . Finally, the last addition to the CIGALE model, a radio module. CIGALE makes full use of the FIRC to derive the radio emission from star formation (Helou et al., 1985), using

$$q_{\text{IR}} = \log \left( \frac{L_{\text{SF,IR}}}{L_{\nu,21\text{cm}} \times 3.75 \times 10^{12}\text{Hz}} \right), \quad (4)$$

where the  $q_{\text{IR}}$  is the correlation parameter and can be input as multiple values by the user. The radio luminosity is also constrained by a power-law slope parameter, which could also be changed by the user. To consider the AGN component in the radio wavelength regime, Yang et al. (2022) implemented a radio-loudness parameter, which is described by the parameter, R (Kellermann et al., 2016), derived as

$$R_{\text{AGN}} = \frac{L_{\nu,5\text{GHz}}}{L_{\nu,2500\text{\AA}}}, \quad (5)$$

where it is simply the ratio between the radio luminosity at 5 GHz and UV luminosity at 2500Å. We note here that the radio-implemented AGN template is oversimplified and does not majorly impact the shape of the SED.

After the aforementioned modules and parameters, one can expect different types of parameters to produce a good fit to the SED, despite it having different physical properties than what the true object has. To counter this, CIGALE implements likelihood-weighted parameters, by applying  $\exp(-\chi^2/2)$  to derive the physical properties. CIGALE would run through all the possibilities ( $n \times n$ ) of the input parameters on its grid mode, temporary save the extrapolated physical properties, and weigh them depending on the wellness of the fit. These are the Bayesian-derived values, which we use in this study, and avoid using ‘best-fit’ values.

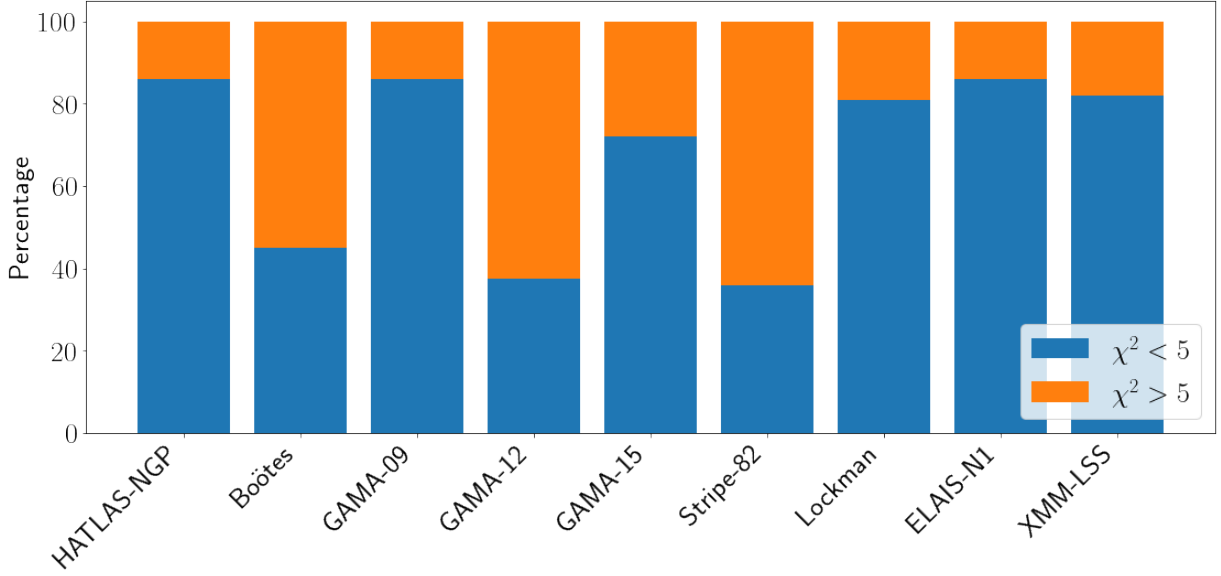


**Figure 16:** The percentage of good and badly fitted SEDs in each of the fields involved in this study. HATLAS-NGP, GAMA-09, GAMA-15, Lockman, ELAIS-N1 and XMM-LSS fields had good ( $\chi^2 < 5$ ) SED fits for  $\sim 80\%$  of their galaxies.

The goodness of the SED fit is determined by  $\chi^2$ , computed as

$$\chi^2 = \sum_i \left( \frac{f_i - \alpha \times m_i}{\sigma_i} \right)^2 + \sum_j \left( \frac{f_j - \alpha \times m_j}{\sigma_j} \right)^2 + \sum_k \left( \frac{f_k - m_k}{\sigma_k} \right)^2, \quad (6)$$

$i$  denotes the properties for  $f_i$  and  $m_i$ , of the observed and modelled flux, respectively, while  $k$  represent the intensive properties and  $j$  are the extensive properties. In this study, we only use SEDs fits with  $\chi^2 < 5$ . Thus, we discard galaxies with SED fits that exceed  $\chi^2 > 5$  as they are unreliable.

Table 3 summaries the section above by displaying all the modules and parameters used to run CIGALE. We note that we lost 20%(146/721) of the galaxies due to bad fits ( $\chi^2 > 5$ ). The redshift range of our galaxies became  $0 < z < 5$ . We show the bad fits contribution for each of the fields in Figure 16. Well-fitted SEDs seem to populate certain fields more than the other. For example, HATLAS-NGP, GAMA-09, GAMA-15, Lockman, ELAIS-N1 and XMM-LSS had  $\sim 80\%$  of their initial sample to have a successful CIGALE run. For Boötes and GAMA-12, most ( $> 60\%$ ) of their sources were simply eliminated after the SED fitting. This could be due to the lack of ancillary data in both fields. Both fields did not have any X-ray counterparts in addition to the low matches acquired from GALEX, which might have unconstrained the high-energy regime of the SED. However, for Stripe-82, it is puzzling why only 13 objects out of 53 had good fits despite noticeable contribution of ancillary data.

We include four examples for some of the best ( $\chi^2 < 1.2$ ) fitted SEDs derived from CIGALE in Figure 17. The SEDs show the big blue bump feature in the UV wavelength range dominated by the AGN (Malkan & Sargent, 1982). The IR bump at  $1 - 100 \mu\text{m}$  due to reprocessed UV emission by dust is also visible (Elvis et al., 1994). We also display four examples of bad ( $\chi^2 > 5$ ) fits with different  $\chi^2$  values from the Boötes and Stripe-82 fields in Figure 18. For the badly fitted SEDs, the top row are two galaxies from Stripe-82 while the bottom two are from Boötes. The model of the top left figure seem to underestimate the fluxes of the whole object. For the top right one, the radio module

ignores the bright flux detected, which ruins the goodness of the fit. Most of the objects in Boötes field, however, have a similar  $\chi^2$  to the bottom figures in Figure 18, where the normalization of the SED seem to slightly differ from the observed fluxes. Despite using multiple parameters for each of the modules, such objects with panchromatic observations could not diverge to a reliable SED fit. A further analysis into why this is the case is needed.

<b>Star Formation History</b>		
sfhdelayed	e-folding time of the main stellar population (Myr)	500, 1000, 2000, 3000, 5000, 6000, 7000
	Age of the main stellar population in the galaxy (Myr)	500, 1000, 2000, 4000, 6000, 7000, 9000
<b>Single Stellar Population</b>		
Bruzual and Charlot, 2003	Initial mass function	Chabrier, 2003
	Metallicity	0.02
<b>Dust Attenuation</b>		
Calzetti et al., 2000	$E(B - V)$	0, 0.05, 0.1, 0.2, 0.3, 0.4, 0.5, 0.7, 0.8, 0.9
	Reduction factor	0.44
	Extinction law	MilkyWay (1)
<b>Dust Emission</b>		
Draine et al., 2014	Mass fraction of PAH	0.47, 1.12, 2.5, 3.9
	Fraction illuminated from minimum to maximum radiation field	0.02, 0.1, 0.5
<b>AGN</b>		
SKIRTOR Stalevski et al., 2016	Average edge-on optical depth at $9.7\mu\text{m}$	3, 7
	Inclination	$30^\circ$
	$\delta$ Power-law index	-0.9, -0.7, -0.5, -0.2, 0.0, 0.2, 0.5
	AGN fraction	0.1, 0.3, 0.5, 0.7, 0.9, 0.99
	$E(B - V)$ of polar dust	0.03
<b>X-ray</b>		
Yang et al., 2020; Yang et al., 2022	Photon index $\Gamma$	1.8
	power slope $\alpha_{ox}$	-2.0, -1.8, -1.6, -1.4, -1.2
	Maximum deviation from $\alpha_{ox}$ - $L_x$ relation	0.2
<b>Radio</b>		
Yang et al., 2022	FIRC coefficient for star formation	2.4, 2.5, 2.6
	Radio loudness parameter	0.1, 1, 10, 20
	Power-law AGN radio emission slope	0.7

**Table 3:** The CIGALE modules and parameters used in this study. We used the ‘sfhdelayed’ SFH model for our sample. We apply solar metallicity to the SSP model of Bruzual and Charlot (2003). For the dust attenuation and emission, we use the models of Calzetti et al. (2000) and Draine et al. (2014), respectively. We use the SKIRTOR AGN model (Stalevski et al., 2016). The X-ray module is based on Equation 2 and Equation 3 while the radio module is based on Equation 4 and Equation 5.

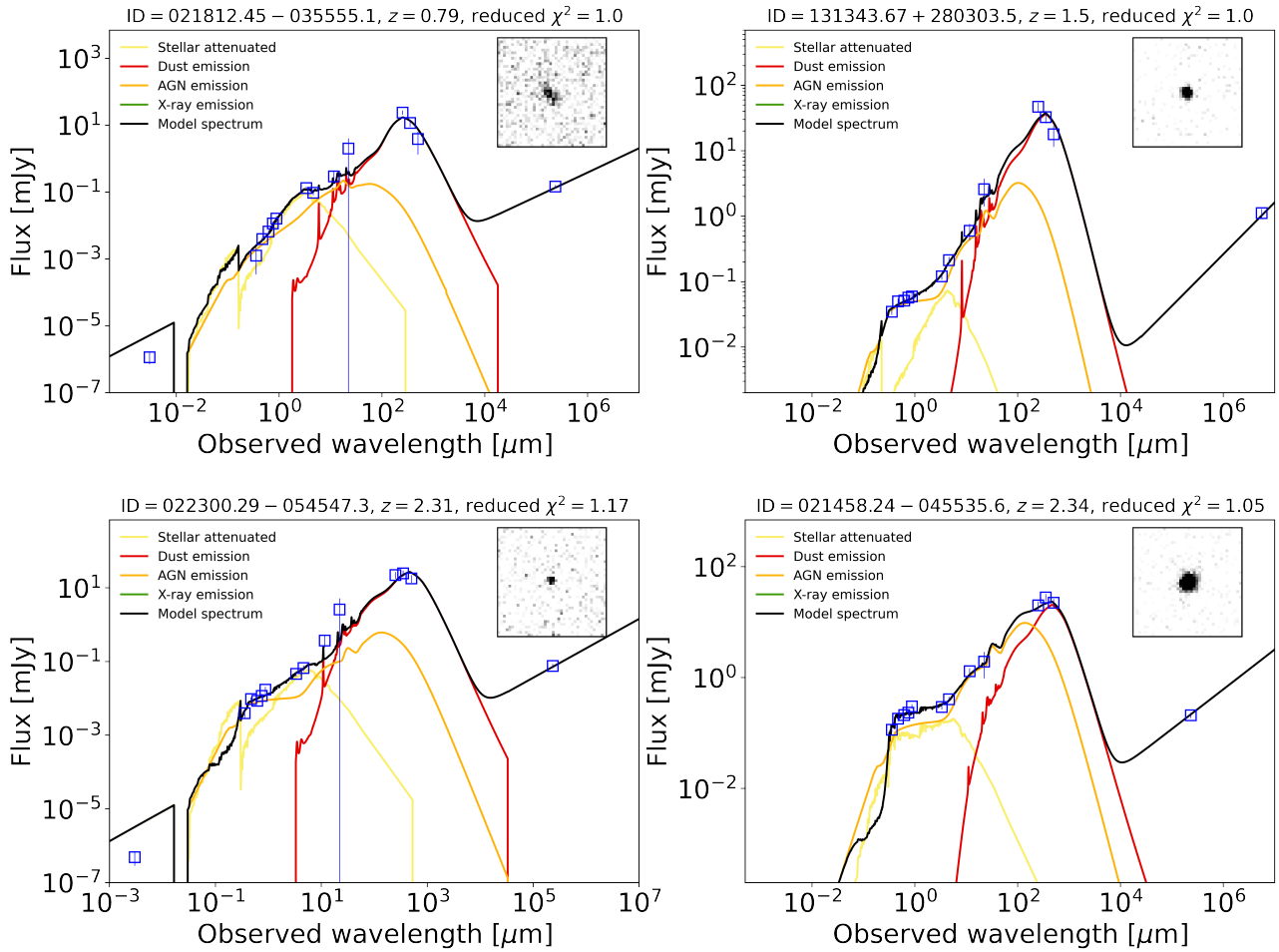


**Figure 17:** Examples for some of the best ( $\chi^2 < 1.2$ ) CIGALE SED fits done on our galaxies. The SEDs contain the Big Blue Bump feature at  $0.1 - 1 \mu\text{m}$  as well as the infrared bump at  $1 - 100 \mu\text{m}$ . The legend specifies the type of emission in the SED and the title includes the SDSS galaxy ID, redshift and reduced chi-square. Image cutouts ( $11.7'' \times 20.9''$ ) in the SDSS i-band are overlaid for each galaxy.

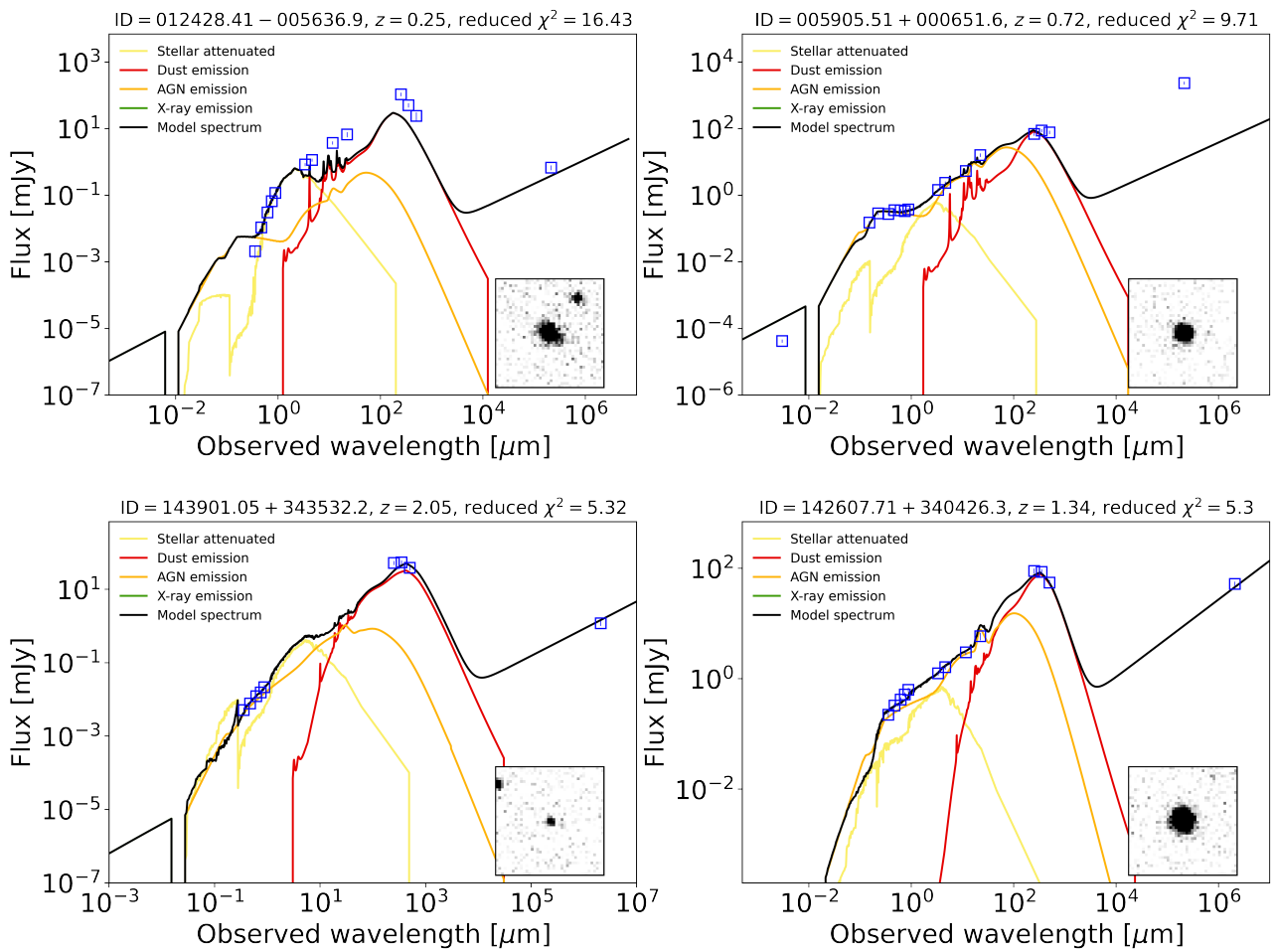


**Figure 18:** Same as Figure 17 but for bad ( $\chi^2 > 5$ ) SED fits in the Stripe-82 (top panel) and Boötes fields (bottom panel).

To test the accuracy of our SED fitting process, we compare our CIGALE AGN luminosities with bolometric luminosity measurements on the entire SDSS DR16Q done by Wu and Shen (2022). Their work fitted spectra of continuum and emission lines from the BOSS spectral measurements. This complements similar work they also did on the SDSS DR7 catalog Shen et al. (2011). We cross-match the SDSS galaxy IDs of our sample with their catalog. The comparison shown in Figure 19 displays a general agreement between both luminosities, as only  $\sim 5\%$  of our sample fall outside of the 0.5 dex offset. Throughout the thesis, we will be using the bolometric luminosities derived by Wu and Shen (2022) for our quasars.

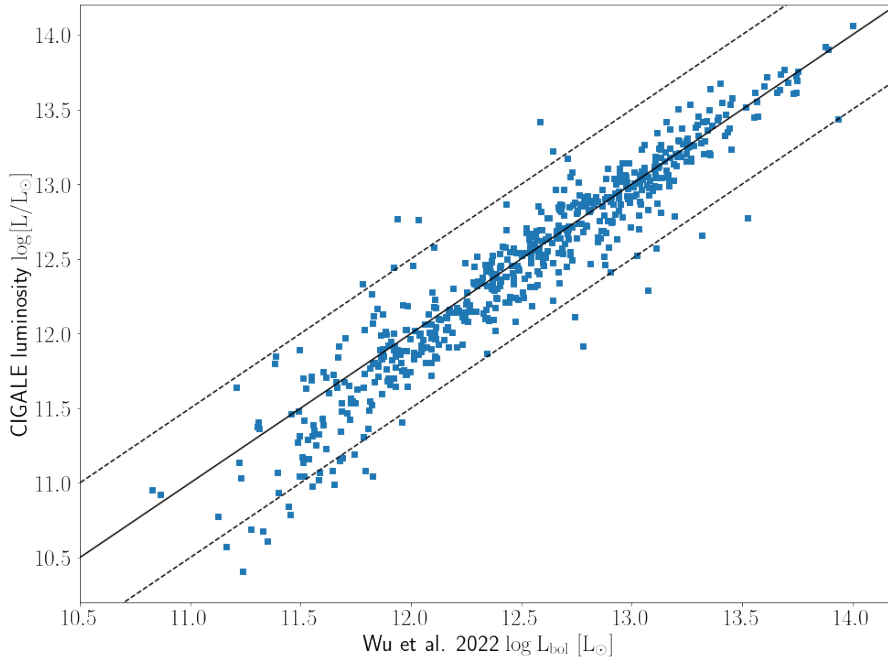


**Figure 19:** A comparison between AGN luminosities of our sample from CIGALE SED fitting and the bolometric luminosities acquired from spectra fitting (Wu & Shen, 2022). The solid black line shows a 1:1 relation, while the dashed lines represent the 0.5 dex offsets.

We further validate the SED CIGALE fittings of our sample by comparing their stellar masses with stellar masses of Li et al. (2021), hereafter L21. Their work involves 2D quasar-host light profile decomposition to construct host galaxy SED fitting to derive its physical properties (see Figure 20). Their study is based on SDSS quasars at  $0.2 < z < 1$ , observed by the Hyper Suprime-Cam Subaru Strategic Program (HSC-SSP; Aihara et al., 2018; Miyazaki et al., 2018) with its exceptional median resolution of  $0.6''$  in five optical bands (*grizy*).

Their work included three fields that are used in our study (GAMA-09, GAMA-15 and XMM-LSS). We therefore directly cross-match the SDSS galaxy IDs in those three fields and we get 14 matches. The small number of matches could be due to our galaxy sample lying in the high mass regime of their stellar mass distribution (see left panel of Figure 22). The stellar mass residuals (difference between L21 mass and  $M_*$ ) for the 14 objects are shown as the blue stars in Figure 21. We see a scatter with a slight trend for CIGALE to overestimate the stellar mass rather than underestimating it. The mean residual is 0.2 dex, shown as the blue dashed line. We cannot however, draw a conclusion about our

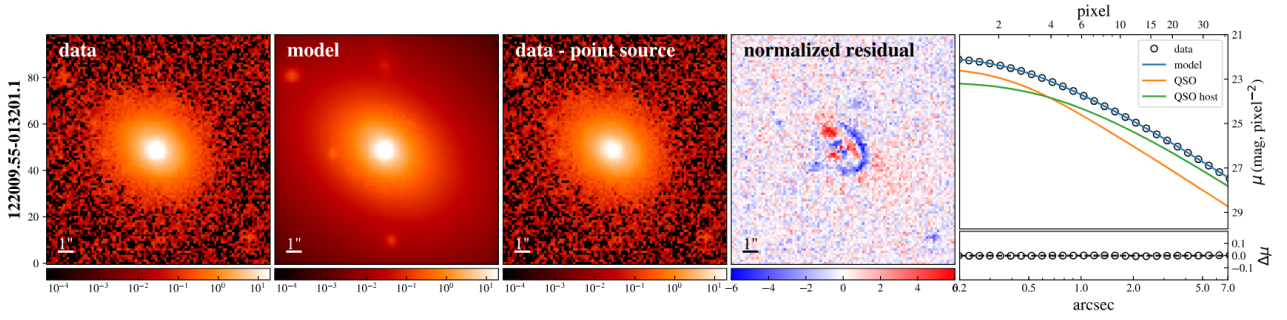


**Figure 20:** The decomposition procedure by Li et al. (2021), from left to right: (1) The HSC *i*-band image; (2) The best point source function model fit and the host galaxy model; (3) The galaxy image subtracted from the model; (5) The residual map between data and the model; (6) A surface brightness profile for the subtracted host galaxy.

SED fitting stellar mass estimation from a sample size of 14 objects.

We thus expanded the validation sample by randomly selecting  $\sim 2000$  (40% of their sample) galaxies from the L21 catalog to fit their host galaxy flux using our CIGALE fitting parameters (see Table 3). The SED fitting produces  $\sim 1500$  good ( $\chi^2 < 5$ ) fits which have a mean mass residual of 0.2 dex, shown as the black solid line in Figure 21. We also see there is an even residual scatter for the L21 galaxies. The residual means of both samples agree and we consider the deviation in stellar mass acceptable in our study.

In addition to using it to verify our SED fitting accuracy, we use Li et al. (2021) galaxy catalog to study our sample of extremely luminous quasars by inspecting the difference in SFR and stellar mass between both samples. The SFR for L21 catalog is derived by our CIGALE parameters. In Figure 22, we plot the difference in distributions of the stellar mass and SFR. We limited our quasar sample to match L21 redshift range ( $0.2 < z < 1$ ). Our quasar population consists of more massive host galaxies that extends to  $10^{12.4} M_{\odot}$  whereas L21 mass distribution contains low-mass galaxies and does not have galaxies with  $M_{*} > 10^{11.5}$ . The SFR of L21 stays approximately the same throughout the whole redshift range. The SFR of our galaxies however, constantly increases with redshift. At  $z = 0.8$ , our galaxies have  $10^2 M_{\odot} \text{yr}^{-1}$  more star formation compared to L21 galaxies. We also note that 70% of L21 sample are star-forming galaxies. Our sample seem to have redder emission (see Figure 14), more massive galaxies and two orders of magnitude higher SFR than the average optical quasar.

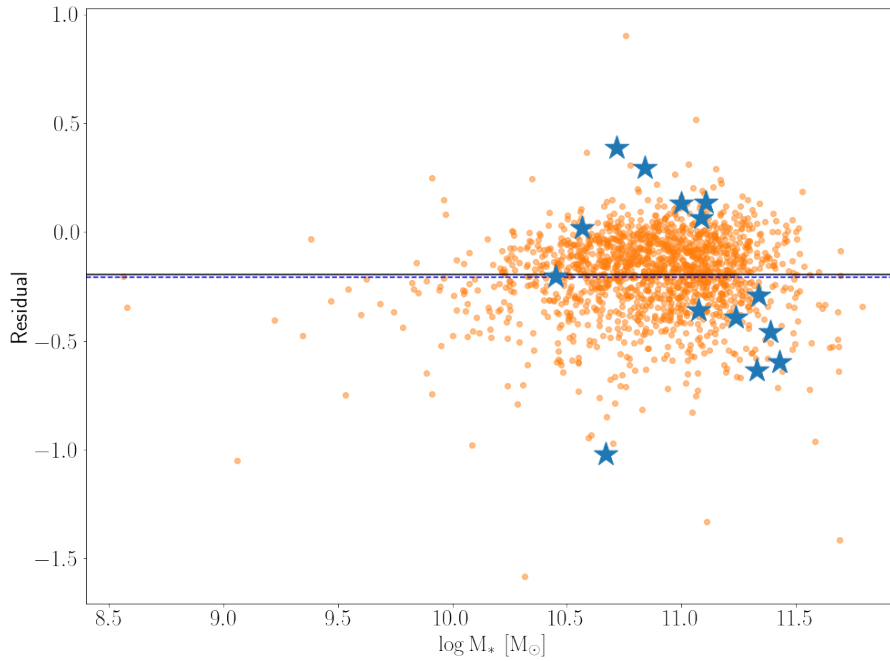


**Figure 21:** A residual plot for stellar masses acquired through two different methods. The Blue stars are the 14 directly matched galaxies between our sample and L21 catalog. The blue dashed line represents their mean residual value. The  $\sim 1500$  HSC-SSP galaxies we fitted using our CIGALE parameters are shown as orange circles. Their mean residual is shown as the black solid line, which overlaps the blue dashed line. The mean residual mass of both galaxy samples is 0.2 dex, which we consider acceptable.

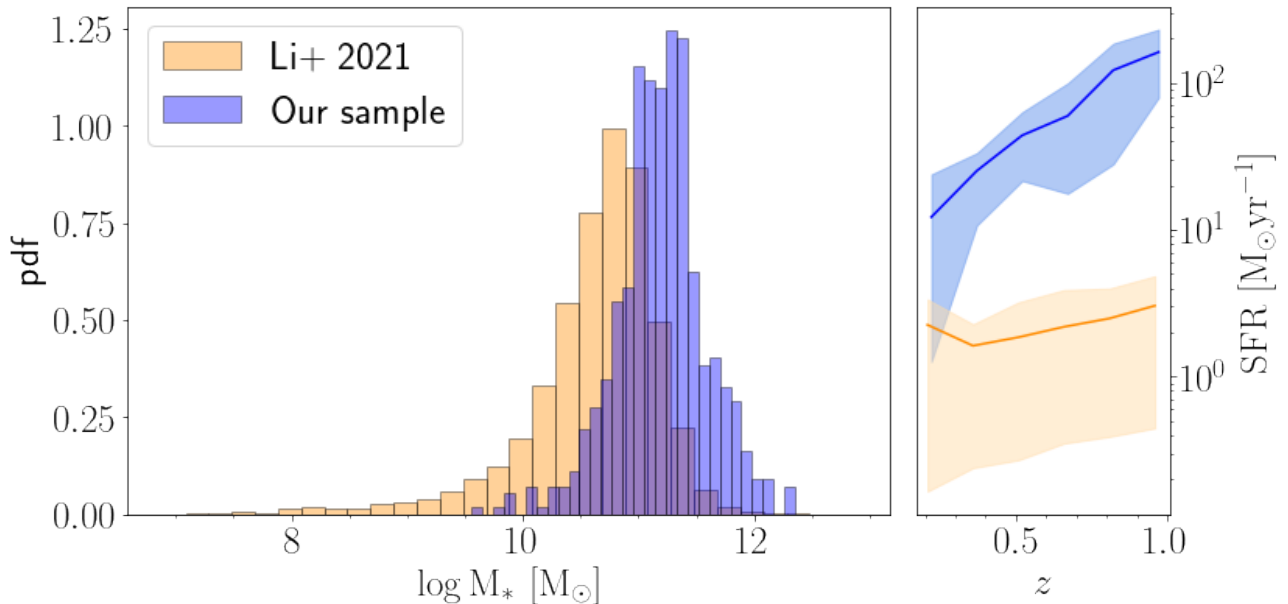


**Figure 22:** We compare physical properties of our galaxies (blue) to unobscured SDSS quasars from Li et al. (2021) (yellow). The panel on the left shows the stellar mass distribution, and the right panel displays the mean SFR derived from CIGALE with  $1\sigma$  as the shaded region. Our sample of galaxies is more massive and show SFRs that are 100 times higher than those occurring in the L21 galaxy sample.

In this study, we make use of the SMBH mass measurements computed by Wu and Shen (2022). Using single-epoch detections of broad-line (H $\beta$ , Mg II and C IV) emissions, they were able to estimate  $M_{\text{BH}}$  (Vestergaard & Peterson, 2006). Such method is commonly used in huge spectroscopic catalogs, especially if the survey contains high redshift objects, such as Shen et al. (2011) and a more recent one, Liu et al. (2022). A major disadvantage of using single-epoch estimators, however, is that they rely on a tight correlation between the BLR size and AGN luminosity which is extrapolated from reverberation mapped AGNs in the local Universe. Reverberation mapping (RM) is a robust method to measure the BLR size by computing the time lag in variability of its continuum emission (Blandford & McKee, 1982). However, measurements by Du et al. (2016), Fonseca Alvarez et al. (2020), and Homayouni et al. (2020) showed that quasar properties in the local Universe could be different to quasars at higher redshift and hence create a selection bias for the BLR size. This bias could overestimate the mass by 0.3 dex, aside from 0.4 dex systematic uncertainty of Wu and Shen (2022).

## 3.2 Luminosity function fitting

Luminosity functions (LF) allow us to understand the distribution of galaxies across cosmic time. The LF directly measures the number of objects that emit a certain luminosity in given volume of the Universe (e.g. Le Floch et al., 2005). We aim to study the distribution of the galaxies in our sample, which have shown to be a rare subsample of the optical quasars (1% of DR16Q, see Section 2.2) population.

As already mentioned in Subsection 1.3, dust plays a major role in understanding the star formation activity in the galaxy. The total IR luminosity ( $L_{\text{IR}}$ ) is assumed to cover the wavelength of stellar emission by old and young stars (Calzetti, 2012; Kennicutt & Evans, 2012). We aim to construct a IR LF using the total IR luminosity derived from CIGALE. The integration of the IR LF would then allow us to derive the SFRD within the redshift range of our study.

X-ray LFs (XLF) could track the AGN activity, since for type 1 quasars (non Compton-thick), the host galaxy emission is orders of magnitude weaker. X-ray surveys are also affected less from obscuration compared to optical emission. When integrating the XLF, we can derive the BHARD as a function of redshift. Madau and Dickinson (2014) showed the BHARD and SFRD to peak at  $z \sim 2$ , which could hint at a possible coevolution scenario. This peak however is then followed by a sharp decline till the current cosmic epoch. The uniqueness of our galaxy sample due to radio observations enabled us to concurrently study the SFRD and BHARD.

### 3.2.1 Total IR LF

The  $L_{\text{IR}}$  is the total integrated emission in the 8 – 1000  $\mu\text{m}$  range of the SED. The comoving number density is then calculated as

$$\Phi = \frac{1}{\Delta \log L_{\text{IR}}} \sum_{\text{bin}} \frac{n_{\text{bin}}}{V_{z_{\text{bin}}}}, \quad (7)$$

where  $\Delta \log L_{\text{IR}}$  is the step size for the  $L_{\text{IR}}$  in a given redshift bin.  $V_{z_{\text{bin}}}$  is the differential comoving volume for the redshift range given. We construct the IR LF throughout the redshift range of  $0 < z < 4$ . We discuss certain limitations in our analysis. Firstly, our cross-matching process involved uniquely matched objects, meaning that, the *Herschel*-detected quasars that had multiple radio counterparts were discarded and not included in this study. This as a result affects the number density derived

from Equation 7.

Furthermore, establishing a  $L_{\text{IR}}$  completeness limit of the sample is essential to ensure a level of certainty. To estimate the completeness of our data, we tried three different methods. The first method was computing the total IR luminosity completeness at which there is 85% identification rate of matched (unique and multiple) sources in the overlapped region (check Figure 9 and Figure 12) between *Herschel* and radio surveys. For example, in the shaded area of Figure 9, there are 31637 *Herschel* sources. If we consider all sources to lie above the total IR luminosity limit implemented, then a 85%  $L_{\text{IR}}$  completeness limit is achieved if there are 26892(85%) *Herschel*-radio matches in the region. We would expect a deep survey to therefore have a low  $L_{\text{IR}}$  completeness limit. We rank the multiplicity rates of our fields based on the  $L_{\text{IR}}$  completeness level achieved (top is lowest  $L_{\text{IR}}$  completeness limit realized). A relatively low  $L_{\text{IR}}$  completeness limit was achieved for the top four most sensitive surveys in our study (XMM-LSS, ELAIS-N1, Lockman and Boötes). The  $L_{\text{IR}}$  limit realized by other fields however, was a factor of three more or higher. It should also be noted that certain fields could not achieve a completeness level as *Herschel* had much more source counts (Stripe-82 and GAMA-12). Moreover, GAMA-09 and GAMA-15 only achieved a completeness of 80% and 65%, respectively.

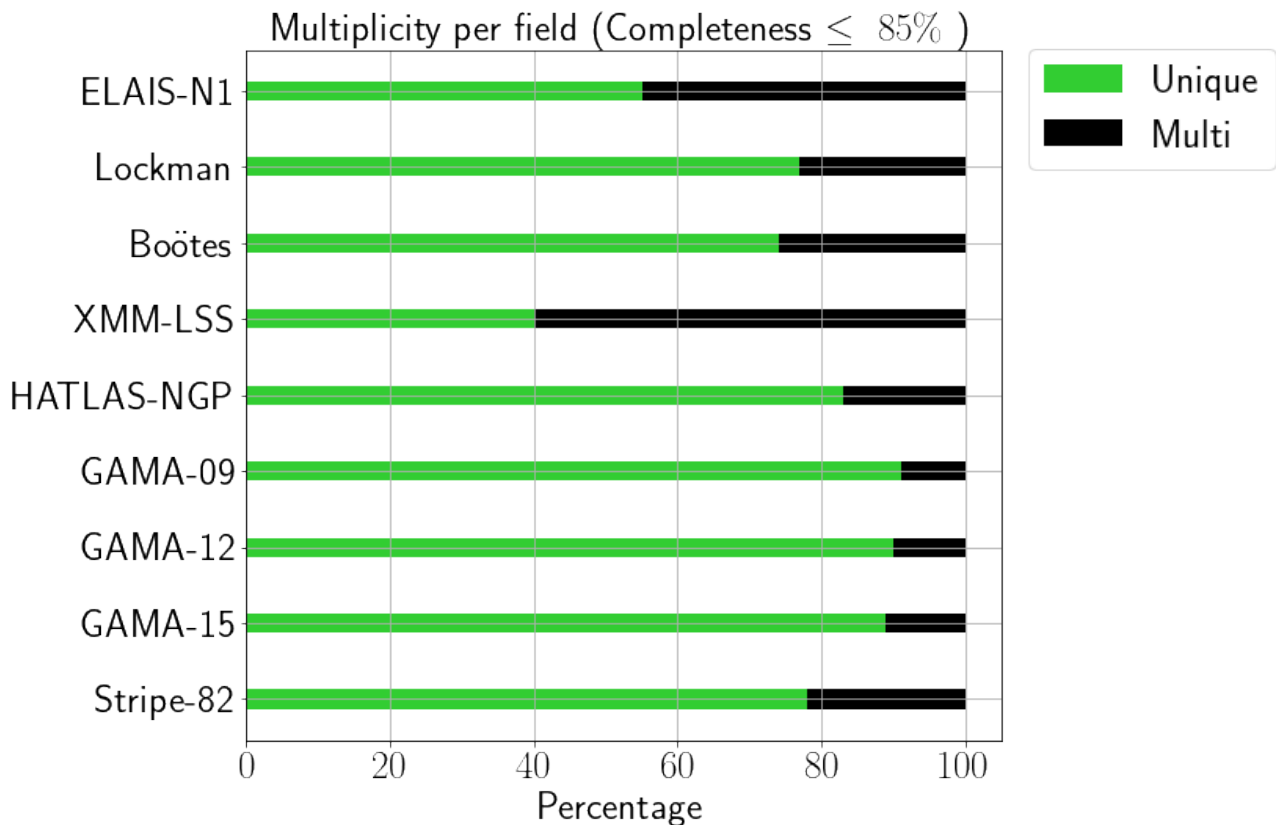


**Figure 23:** Unique (green) and multiple (black) percentage of matches for all fields ranked as a function of the  $L_{\text{IR}}$  85% completeness limit (i.e. ELAIS-N1 is the deepest field). We note that GAMA-09 and GAMA-15 achieved only a completeness of 80% and 65%, respectively, while it was not possible to reach a sophisticated completeness for Stripe-82 and GAMA-12.

As we mentioned before, a significant amount of data (20%) was eliminated due to their bad fits.

Furthermore, if we apply the aforementioned  $L_{\text{IR}}$  completeness limits, we would lose more data, especially in the fields shallower than XMM-LSS, ELAIS-N1, Lockman and Boötes. Therefore we chose to not apply this method to derive the  $L_{\text{IR}}$  completeness limit.

Another method to constrain the completeness of the IR LF was adopted from Wang et al. (2021), who used the  $250\mu\text{m}$  flux limit to compute the  $L_{\text{IR}}$  completeness limit. It is based on plotting the  $L_{\text{IR}}$  distribution of sources which lie close to the  $250\mu\text{m}$  flux limit in each of the fields against redshift. For instance, if we take sources with  $S_{250\mu\text{m}} < 41$  mJy in Lockman and observe the upper limit of  $L_{\text{IR}}$  in each redshift bin. The upper limit is then the completeness limit derived. However, this was difficult to implement in our study since very few sources lie close to the selection limit of  $S_{250\mu\text{m}}$  in each redshift bin.

To overcome the statistical issue in our study, we derive the  $L_{\text{IR}}$  completeness limit by applying a conversion factor to the  $S_{250\mu\text{m}}$  limit. We use the simulated infrared dusty extragalactic sky (SIDES) model by Béthermin et al. (2017). SIDES aimed to connect simulation models and observations by correcting the intrinsic number of galaxy counts through a  $2 \text{ deg}^2$  light cone for dark matter haloes. The simulated galaxies are connected to their parent haloes using abundance matching of peak circular velocity (highest velocity galaxy is matched to the most massive halo, see Reddick et al., 2013), after which their properties are derived through SED fitting. The simulation contains flux density in the  $250 \mu\text{m}$  SPIRE band as well as  $L_{\text{IR}}$  for over 5 million sources.

Therefore, for each of our redshift bins, we derive the completeness factor by multiplying the  $S_{250\mu\text{m}}$  85% completeness limit (see Table 2) of SPIRE observations with the mode of the  $L_{\text{IR}}/L_{250\mu\text{m}}$  ratio derived from the simulation.  $L_{250\mu\text{m}}$  is the derived luminosity using the  $250 \mu\text{m}$  SPIRE flux density and redshift of the simulated galaxies. We plot the distribution of the  $L_{\text{IR}}/L_{250\mu\text{m}}$  ratio in Figure 24. We note that there is a negligible (0.27%) fraction of galaxies that had  $L_{\text{IR}}/L_{250\mu\text{m}}$  ratio less than 1. This is physically impossible and we do not take them into account when computing the mode. As the completeness limit of our IR LF is now established, we can fit the IR LF function. We only use HATLAS-NGP field in constructing the LF. It is the only field in this study that contains a sufficient amount of data after the SED fitting process. We note that combining all fields to overcome the aforementioned issue would introduce an observational bias. This is because not all fields have the same FIR depth (refer to Table 1), which would contaminate the faint-end of the IR LF slope. We assume a modified Schechter function derived by Saunders et al. (1990) to parametrize our fits. It is given by,

$$\Phi(L) = \Phi_* \left( \frac{L}{L_*} \right)^{1-\alpha} \exp \left[ -\frac{1}{2\sigma^2} \log_{10}^2 \left( 1 + \frac{L}{L_*} \right) \right]. \quad (8)$$

The LF in this case depends on four free parameters.  $L_*$  is the characteristic luminosity at which the power-law of the slope breaks,  $\Phi$  is the normalization component of the LF,  $\alpha$  is the faint-end slope parameter and  $\sigma$  shapes the cut-off around the characteristic luminosity. We choose to fit the  $L_*$  and  $\Phi$  parameters across our redshift bins and fix the faint-end slope  $\alpha$  and  $\sigma$  Gaussian due to the lack of data points in each redshift bin. We adopt  $\alpha = 1.26$  and  $\sigma = 0.44$  values from a IR LF study on dusty star-forming galaxies by Wang et al. (2019). We also bin our data in the same redshift ranges as their study. To therefore compute the comoving number density for IR ( $\Psi_{\text{IR}}$ ), we integrate the aforementioned Schechter function

$$\Psi_{\text{IR}} = \int_{L_{\text{limit}}}^{L_{\text{upper}}} L \Phi(L) dL. \quad (9)$$

We chose the upper limit to be  $10^{15} L_{\odot}$ . The lower limit is the assigned completeness limit in each

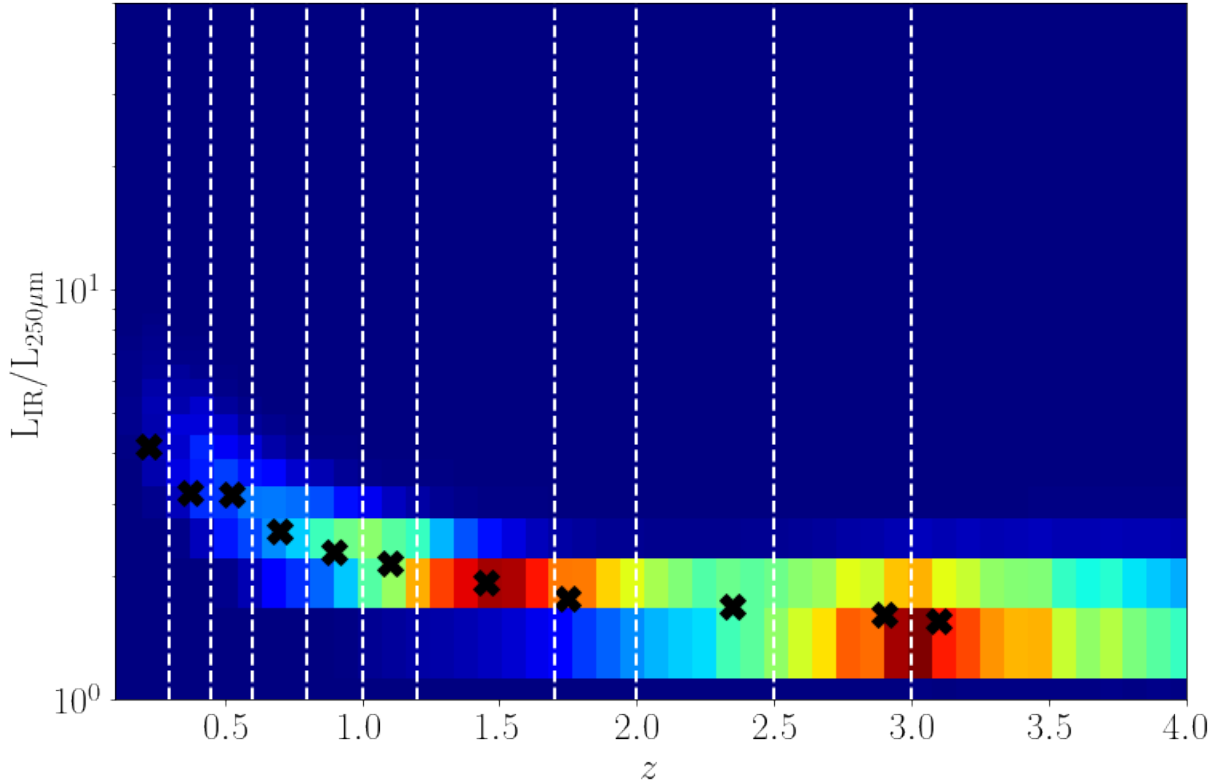


**Figure 24:** A 2D histogram distribution of the  $L_{\text{IR}}/L_{250\mu\text{m}}$  ratio where dense regions are redder.  $L_{\text{IR}}$  and  $L_{250\mu\text{m}}$  were derived from SIDES across the redshift range of our IR LF (Béthermin et al., 2017). The vertical white dashed lines represent the binnings for our IR LF and the black crosses represent the mode value of the ratio for each redshift bin.

redshift bin, shown as the black line in Figure 34. Data points lying close or behind the completeness limit at the faint-end slope of the plot were simply ignored in the fitting process. We also did not fit the redshift bin of  $3 < z < 4$  since it lacked data.

### 3.2.2 X-ray LF

Fitting a XLF to our data is much more challenging than fitting a IR LF. For the IR LF, the  $L_{\text{IR}}$  is derived from CIGALE SED fitting for all the HATLAS-NGP good fits. For the X-ray however, our multi-wavelength catalog does not have extensive detections in the high energy range beyond UV. Moreover, the derived soft and hard X-ray bands from CIGALE, are based on a uniform sensitivity (boxcar filter) which will not be robust enough to fit a XLF. In HATLAS-NGP, we only have 32 sources with total band (0.2 – 12 keV) XMM detections prior to SED fitting. This number decreased to 26 sources after the CIGALE fitting process, which is about 7% of the sample size we had for the IR LF. For calculating the volume density in X-ray, we use Equation 7 for much larger redshift bins.

The completeness of the XLF can be directly derived from the EPIC observations. The EPIC depth limit in the hard (2 – 12 keV) X-ray is  $6.8 \times 10^{-15} \text{ erg cm}^{-2} \text{ s}^{-1}$ . We used the hard band limit to avoid the excess emission in the soft X-ray from Comptonized UV photons emitted by the accretion disk (Zdziarski et al., 1995; Boissay et al., 2016). To parametrize our data, we use the Luminosity-

dependent density evolution (LDDE) model described by (Ueda et al., 2014):

$$\Phi(L_X, z) = \Phi(L_X, z = 0) e(z, L_X) \quad (10)$$

The LDDE model is based on two components; the first one describes the volume density of the XLF at  $z = 0$ ,  $\Phi(L_X, z = 0)$  using a double power-law which has  $\gamma_1$  and  $\gamma_2$  as the faint- and bright-end power-law slopes, respectively and is given as

$$K \left[ \left( \frac{L_X}{L_*} \right)^{\gamma_1} + \left( \frac{L_X}{L_*} \right)^{\gamma_2} \right]^{-1}, \quad (11)$$

where  $K$  is the normalization factor and  $L_*$  is the break luminosity. The second term of the LDDE model is an evolution term,  $e(z, L_X)$ . This factor changes depending on the redshift of the XLF. Originally developed by Ueda et al. (2003), the evolution term depended on one redshift cut-off term. It was the bright-end observations of luminous AGNs that suggested a drop in the number density at  $z \gtrsim 3$  (Silverman et al., 2005; Hiroi et al., 2012). Therefore, a second cut-off term was introduced into the evolution term, which is described by (Ueda et al., 2014):

$$e(z, L_X) = \begin{cases} (1+z)^{e_1}, & [z < z_{c1}(L_X)] \\ (1+z_{c1}(L_X))^{e_1} \left( \frac{1+z}{1+z_{c1}(L_X)} \right)^{e_2}, & [z_{c1}(L_X) < z < z_{c2}(L_X)] \\ (1+z_{c1}(L_X))^{e_1} \left( \frac{1+z_{c2}(L_X)}{1+z_{c1}(L_X)} \right)^{e_2} \left( \frac{1+z}{1+z_{c2}(L_X)} \right)^{e_3}, & [z > z_{c2}(L_X)] \end{cases} \quad (12)$$

where the cut-off redshifts are given by power-law functions of  $L_X$ ,

$$z_{c1}(L_X) = \begin{cases} z_{c1}^* & [L_X \geq L_{a1}] \\ z_{c1}^* \left( \frac{L_X}{L_{a1}} \right)^{\alpha_1} & [L_X < L_{a1}] \end{cases} \quad (13)$$

and

$$z_{c2}(L_X) = \begin{cases} z_{c2}^* & [L_X \geq L_{a2}] \\ z_{c2}^* \left( \frac{L_X}{L_{a2}} \right)^{\alpha_2} & [L_X < L_{a2}]. \end{cases} \quad (14)$$

There is also a further parametrization for the  $e_1$  parameter but we do not use it. The evolution parameter of the LDDE model contains 9 free parameters in addition to the 4 parameters in the double power-law function. Due to our limited sample of data, we only parametrize the normalization and the break luminosity terms. We take the rest of the parameters from Aird et al., 2015 who measured the XLF in hard X-ray (2 – 7 keV) band. We use the parameters displayed in Table 4 to complete the fitting process. The XLFs of our study are divided into 5 bins throughout the redshift range of  $0 < z < 4$ . The IR LF on the other hand, had 11 redshift bins.

To derive the BHARD however, it is important to account for the entire luminosity emitted by the AGN and not just the X-ray. To do that, a bolometric correction factor, given by  $K_X = L_{bol}/L_X$ , can be applied. The AGN emission spans the entire SED range. It is therefore vital to understand the characteristics of its emission in addition to their physical origin. For example, correction factor models for X-ray emission need to consider the surrounding torus, as already mentioned in Subsection 1.3, a large quantity of the AGN population suffer large X-ray absorption (Brightman et al., 2017). Optical

Parameters	$\gamma_1$	$\gamma_2$	$e_1$	$e_2$	$e_3$	$z_{c1}^*$	$z_{c2}^*$	$L_{a1}$ (erg s <sup>-1</sup> )	$L_{a2}$ (erg s <sup>-1</sup> )	$\alpha_1$	$\alpha_2$
LDDE	0.73	2.22	4.34	-0.3	-7.33	1.85	3.16	$10^{44.78}$	$10^{44.46}$	0.23	0.12

**Table 4:** Best estimates of hard (2 – 7 keV) X-ray LDDE model parameters taken from Aird et al. (2015).

corrections are needed in the case of a low-luminous AGN (Duras et al., 2020), as well as dust absorption of UV emission (Runnoe et al., 2012). Several works have already performed such analysis (e.g. Elvis et al., 1994; Marconi and Hunt, 2003) as well as more recent work (e.g. Netzer, 2019). However, their work focused on bright X-ray sources as well as type 1 quasars for a limited range of AGN luminosity. Establishing a correction factor for type 1 AGNs is much easier than type 2 AGNs since there is much less obscuration.

We use the work of Duras et al. (2020) who fitted SEDs for type 1 and type 2 AGNs across a wide range of redshift ( $0 < z < 5$ ). They derived bolometric correction factors for hard X-ray (2 – 10 keV) emission for a huge AGN luminosity range of  $\sim 10^7 - 10^{15} L_{\odot}$ . Their work agrees well with Lusso et al. (2012) who also characterized the  $K_X$  for bolometric luminosities of type 1 AGNs. Duras et al. (2020) linked the the X-ray luminosity to  $K_X$  by:

$$K_X(L_X) = a \left[ 1 + \left( \frac{\log(L_X/L_{\odot})}{b} \right)^c \right]. \quad (15)$$

The correction factor derived for type 1 and type 2 AGNs was similar, yielding the same best fit parameters,  $a$ ,  $b$  and  $c$ , which are available in Table B.1. To derive the black hole accretion rate (BHAR) from the derived AGN bolometric luminosity, we assume an accretion disk radiation efficiency of  $\epsilon = 0.1$  (Soltan, 1982). The BHAR is then given as

$$\text{BHAR} = \frac{1 - \epsilon}{\epsilon c^2} L_{bol}. \quad (16)$$

We plug in the BHAR term into the integral of the XLF to derive the BHARD,  $\Psi_{\text{BHARD}}$ ,

$$\Psi_{\text{BHARD}} = \int_{L_{X,\text{lower}}}^{L_{X,\text{upper}}} \frac{1 - \epsilon}{\epsilon c^2} L_{bol} \Phi(L_{bol}) d \log L_{bol}, \quad (17)$$

The upper limit for the integration is  $10^{13.5} L_{\odot}$  and the lower limit is the completeness threshold of the XLF. We note that these limits are X-ray luminosities, so we applied the bolometric correction factor to them. We further simplify the integral into

$$\Psi_{\text{BHARD}} = \frac{1 - \epsilon}{\epsilon c^2} \int_{L_{X,\text{lower}}}^{L_{X,\text{upper}}} \Phi(L_{bol}) dL_{bol}. \quad (18)$$

We show the derived BHARD and SFRD for our galaxy population in Figure 38.

## 4 Results

We present our findings in this section. We discuss the star activity in our sample, the stellar mass of our galaxies and its evolution with the black hole mass. We show the downsizing phenomenon. We explore whether the black hole affects the growth of its host galaxy in a wide range of redshifts ( $0 < z < 5$ ), and lastly we show the SFRD and BHARD evolution through cosmic time.

### 4.1 Star formation activity

We first analyse how the galaxies in our sample relate to the well-established relation between SFR and stellar mass, which flattens towards high stellar masses (e.g. Daddi et al., 2007; Elbaz et al., 2007; Lee et al., 2015). We adopt the approach by Popesso et al. (2022) (hereafter P22) who compiled 27 published work focused on MS measurements to reach a normalized MS function that covers  $0 < z < 6$ . Calibrating the IMF, SFR indicators and cosmology were primary corrections to align the studies and remove any impactful systematic effect. P22 adapted from Lee et al. (2015) a fitting function that constrains the shape of the MS fit depending on characteristics that can be interpreted physically. The MS fit is hence described as (Popesso et al., 2022),

$$\log(\text{SFR}(t, M_*)) = a_0 + a_1 t - \log(1 + (M_*/10^{a_2 + a_3 t})^{-a_4}). \quad (19)$$

Fitting as a function of redshift can lead to more complex fittings. Thus, P22 fitted Equation 19 as a function of time, as adapted from Speagle et al. (2014). The fitting parameters used are available in Table C.1. The functional form show a bending of the MS fit in the high stellar mass regime. The bending feature depends on the turnover mass. If the stellar mass surpasses the turnover mass, it is thought that cold streams feeding the accretion become suppressed. The suppression of the infalling cold gas hence downturns the increase in SFR, causing the MS fit to bend, as seen in Figure 26.

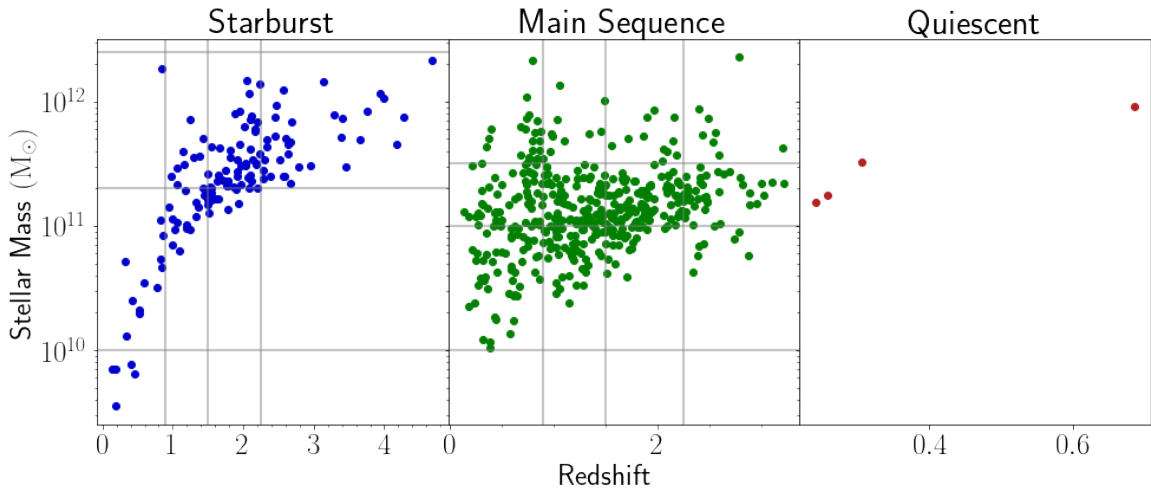


**Figure 25:** Stellar mass as a function of redshift for our classified galaxy sample. The classification is done through Equation 19, and the gray vertical and horizontal lines represent the redshift and stellar mass bins used in this thesis. We ignore the SB galaxies with  $M_* < 10^{10} M_\odot$ . Most (77%) of our galaxies are SFGs while only four galaxies are quiescent.

The causes behind the diminishing of cold gas reservoir for galaxies is an active area of research where AGN feedback (Ma et al., 2022), mergers (Spilker et al., 2022) or instability (Kalita et al.,

2022) are the most frequent phenomenon suggested. We classify our galaxies as follows, a galaxy is selected as a star-forming galaxy (SFG) if its SFR lie within  $3\sigma$  (0.9 dex) of Equation 19. This criteria classifies 77% (451/585) of our galaxy population as SFGs while quiescent galaxies count for only four in our sample. Those quenched galaxies could perhaps be gas-poor, which thus limits their star formation activity. All four quenched massive galaxies are located in the lowest redshift bin. 'Starburst' (SB) galaxies on the other hand, possess an intense star-forming episode that is much higher than the average SFG. They account for 22% (130/585) of our galaxy sample and reach extreme values of SFR ( $10^3 - 10^4 M_{\odot} \text{ yr}^{-1}$ ).

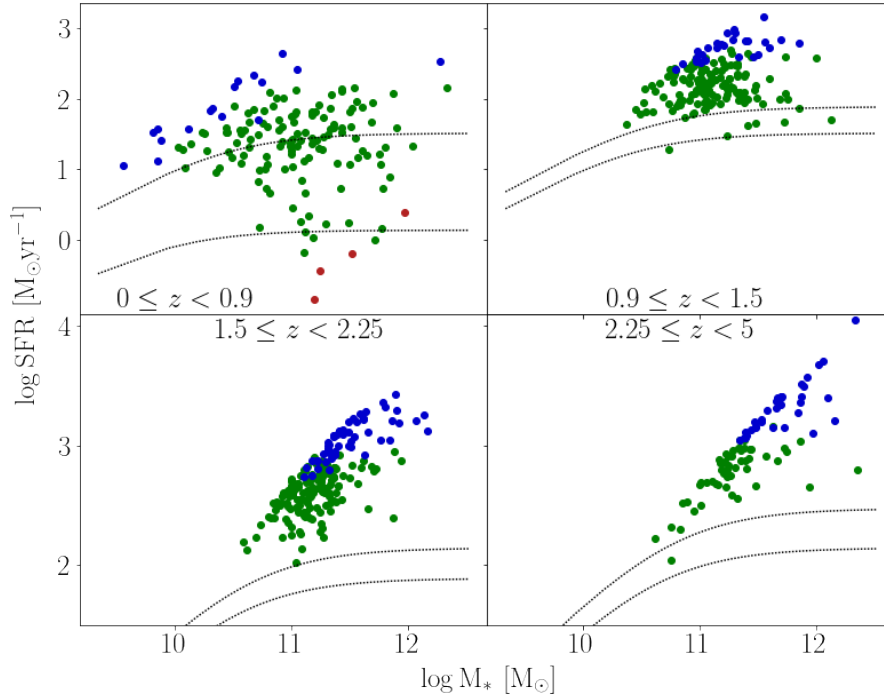


**Figure 26:** SFR vs stellar mass in four redshift bins. The dashed lines are the MS fits (from Equation 19) representing low and upper limits of each redshift bin. The green data points are classified as SFGs, SB galaxies are in blue and quiescent galaxies are dark red Figure 25.

Our fraction of SB galaxies increases from 0.12 at  $0 \leq z < 0.9$  to 0.38 at  $2.25 \leq z < 5$ , marking an increase of 26%. The SB fraction estimated by Rinaldi et al. (2022) represents  $\sim 30\%$  of their galaxy sample. Their findings approximately matches ours, however their sample expands a lot more into the low mass galaxy regime ( $\sim 10^5 M_{\odot}$ ). Coleman et al. (2022) found 60% of their 20 cold quasar sample to be starburst galaxies and share our extreme SFR values. Figure 26 contains MS fits for upper and lower limit of each redshift bin. The first redshift bin ( $0 \leq z < 0.9$ ) covers almost half of the cosmic time, which also explains the 1.3 dex offset between both MS lines. The bending feature occurs at higher stellar masses as the redshift increases, which could be due to the high cold gas density at high redshifts (Daddi et al., 2022; Teklu et al., 2023). Moreover, the scatter of SFGs shifts upwards compared to the MS fits as the redshift increases. For instance, 53 sources lie within both MS fits in our lowest redshift bin, but after  $z \sim 1.5$ , all the MS galaxies have  $\text{SFR} > 100 M_{\odot} \text{ yr}^{-1}$  and are found at the higher-end of MS galaxies.

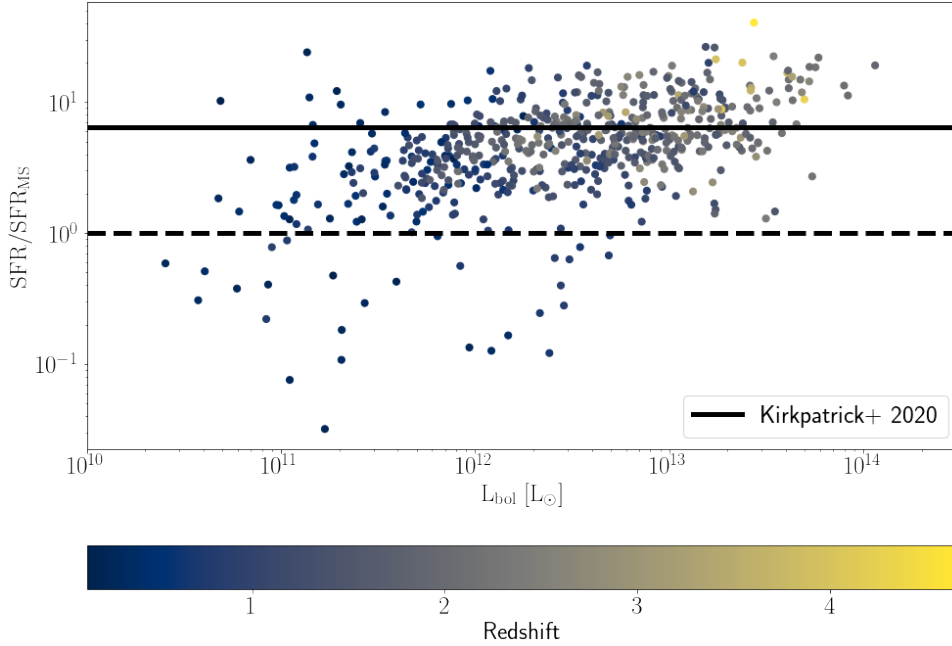


**Figure 27:** SFR/SFR<sub>MS</sub> ratio of our galaxies as a function of their bolometric luminosity and color coded by their redshift. The solid line is the average ratio derived by Kirkpatrick et al. (2020), which is 9.3 while the dashed line marks a starburstiness of 1. The starburstiness of our sample is 6.

To further illustrate the star formation activity in our sample, we show in Figure 27 the ratio between the SFR of each galaxy and the expected SFR for a typical galaxy on the main sequence (SFR<sub>MS</sub>) for their respective redshift, SFR/SFR<sub>MS</sub>, also known as the ‘starburstiness’ (Elbaz et al., 2011). Our galaxies have a factor of 6 for their starburstiness. Cold quasars of Kirkpatrick et al. (2020) had a ratio of 9.3 with a huge standard deviation of 6.4. The ratio increases as we go to higher redshifts, which was also observed by Coleman et al. (2022).

The distribution of the optical and MIR emission (see Figure 14 and Figure 15) for our galaxies suggested that a significant sample of our study may be cold quasars. A selection criteria has been implemented by Kirkpatrick et al. (2020) to classify cold quasars based on their emission. The classification depends on the X-ray luminosity, the blueness and the FIR emission of the galaxy. We use the hard (2 – 10 keV) X-ray luminosities ( $L_{2-10 \text{ keV}}$ ) derived from CIGALE, which would roughly allow us to apply the selection criteria. However, it is worth noting that the X-ray luminosities derived from CIGALE are based on Equation 3. The criteria for cold quasars are as follows; (i) ( $L_{2-10 \text{ keV}} > 10^{44} \text{ erg s}^{-1}$ ), (ii)  $W3 [\text{Vega}] < 11.5$ , (iii) detection in all FIR SPIRE bands and (iv)  $M_B < -23$  where  $M_B$  is the B-band of the Johnson photometric system (Johnson & Morgan, 1953).

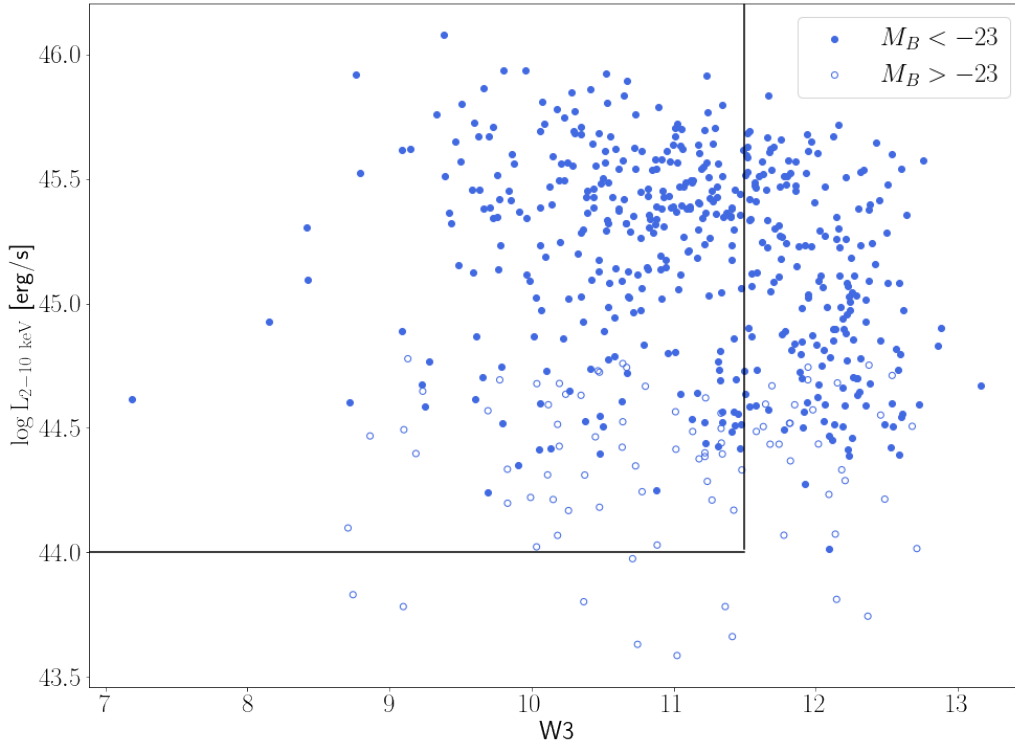


**Figure 28:** Classification diagram for cold quasars set by Kirkpatrick et al. (2020). Filled circles have  $M_B < -23$  while empty circles did not achieve the required B-band magnitude. The solid line is at  $W3 = 11.5$  and  $L_{2-10 \text{ keV}} = 10^{44} \text{ erg s}^{-1}$ . 56% of filled circles lie inside of the solid line rectangle and thus fit the cold quasar classification.

The result of the aforementioned classification is shown in Figure 28. Out of 585 galaxies, 281 satisfied all conditions to be cold quasars. Our quasar sample contains galaxies which extend to a much bluer  $W3$  range than Kirkpatrick et al. (2020) sample where they mostly lie between  $W3 = 10 - 11$ . Galaxies with  $M_B < -23$  seem to also have brighter X-ray luminosities. The criteria applied by Kirkpatrick et al. (2020) is not a definitive classification method for cold quasars. Their criteria involved applying the MIR limit to exclude optical quasars. However, 19% of optical quasars in their sample had  $W3 < 11.5$ .

Kirkpatrick et al. (2020) argued that establishing a different AGN class for cold quasars may not be needed if they are intrinsically red quasars. Red quasars are thought to be a preceding stage before optical quasars. The galaxy is then fully shrouded in dust and gas while the AGN accrete close to its Eddington limit as the feedback is not fully activated yet (Kim & Im, 2018). Kirkpatrick et al. (2020) suggested that the AGN emission might have been able to poke a hole through the center of the dusty envelope for red quasars. This would hence make the galaxy optically visible to us, while the rest of the galaxy is still covered in dust. To roughly test that, we plot the  $M_{\text{BH}}$  against  $L_{\text{bol}}$  as a function of the Eddington ratio ( $L_{\text{bol}}/L_{\text{Edd}}$ ). We compare our quasars with 16 red quasars from Kim et al. (2015). Figure 29 shows a relative difference between our cold quasars sample and the red quasars. These red quasars have a high mean Eddington ratio of 0.69, while our sample has 0.24, which is slightly higher than what Kim et al. (2015) derived for their type 1 quasars sample (0.16). This result does not support cold quasars being fundamentally red quasars. A method to further investigate this theory could be through radio observations to probe molecular gas around the galaxy, as red quasars

have prominent merger features (Urrutia et al., 2012). Moreover, it is worth noting that the Eddington ratio being somewhat higher than typical optical quasars might indicate that cold quasars are part of the AGN evolution paradigm. Kirkpatrick et al. (2020) suggested that they could be 3% – 4% of the optical quasar lifetime, which would be  $\sim 40$  Myr.

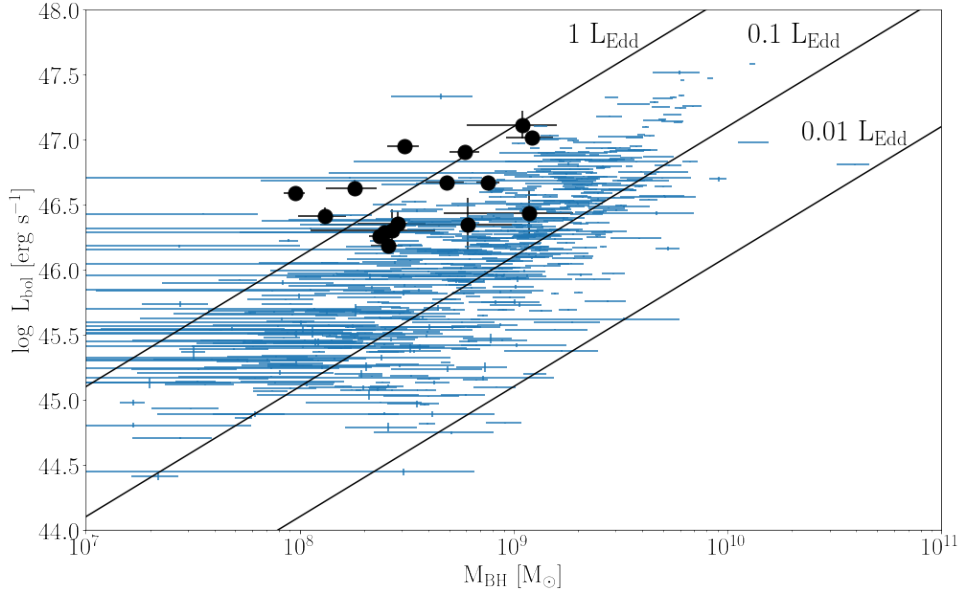


**Figure 29:**  $M_{\text{BH}}$  against  $L_{\text{bol}}$  plot. The Eddington ratios of 1, 0.1, 0.1 are overlaid as the black lines. 16 red quasars from Kim et al. (2015) are shown as the black circles. Our galaxies are shown as the blue scatter dots. Cold quasars do not share similar Eddington ratios to that of red quasars.

## 4.2 The role of BH in SFR growth

In this section, we focus on comparing AGN properties (black hole accretion rate (BHAR), specific BHAR (sBHAR) and  $M_{\text{BH}}$ ) with their host galaxy properties (SFR, specific SFR (sSFR) and  $M_*$ ).

### 4.2.1 sSFR-sBHAR relation with redshift

We show the sBHAR ( $\frac{\text{BHAR}}{M_{\text{BH}}}$ ) and sSFR ( $\frac{\text{SFR}}{M_*}$ ) evolution throughout redshift in Figure 30. Downsizing phenomenon is the general trend seen, where massive galaxies show low SFR at low redshifts compared to lower mass galaxies (Mortlock et al., 2011). This was also tracked by the high metallicity found in massive galaxies. Maiolino and Mannucci (2019) found their current metallicity to be already achieved  $z \sim 1$  by transforming a significant fraction of their gas into metals. Lower mass galaxies are conversely, accreting their mass at a much slower rate and thus maintaining a higher SFR average over time. It is important to mention that this does not disregard the hierarchical galaxy formation theory; small galaxies merging and forming the large structures we observe today (Cole et al., 2002). Downsizing is suggested to be environmental dependent. Our sSFR results for SFG galaxies are roughly higher than Carraro et al. (2020) fittings. Using X-ray stacking analysis, Carraro et al. (2020) derived the SFR for SFGs and SB galaxies through SED fitting. Our mass bin of  $11.5 \leq \log(M_*/M_\odot) < 12.5$  is compared to their best-fit for mass bin of  $11 < \log(M_*/M_\odot) < 12$  (dark green line). Taking downsizing into consideration and our larger bin mass, our sample should lie below their relation, but they overlap the line well. For our mass bin of  $10 \leq \log(M_*/M_\odot) < 11$  which

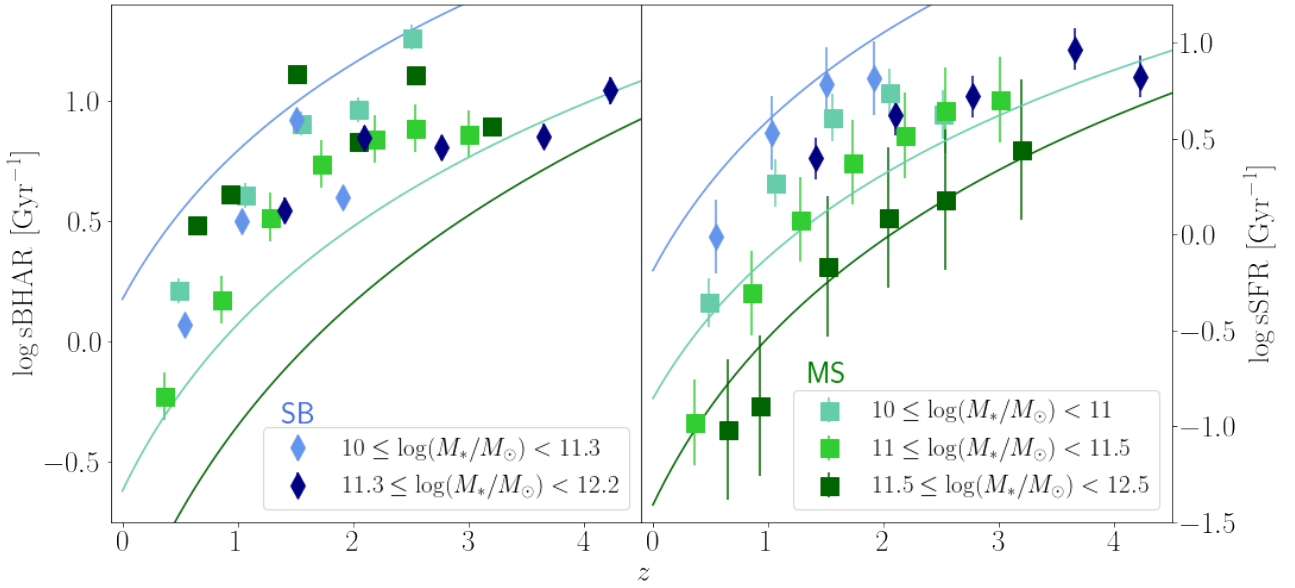


**Figure 30:** sBHAR (*left panel*) and sSFR (*right panel*) divided into stellar mass bins and plotted as a function of redshift for SB (blue) and SFG (green) galaxies. The solid lines are best-fits of Carraro et al. (2020) and their colors roughly represent which mass bin of our study they correspond to.

is directly compared to their fit (light green) for masses of  $10 \leq \log(M_*/M_\odot) < 11$ . The line seems to match at low redshifts but our galaxies have higher accretion rates earlier in the cosmic epoch. As we discuss below in Section 4.2.3, it could be due to the massive difference in SFR between both populations. For SB galaxies, we see the same tendency as our mass bin matches well with their SB galaxy fit, despite our mass bin spanning an additional 0.3 dex compared to their mass bin upper limit. Additionally, the mass-doubling timescale for SFG galaxies agrees well with Carraro et al. (2020). This timescale is the inverse of both sSFR and sBHAR, and it indicates the time needed to double the stellar and black hole mass, respectively. However for SB galaxies, it is difficult to compare due to the lack of samples in our data in addition to the different mass bins where our galaxies are generally more massive.

The sBHAR side of the plot, which tracks the evolution of black hole mass, does not display the downsizing phenomenon. Given the overall large scattering for the mass bins, it is most likely because our bins are based on the stellar masses. As previously mentioned in Section 1.1, the inconsistency in the  $M_* - M_{\text{BH}}$  scaling relation at high redshifts shows that black holes are overmassive compared to local ones with similar host galaxy masses (e.g. Übler et al., 2023) galaxies. We suspect this could be the reason for such a scatter and to further investigate the reasoning, we plot and discuss the  $M_* - M_{\text{BH}}$  relation of our sample in Section 4.2.2.

#### 4.2.2 $M_* - M_{\text{BH}}$ relation

We plot the  $M_* - M_{\text{BH}}$  relation for our redshift bins in Figure 31. It is important to note that the  $M_{\text{BH}}$  mass measurements could contain a systematic error up to  $\sim 0.4$  dex (Shen, 2013). Also a couple ( $< 6$ ) of galaxies in our sample were flagged with bad black hole mass measurements. We also showed the mean deviation for CIGALE mass estimates to be 0.2 dex. The black hole mass correlates with the stellar mass of their host galaxy. We computed the Pearson correlation coefficients ( $r$ ) for each of our bins. The coefficient does not vary significantly between redshift bins but it peaks in the

$1.5 \leq z < 2.25$  bin. We overlay our  $M_* - M_{\text{BH}}$  plot with two local relations. The Kormendy and Ho (2013) relation probed massive elliptical and pseudobulge galaxies. The other relation is from Reines and Volonteri (2015), where they probed AGNs in the nearby Universe ( $z = 0.055$ ) with visible  $\text{H}\alpha$  emission in the BLR.

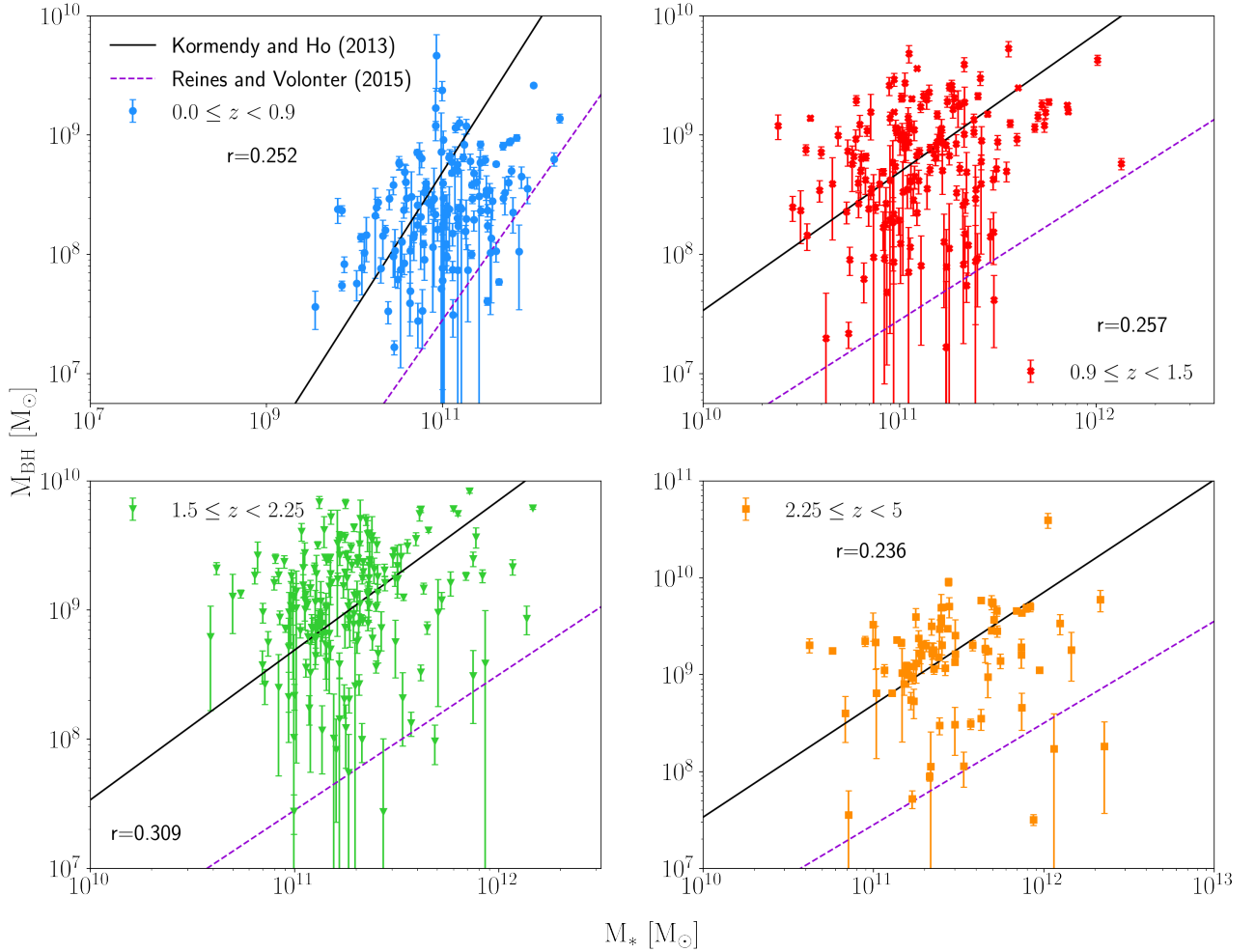


**Figure 31:** The  $M_{\text{BH}}$  vs.  $M_*$  per redshift bin. We display the Pearson correlation coefficient ( $r$ ) for each redshift. There is a weak correlation which does not greatly vary between our redshift bins. The black solid and purple dashed lines are from Kormendy and Ho (2013) who and Reines and Volonteri (2015) local black hole–to–stellar mass relation, respectively. Kormendy and Ho (2013). The relation by Kormendy and Ho (2013) was derived from elliptical galaxies, while Reines and Volonteri (2015) used type 1 AGNs to derive theirs.

If we focus at our lowest redshift bin to directly compare our sample with both local relations. The scaling relation of Kormendy and Ho (2013) seem to underestimate the growth of the galaxy, as a significant number of them fall below the relation, where the stellar mass varies massively (1.5 dex) for the same  $M_{\text{BH}}$ , which are already massive ( $> 10^8 M_\odot$ ). We also compare our results with Li et al. (2023), who also studied the scaling relation using RM on 38 quasars at  $0.2 \lesssim z \lesssim 0.8$ . With no impactful bias effects, their relation agrees with Kormendy and Ho (2013) with a scatter of 0.47 dex, which is smaller than ours ( $0.68 \pm 0.04$  dex, in  $0 \leq z < 0.9$  bin). On the other hand, most of our

galaxies lie above the Reines and Volonteri (2015) relation. The study by Carraro et al. (2020), which involved wide redshift range ( $0 < z < 3.5$ ), also agrees with the local relation of type 1 AGNs, though their sample includes different types of galaxies.

If we go to higher redshifts however, the trend shifts systematically towards the Kormendy and Ho (2013) relation, where the scatter decreases to  $0.36 \pm 0.16$  and  $0.47 \pm 0.13$  for the  $1.5 \leq z < 2.25$  and  $0.9 \leq z < 1.5$  redshift bins, respectively. In those bins, a significant amount of galaxies have BH masses which are comparable to the local ellipticals, which in contrast, make our BH masses overmassive compared to the Reines and Volonteri (2015) relation. A similar result was observed by Zhang et al. (2023), who studied type 1 AGNs at redshift of  $z = 2 - 2.5$ . They suggested the increase of normalization for the local relation at higher redshift could be linked to the availability of denser gas reservoirs at higher redshifts, as shown by simulations (e.g. Habouzit et al., 2019).

A trend where galaxies lie above the local relation was also observed by Ding et al. (2020). However, their sample was overmassive for the Kormendy and Ho (2013) relation. They studied 8 lensed quasars at intermediate redshifts. They suggested a backwards growth scenario where the black hole evolution occurred prior to the galaxy. This was also proposed by Mintz et al. (2024), who applied SED fittings to 64 cold quasars.

The scaling relation is thought to depend heavily on the galaxy type observed. Shankar et al. (2019) performed a study to constrain this relation, they argue that, the dependence on the velocity dispersion to carry out black hole mass measurements ( $M_{\text{BH}} \propto \sigma^{4-5}$ , (Bernardi et al., 2007)) in ellipticals causes a bias in the scaling relation. Such a relation would lead to a higher black hole mass due to a high velocity dispersion value, while the host galaxy mass is still constant. Shankar et al. (2019) also added the absence of dependency on morphological parameters for this relation. This claim is supported by Davis et al. (2019) findings, who derived  $M_{\text{BH}} - M_*$  relation for local quiescent spiral galaxies and their relation agreed well with Reines and Volonteri (2015). Thus if we directly compare our sample to the local derived from type 1 AGNS, then our sample contains overmassive black holes. To match the local relation of Reines and Volonteri (2015), our sample would have to grow in stellar mass. We can view our plots as snapshots for the population at different times. At the lowest redshift bin, one can interpret what we observe as the stage where the galaxies are approaching the local AGN relation. If we go back further in time, so higher redshift, we see galaxies have  $> 1$  dex scatter and are generally farther from the local AGN relation. This could perhaps support the idea of backwards growth of black holes. To have a better look at the growing behavior for the black hole and its host galaxy, we plot the accretion rate in the next section.

### 4.2.3 SFR-BHAR evolution

We further explore the coevolution between the black hole and the host galaxy by plotting the SFR against the BHAR in Figure 32. There is a general trend of positive correlation in all redshift bins. This, however, does not mean there is a direct connection between both aspects. High gas fraction in the galaxy could cause simultaneous feeding for both the black hole and host galaxy (Shimizu et al., 2019; Woo et al., 2020; Zhuang et al., 2021). For  $0 \leq z < 0.9$  bin, there is a rough agreement between our work and the overlaid findings (Zhuang & Ho, 2020; Spinoglio et al., 2022; Torbaniuk et al., 2023). Spinoglio et al. (2022) derived their SFR for type 1 quasars using [CII] 158  $\mu\text{m}$  emission line to avoid AGN contamination. Their BHAR was traced using the MIR [O IV] forbidden line, which correlates well with AGN X-ray emission. Zhuang and Ho (2020) performed SFR measurements

using the forbidden [O III] emission line, which is contaminated by the AGN but is thought to not affect the SFR measurements by more than 0.2 dex. Torbaniuk et al. (2023) used X-ray data to derive the BHAR for optically selected quasars.

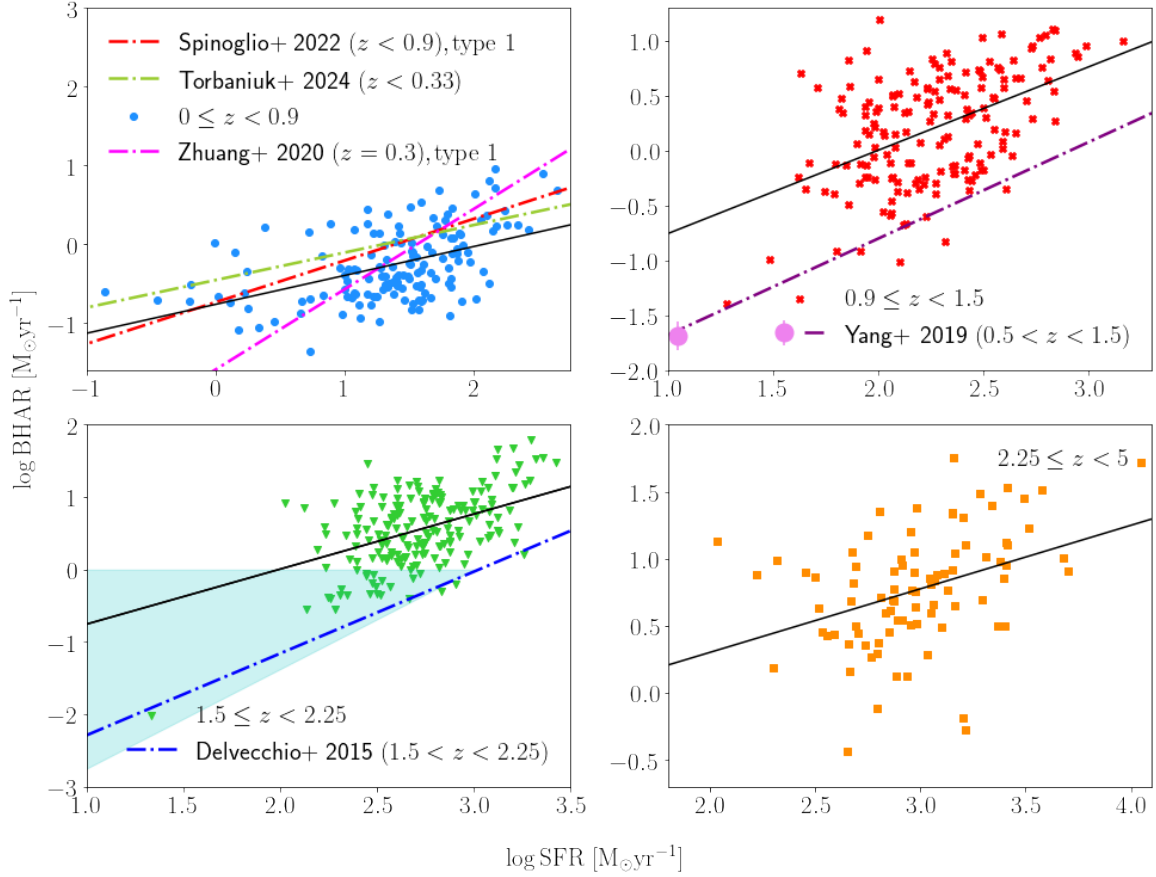


**Figure 32:** The  $\log\text{BHAR} - \log\text{SFR}$  relation divided in four redshift bins. The solid black lines represent the fits for this study (see Table D.1 for best-fitting parameters) and the dashed dotted lines represent the relations from Delvecchio et al. (2015), Yang et al. (2019), Zhuang and Ho (2020), Spinoglio et al. (2022) and Torbaniuk et al. (2023). The pink data point in the  $0.9 \leq z < 1.5$  bin plot represents the most 'active' data point in Yang et al. (2019). The shaded blue region in the  $1.5 \leq z < 2.25$  plot represents the dynamical range studied by Delvecchio et al. (2015).

The slopes from Spinoglio et al. (2022) and Torbaniuk et al. (2023) matches well with our findings, however the type 1 AGN study by Zhuang and Ho (2020) has a steeper slope than ours, indicating a greater black hole growth. Their sample cover black hole masses of  $10^{5.4} - 10^{9.4} M_{\odot}$ , and their BHAR and SFR had similar values to our sample in the redshift bin.

At bins of higher redshifts, there is a significant difference in the dynamical range of BHAR and SFR values between our work and other studies. For example, in  $0.9 \leq z < 1.5$  bin, our fit lies 1 dex above the relation by Yang et al. (2019). To demonstrate the difference further, the pink data point represents the most active bin in their study, where the bin contains 361 galaxies. It is worth mentioning however, that they used bulge-dominated galaxies, which are thought to be significantly quenched by  $z \lesssim 1.0$  (M. Du et al., 2021), which might explain the gap. Moreover, Stemo et al.

(2020) studied X-ray and IR selected AGN host galaxies that are optically detected galaxies by the *Hubble Space Telescope*. Their BHAR and SFR are 1 and 1.8 dex less than our measurements in the  $0.9 \leq z < 1.5$ , respectively. Rodighiero et al. (2015) included 231 starbursts at  $1.5 < z < 2.5$  with high SFR ( $\sim 500 - 750 M_{\odot} \text{ yr}^{-1}$ ). They derived their BHAR using X-ray stacking analysis but the galaxies did not have equally strong BHAR (only  $10^{-1} M_{\odot} \text{ yr}^{-1}$ ). There is also a similar case in the  $1.5 \leq z < 2.25$  bin plot, where Delvecchio et al. (2015) studied FIR-selected galaxies and their X-ray counterparts. Their data lie in the shaded region of the  $1.5 \leq z < 2.25$  redshift bin plot, where their BHAR values are  $\sim 2$  dex less than our findings. Our cold quasars sample could indeed be a brief phase between the red and optical quasar stage where there AGN is partially shrouded in dust and gas, enabling the central engine and star-forming regions to grow further (Kirkpatrick et al., 2020). The derived SFR and BHAR values in our study expand the previously known empirical range for such properties. Carraro et al. (2020) studied SB galaxies up to  $z = 3.5$  to which their IR-derived SFR peaked at  $1229 M_{\odot} \text{ yr}^{-1}$ . That is 9 times less than our most active galaxy in the  $2.25 \leq z < 5$  redshift bin.

As the redshift increases, our best-fittings become less steep. This disagrees with the other studies involved in our plot. The slope and y-intercept for each bin can be found in Table D.1. We note that our highest redshift contains the steepest best-fit line. However, due to the large scatter around the relation, we cannot conclude such a trend. It is difficult to make a direct comparison as the selection criteria of each work differs from one another. For example, Yang et al. (2019) found a slightly steeper trend in their  $1.5 - 3$  redshift bin compared to the  $0.5 - 1.5$  redshift bin. In the case of Delvecchio et al. (2015), their highest redshift bin ( $1.5 < z < 2.5$ ) slope doubles with respect to their lowest redshift bin ( $0.01 < z < 0.25$ ). Stemo et al. (2020) found a flatter slope trend as the redshift increased.

The scatter of BHAR increases at higher redshifts. That is, the SFR is maintaining its growth while the BHAR slowed down in comparison. The depletion of gas fraction in the galaxy is likely not the case, since star formation activity is still occurring. It may be a due to the AGNs expelling the gas from its central region, hence halting their own accretion as observed by Ellison et al. (2021). We explore possible links for coevolution by plotting the BHAR/SFR ratio against stellar mass in ??.

#### 4.2.4 BHAR/SFR ratio against the stellar mass

As seen in Figure 32, there is a correlation between both systems that weakens at higher redshifts. We further illustrate the relation by plotting the BHAR/SFR ratio as a function of the stellar mass. A linear trend in Figure 33, as derived by Aird et al. (2019) and Carraro et al. (2020), indicates that black holes become more efficient at accreting matter compared to star formation as the galaxy grows in mass. Aird et al. (2019) used X-ray luminosity to measure the BHAR and used UV to MIR wavelengths to derive SFR and stellar mass from SED fitting. They argued that low mass galaxies are less likely to trigger an AGN due to the supernova feedback preventing the gas clouds from falling into the central region. However, once an AGN in a low mass galaxy is triggered, it starts accreting at similar rates to that of massive galaxies. Torbaniuk et al. (2023) derived a flat trend. They suggest it could be linked to the growth of the black hole potential well, enabling more gas to fall into the center (Ni et al., 2020).

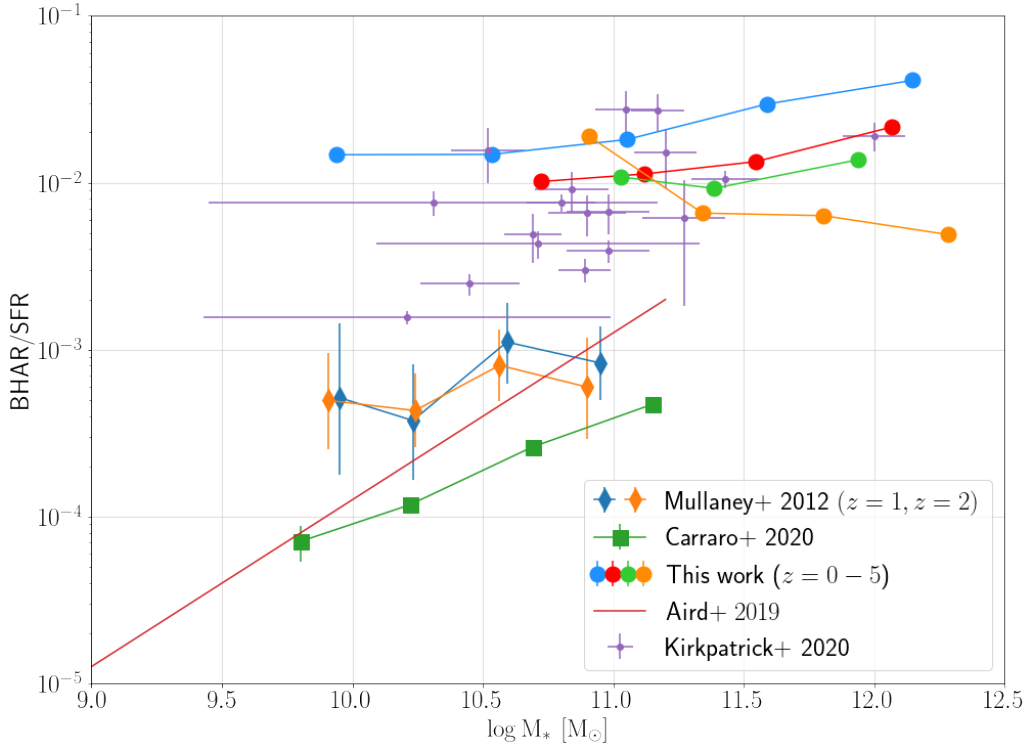


**Figure 33:** BHAR/SFR ratio as a function of the stellar mass. As previously shown, our work is split in four redshift bins,  $0 \leq z < 0.9$  (blue),  $0.9 \leq z < 1.5$  (red),  $1.5 \leq z < 2.25$  and  $2.25 \leq z < 5$  (orange). The work of Mullaney et al. (2011), Aird et al. (2019), Carraro et al. (2020), and Kirkpatrick et al. (2020) is also overlaid. Our sample show a flat trend in all redshift bins.

A flat trend was also observed in Mullaney et al. (2011). They studied the BHAR using X-ray stacking analysis for a redshift range of  $0.5 < z < 2.5$  and measured the SFR from MIR and UV observations. Binned at  $z \sim 1$  and  $z \sim 2$ , they derived a constant flat trend that has the ratio  $\text{BHAR/SFR} \approx 10^{-3}$ . From this ratio, they inferred the black hole mass and found that  $\text{BHAR/SFR} = M_{\text{BH}}/M_*|_{z=0}$ . This implies that the growth of the BHAR and SFR in their galaxies will maintain the same ratio for their masses. For their galaxy sample, which included mergers (Ni et al., 2020), this ratio indicates no enhancement in the SFR activity despite merger interactions. They argue that gas fraction is the deciding factor for the overall galaxy growth. For our findings, we observe a flat trend for all redshift bins. Moreover, our redshift bins share a BHAR/SFR ratio of  $\sim 10^{-2}$ , which is about  $\sim 1$  dex higher than other studies (Mullaney et al., 2011; Aird et al., 2019; Delvecchio et al., 2019; Carraro et al., 2020; Torbaniuk et al., 2023), but agrees with Kirkpatrick et al. (2020). Both their sample and ours expand the dynamical range of this plot into higher ratios and more massive galaxies. The trend translates into a consistent growth rate between the SMBH and the host galaxy. We note however, that our lowest redshift bin shows the highest BHAR/SFR ratio whereas our highest redshift bin show the lowest ratio. This might indicate a decline in BHAR at high redshifts that is then followed by an episode of active accretion once again at low redshifts.

### 4.3 LF fitting

We compare our IR LF to Wang et al. (2019) who adopted a double Schechter function as well. Their work is based on implementing the XID+ probabilistic tool on 30 optical bands as prior information

to derive confusion-limited SPIRE 250, 350 and 500  $\mu\text{m}$  flux densities in addition to 870  $\mu\text{m}$  ALMA waveband for dusty star-forming galaxies. Those flux densities were then used in CIGALE to derive the physical properties of galaxies. Their deblending tool have shown similar source counts as other FIR observations (e.g. Casey et al., 2013; Valiante et al., 2016; Geach et al., 2017; Zavala et al., 2017). They achieved ten times the source counts of source extraction techniques. Their de-blending catalog also obtained deeper galaxy counts for submillimetre wavelengths (870  $\mu\text{m}$ ) compared to observations done by the Submillimetre Common-User Bolometer Array at (850  $\mu\text{m}$ ) (Holland et al., 1999).

Firstly, the volume density of our sample shown in Figure 34 is orders of magnitude less than the work of Wang et al. (2019). While our galaxy population is a subsample of dusty star-forming galaxies, there could also be limitations attributing to such low volume densities. Firstly, HATLAS-NGP radio data were part of the LoLSS, which is a wide radio survey. As seen from multiplicity plots (Figure 10 and Figure 23), deep fields have more multiplicities which could be directly linked to more source detections. In addition to the undetected sources, the elimination of *Herschel* objects with multiple radio counterparts also contributed to the low comoving number density achieved for such a wide area field ( $\sim 179 \text{ deg}^2$ ). The bright-end of the slope of our galaxies at low redshift bins ( $0 < z < 0.3$ ,  $0.3 < z < 0.45$ ,  $0.45 < z < 0.6$ , and  $0.6 < z < 0.8$ ) is on average 0.5 dex less than Wang et al. (2019). At higher redshift bins, the bright-end cut-offs still do not agree with each other but the discrepancy in the break luminosity decreases between both studies. If we compare our results to the work of Wang et al. (2021) where they studied ULIRGS in Lockman, ELAIS-N1 and Boötes. Our densities are  $\sim 1$  dex lower than their sample, while the  $L_{\text{IR}}$  are fairly similar beyond the completeness limit of both IR LF.

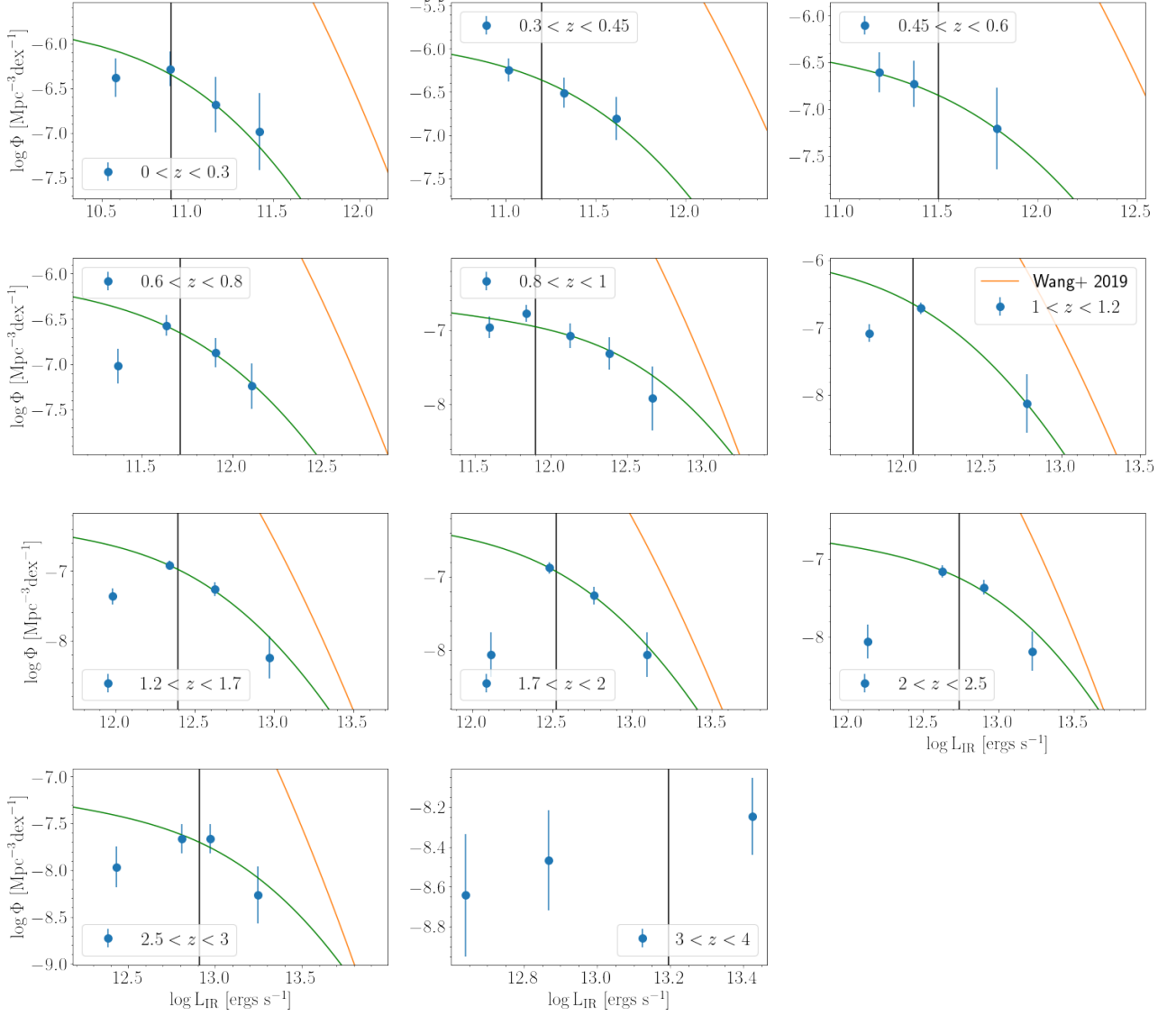


**Figure 34:** The Total IR LF derived from Equation 8 in ten redshift bins. The blue data points are the HATLAS-NGP binned data, with Poisson errors. The vertical black solid line represents the 85%  $L_{\text{IR}}$  completeness limit derived in this study. Our highest redshift bin IR LF could not be fitted due to insufficient data points available beyond the completeness limit.

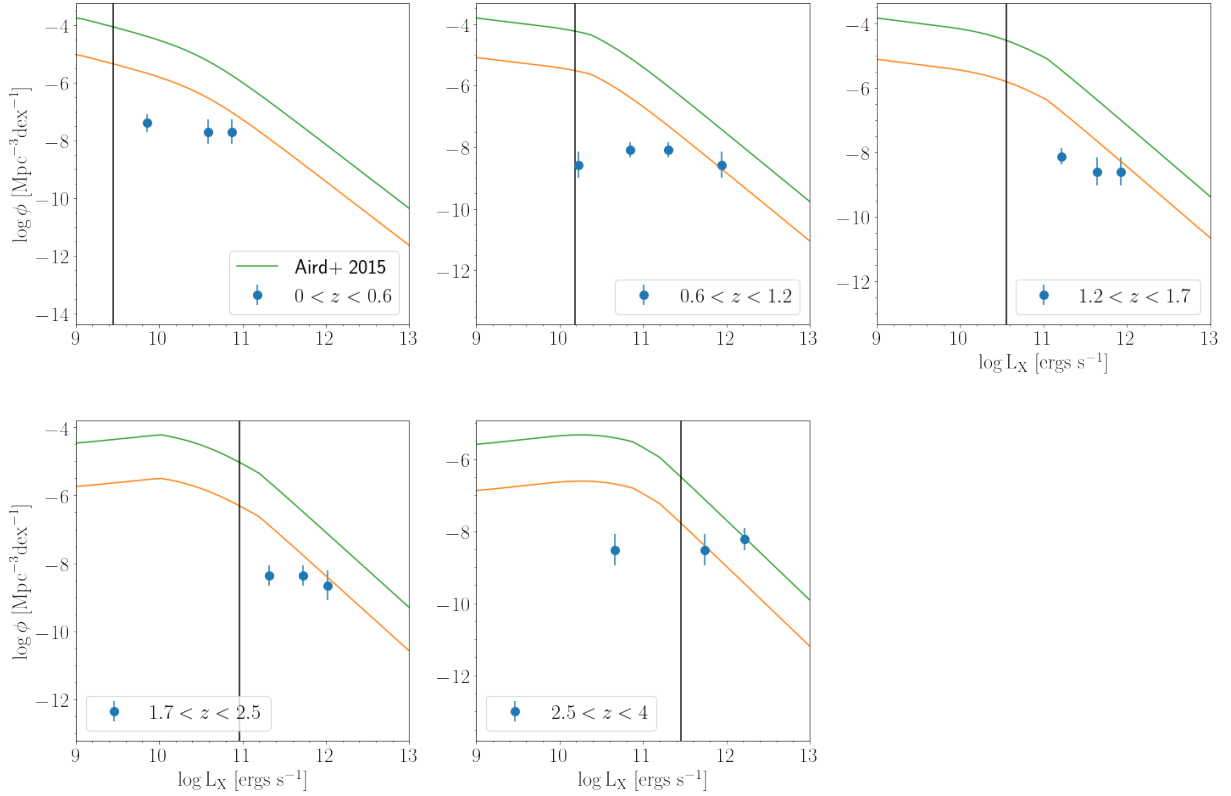


**Figure 35:** The XLF of our galaxies derived from Equation 10, using the LDDE model. The blue data points are the binned HATLAS-NGP X-ray (0.2 – 12 keV) data with their Poisson errors. We also plot the LDDE best-fit of Aird et al., 2015 shown in green. The black solid line represents the depth limit of the XMM observations.

The LDDE XLF is plotted in Figure 35. As mentioned before, we expand the step size of our redshift bins compared to IR LF to have a reasonable volume density plot that can be fitted. Despite this, the XLF does not fit the data perfectly, only the bright-end of the XLF partly agrees with our volume density. The great number of free parameters in the LDDE model as well as the low number of X-ray data do not result in an overall good fit. One can see it best by plotting the best-fit of Aird et al., 2015. Our XLF is very similar to Aird et al., 2015 in terms of the 'knee' feature and also the faint- and bright-end of the slopes. Our XLF is just shifted downwards and that is due to the normalization factor. This is our major uncertainty in the XLF and thus affects the BHARD as well.

#### 4.4 SFRD and BHARD across cosmic time

We plot the total IR luminosity density as a function of our redshift range  $z = 0 - 3$  in Figure 36. The luminosity density of our sample is three orders of magnitude less than Wang et al. (2019). The density of our sample does not vary massively after  $z > 0.5$ , but it peaks at  $z \sim 1.5$ , which roughly agrees with Wang et al. (2019). We derive the cosmic star formation history (CSFH) of our sample by multiplying the IR luminosity density with a constant factor of  $10^{-10} M_{\odot} \text{ yr}^{-1} L_{\odot}$  (Béthermin et al., 2017), obtained from the conversion factor of Kennicutt (1998).

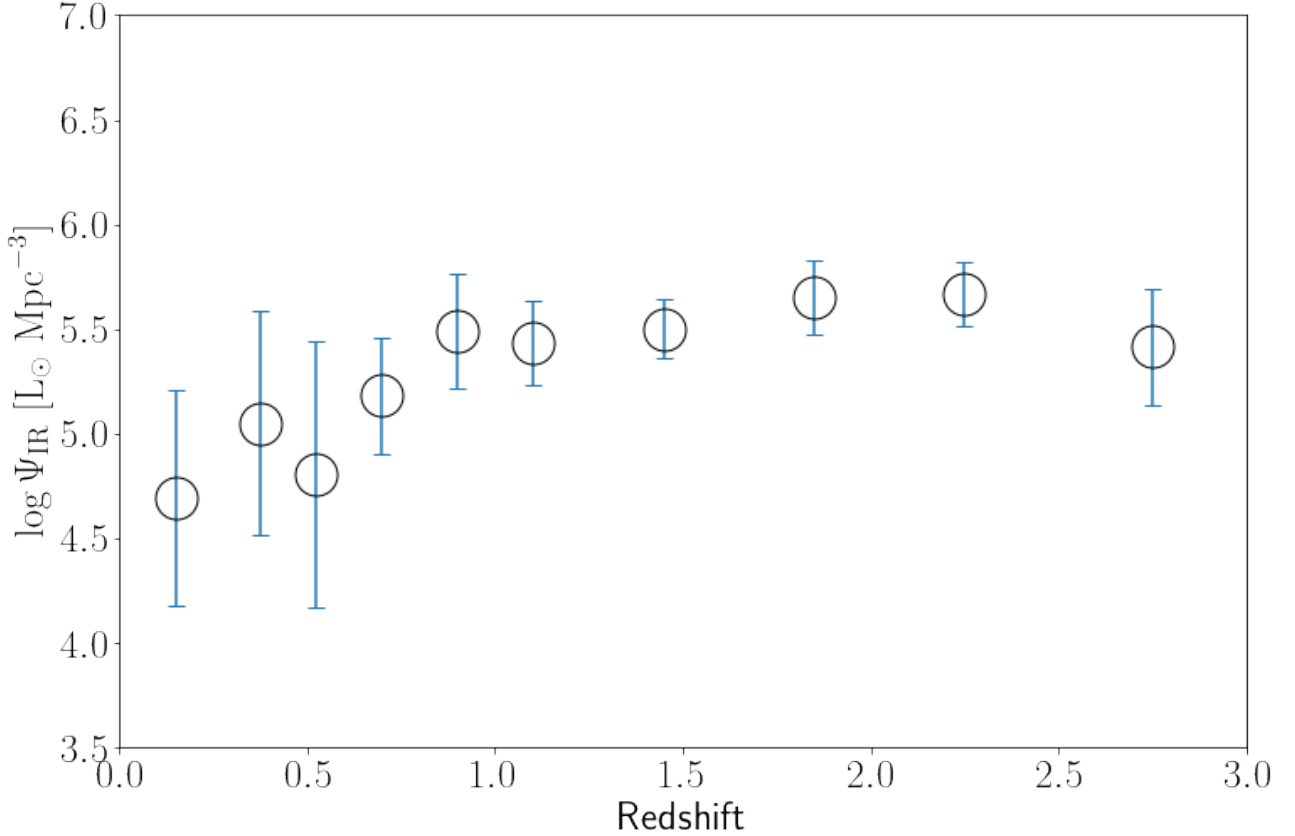


**Figure 36:** The IR luminosity density as a function of redshift. This density was derived from integrating the IR LF.

We plot the derived CSFH in [Figure 37](#) and compare it with Madau and Dickinson (2014). For a direct comparison between the trends, we multiplied our SFRD with a factor  $10^{3.4}$  to align it with the other study. We see a general agreement between our data points and their fit. We fit our data to the analytical function of Madau and Dickinson (2014), expressed as (Son et al., 2023),

$$\Psi(z) = K \frac{(1+z)^a}{1 + [(1+z)/b]^c}, \quad (20)$$

where  $K$  is the normalization factor,  $a$  is the power-law slope to shape the trend from the peak to the present day, while the  $b$  and  $c$  terms are for shaping the fit from the peak to high redshifts. We show the best-fitting parameters for SFRD in the second row of [Table 5](#). We did not include the normalization, as, for our case we input it to match it with Madau and Dickinson (2014). Both fits are within our error bars.

Best-fitting parameters			
Function/Parameters	a	b	c
SFRD	1.05	2	1.3
BHARD	3.1	2	6.1

**Table 5:** The best-fitting parameters for our SFRD and BHARD derived from Equation 20. The high- and low-redshift slope of BHARD is much steeper compared to the SFRD slope for our galaxies.

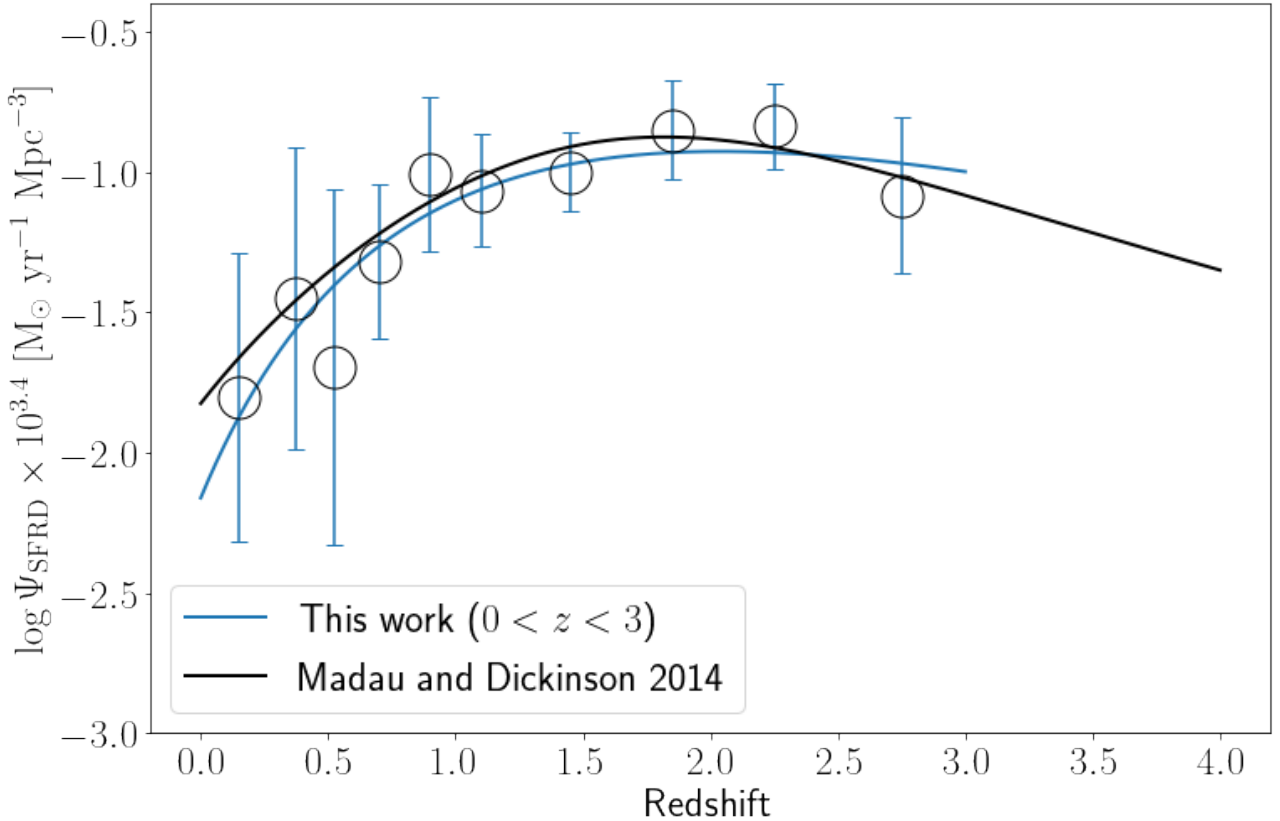


**Figure 37:** The CSFH of our sample normalized to the work of Madau and Dickinson (2014). Their fit is the black solid line. The blue line is the best-fit for our data. Our best-fit agrees well with their trend.

Furthermore, we computed the BHARD of our sample by integrating Equation 18. We also fit the BHARD trend using Equation 20, and we show the best-fitting parameters in Table 5. We plot the SFRD and BHARD of our sample in Figure 38, normalized to the work of Madau and Dickinson (2014). At high redshifts, the accretion rate of the black holes seem much lower than the SFR. The BHARD then slowly increases, and peaks at  $z \sim 1$ , which is later than the peak of SFRD. The decline of the BHARD afterwards is also much steeper compared to the other two fits. The general trend displayed therefore shows the black hole accretion rate lagging behind star formation at high redshifts. Only at  $z \sim 1$  does the BHARD peak and catch up again with the SFRD, but immediately after this peak, the decline in the slope of BHARD is much sharper than that of SFRD. Moreover, Figure 38 does not show any evidence of AGN feedback affecting the star formation activity. However, we still cannot exclude such a possibility due to our uncertainties in assembling the BHARD and CSFH.

We suggest multiple physical interpretations that may explain the low accretion rates of the black hole at high redshifts. Firstly, it could simply be due to the AGN exhausting the gas reservoir in its vicinity (Ellison et al., 2021). It could also be due to AGN outflows expelling the gas from the central region. The hydrodynamical simulations by Costa et al. (2018) showed the possibility for AGNs to only shock and accelerate the gas existing in their galactic center.

As for the active accretion episode that the black hole experience at lower redshifts ( $z \sim 1$ ), we suspect it might be due to the availability of the recycled gas. A recent hydrodynamical simulation showed that recycled gas from dying intermediate mass stars in the central region could contribute up to 38% of the total accreted material by a SMBH (Choi et al., 2024). This was further supported by a spectra study done on the stellar population of low luminosity AGNs (Riffel et al., 2024). They found a large amount of intermediate-age ( $200 \text{ Myr} \leq t \leq 2 \text{ Gyr}$ ) stellar population near the galactic center, suggesting that the stars will enrich the central region with metals during their late evolution stage. Moreover, recycled gas accretion is thought to also be possible from AGN outflows. The ambient medium at large scales slows down the outflows through shocks (see Section 1.2). The outflows thus decelerate and lose energy, allowing themselves to cool down into gas clumps, which could then be reaccreted by the AGN (Van De Voort, 2017).

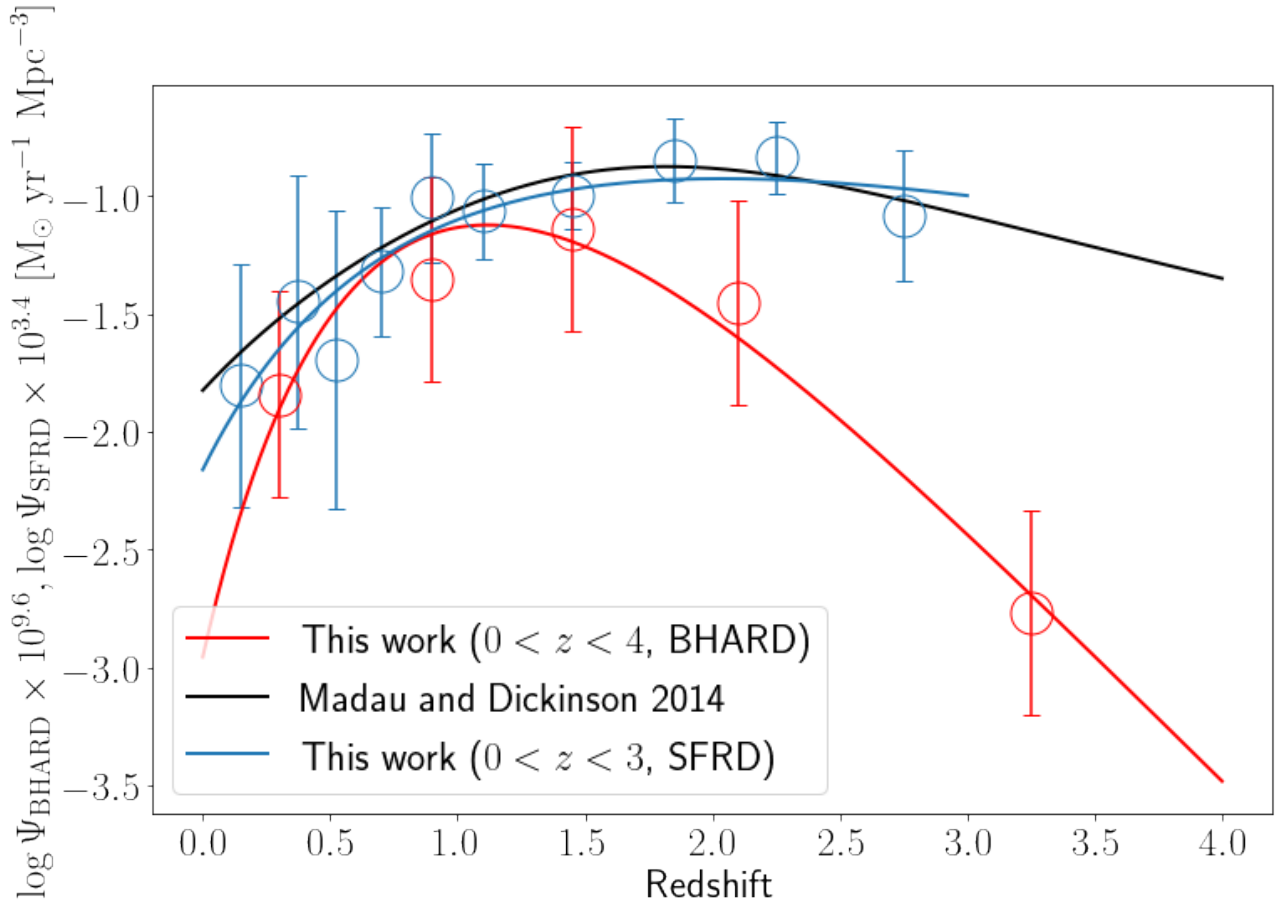


**Figure 38:** The BHARD and SFRD of our sample in red and blue, respectively. The normalization of our SFRD is the same as in Figure 37. For the BHARD, we multiplied it  $10^{9.6}$  to be able to overlap it with the SFRD. The SFRD of our sample peaks at  $z = 1.5 - 2$ , which agrees well with Madau and Dickinson (2014), shown in the black solid line. The decline in BHARD after and before its peak ( $z \sim 1$ ) is more extreme than the SFRD.

## 5 Discussion and Conclusion

In this thesis, we utilized the high angular resolution of radio observations and the FIRC to locate a subsample of optical quasars which have a bright FIR emission, known as cold quasars. We studied 585 cold quasars in nine fields (Lockman, Boötes, ELAIS-N1, GAMA-09, GAMA-12, GAMA-15, Stripe-82, XMM-LSS and HATLAS-NGP ) across a wide redshift range ( $z = 0 - 5$ ). We cross-matched deep (LoTSS, MIGHTEE and VLA) and wide (LoLSS) radio surveys with the *Herschel* SPIRE blind source catalog. The matched objects were then split into two classes. *Herschel*-detected sources with a single radio match were classified as unique and are included in our study. On the other hand, *Herschel*-detected sources with multiple radio sources matched to them were eliminated. We find that the number of multiple matches in a field is related to the depth of the radio observations. Deep radio surveys had a higher multiplicity rate than shallower radio surveys. After selecting the uniquely matched objects, we cross-matched them with the SDSS quasar catalog, resulting in a 1% matching rate. We also added ancillary data to create a multi-wavelength catalog. We studied this rare subsample of optical quasars by performing SED CIGALE fitting as well as constructing XLF and IR LF. We studied the same galaxy population across cosmic time to investigate the link in evolution or the lack thereof between AGNs and their host galaxies.

Our main findings are:

- Our cold quasar sample is, generally brighter in the MIR than most unobscured quasars. They are also slightly redder in the optical, which could be due to obscuring cold dust. Comparing our sample to a SDSS quasar study by Li et al. (2021), our sample, are on average, more massive and show two orders of magnitude more SFR. This gives a strong indication that cold quasars might be intrinsically different than the general SDSS population.
- We only have four quiescent galaxies in our sample. The majority (77%) of the sample are SFGs and the rest are SB galaxies. Most of our SFGs lie close to the upper limit of being a main sequence galaxy. We computed the starburstiness of our sample to be 6, that is, our galaxies are six times more active in star formation than the average main sequence galaxy.
- We observe the downsizing effect in the stellar mass of our galaxies. Our most massive galaxies show that they accreted most of their mass at higher redshifts and are now accreting at lower rates compared to low mass galaxies. We do not observe the downsizing effect for the black hole mass.
- The  $M_* - M_{\text{BH}}$  relation for our sample displays a large scatter of stellar mass for the same black hole mass. If we compare our distribution to the local  $M_* - M_{\text{BH}}$  relation for type 1 AGN, we find our sample to be overmassive in black hole mass. We also find that our lowest redshift bin is closer to the local relation than the higher redshift bins. This could be an indication of a backwards growth evolution for the galaxy, where the black hole formed first and is now growing much less compared to the stellar mass.
- The empirical range of our SFR and BHAR at high redshift bins is much higher ( $> 1.5$  dex) than in previous works. The SFR-BHAR relation shows a positive slope that flattens as the redshift increases. The flattening of the slope at high redshifts indicates a decline in BHAR growth compared to the SFR.
- The BHAR/SFR ratio as function of stellar mass shows a flat trend in all redshift bins. The ratio is 1 dex higher than previous studies, which indicates a high BHAR in our sample. We

observe the highest redshift bin of our study to have the lowest BHAR/SFR ratio while the lowest redshift bin to have the highest ratio. This suggests a retriggering event for the black hole where it starts accreting actively again at low redshifts.

- Using IR LF and XLF, we computed the SFRD and BHARD of our sample, respectively. The accretion history shows low black hole activity at high redshifts. However, as the redshift decrease, BHARD increases, peaking at  $z \sim 1$ , which is later than the peak of the SFRD ( $z = 1.5 - 2$ ). Following the peak, there is a strong decline in the BHARD compared to the SFRD.

Our coevolution study does not display any form of AGN feedback that might be affecting the star formation activity of the galaxies. The black hole lagging behind in accretion could be due to gas exhaustion in the center or the outflows expelling the gas in the central region. Furthermore, we suspect the recycled gas could be the reason for the growth in black hole accretion rate once again at low redshifts.

Our work suffered from several caveats that could potentially be minimized in future projects. First, the exclusion of *Herschel* sources with multiple matches decreased the sample size and did not allow us to directly compute the completeness limit of our LFs. A probabilistic de-blending tool such as XID+ to properly assign the *Herschel* sources with multiple matches would have improved our LF fitting process immensely. The low number of data points limited our parametrization of the LF, especially for the XLF, where we only fitted two parameters out of 13. This as a result affected the computation of the BHARD. Furthermore, our work lost 20% of its initial sample size due to bad ( $\chi^2 > 5$ ) SED fittings. In addition, Kirkpatrick et al., 2020 deemed SED fitting via CIGALE to be unreliable. They tested it and found CIGALE to derive SFR values three times higher than what was computed by their template. Moreover, the SED fittings of their cold quasars produced by CIGALE showed the UV and optical emission to be dominated by the galaxy, which did not align with their spectra observations. Further investigation is needed to compare whether different SED fitting tools might imply significant difference in the physical properties.

## Appendices

### A Separation distribution

We show here the positional separation distribution between *Herschel* and radio data. All fields except GAMA-12 share the same trend.

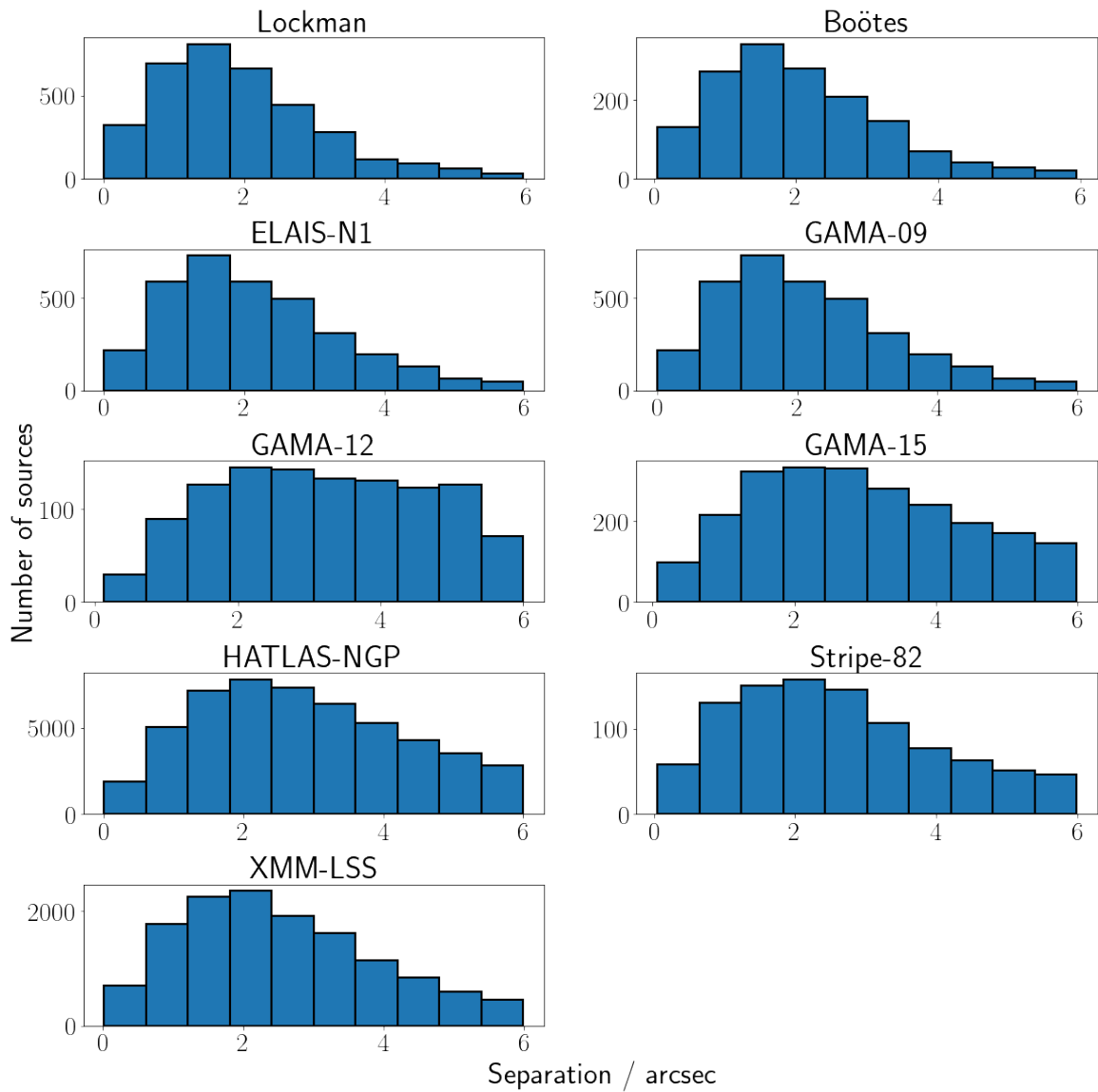


**Figure A.1:** Distribution of positional separation between *Herschel* and their unique radio counterparts for each field individually.

## B Bolometric correction factor

Parameters	$a$	$b$	$c$
Duras et al., 2020	15.33	11.48	16.2

**Table B.1:** Best-fit parameters for the bolometric correction factor.

## C Main sequence fitting

Parameters	$a_0$	$a_1$	$a_2$	$a_3$	$a_4$
Best-fit	0.73	2.22	4.34	-0.3	-7.33

**Table C.1:** Best-fit parameters of MS fit derived from Popesso et al., 2022.

## D SFR-BHAR fitting parameters

Redshift range	Slope	Intercept
$0 \leq z < 0.9$	0.36	-0.76
$0.9 \leq z < 1.5$	0.76	-1.5
$1.5 \leq z < 2.25$	0.86	-1.79
$2.25 \leq z < 5$	0.47	-0.65

**Table D.1:** Best-fitting parameters for linearly fitting the relation between  $\log(\text{SFR})$  and  $\log(\text{BHAR})$  [Figure 32](#). We note that the highest redshift show a steep fit, however from large scatter of the  $2.25 \leq z < 5$  bin, we cannot confirm such steepening.

## References

- Aalto, S., Garcia-Burillo, S., Muller, S., Winters, J. M., Gonzalez-Alfonso, E., van der Werf, P., Henkel, C., Costagliola, F., & Neri, R. (2015). High resolution observations of HCN and HCO+j = 3-2 in the disk and outflow of mrk 231. detection of vibrationally excited HCN in the warped nucleus [ADS Bibcode: 2015A&A...574A..85A]. *Astronomy and Astrophysics*, 574, A85. <https://doi.org/10.1051/0004-6361/201423987>
- Aihara, H., Arimoto, N., Armstrong, R., Arnouts, S., Bahcall, N. A., Bickerton, S., Bosch, J., Bundy, K., Capak, P. L., Chan, J. H. H., Chiba, M., Coupon, J., Egami, E., Enoki, M., Finet, F., Fujimori, H., Fujimoto, S., Furusawa, H., Furusawa, J., ... Yuma, S. (2018). The hyper supprimecam SSP survey: Overview and survey design. *Publications of the Astronomical Society of Japan*, 70, S4. <https://doi.org/10.1093/pasj/psx066>
- Aird, J., Coil, A. L., & Georgakakis, A. (2019). X-rays across the galaxy population – III. the incidence of AGN as a function of star formation rate. *Monthly Notices of the Royal Astronomical Society*, 484(3), 4360–4378. <https://doi.org/10.1093/mnras/stz125>
- Aird, J., Coil, A. L., Georgakakis, A., Nandra, K., Barro, G., & Pérez-González, P. G. (2015). The evolution of the x-ray luminosity functions of unabsorbed and absorbed AGNs out to  $z = 5$ . *Monthly Notices of the Royal Astronomical Society*, 451(2), 1892–1927. <https://doi.org/10.1093/mnras/stv1062>
- Aird, J., Nandra, K., Laird, E. S., Georgakakis, A., Ashby, M. L. N., Barmby, P., Coil, A. L., Huang, J.-S., Koekemoer, A. M., Steidel, C. C., & Willmer, C. N. A. (2010). The evolution of the hard x-ray luminosity function of AGN. *Monthly Notices of the Royal Astronomical Society*, 401(4), 2531–2551. <https://doi.org/10.1111/j.1365-2966.2009.15829.x>
- Albert, J. G., Van Weeren, R. J., Intema, H. T., & Röttgering, H. J. A. (2020). Probabilistic direction-dependent ionospheric calibration for LOFAR-HBA. *Astronomy & Astrophysics*, 635, A147. <https://doi.org/10.1051/0004-6361/201937424>
- Almeida, C. R., Levenson, N. A., Alonso-Herrero, A., Ramos, A. A., Espinosa, J. M. R., Garcia, A. M. P., Packham, C., Mason, R., Radomski, J. T., & Diaz-Santos, T. (2011). Testing the unification model for AGN in the infrared: Are the obscuring tori of type 1 and 2 seyferts different? *The Astrophysical Journal*, 731(2), 92. <https://doi.org/10.1088/0004-637X/731/2/92>
- Antonucci, R. (1993). Unified models for active galactic nuclei and quasars. [ADS Bibcode: 1993ARA&A...31..47]. *Annual Review of Astronomy and Astrophysics*, 31, 473–521. <https://doi.org/10.1146/annurev.aa.31.090193.002353>
- Avachat, S. S., Perlman, E. S., Sparks, W. B., Cara, M., & Owen, F. N. (2014). Multi-wavelength polarimetry and variability study of the m87 jet. *Proceedings of the International Astronomical Union*, 10, 116–121. <https://doi.org/10.1017/S1743921315002033>
- Azadi, M., Coil, A. L., Aird, J., Reddy, N., Shapley, A., Freeman, W. R., Kriek, M., Leung, G. C. K., Mobasher, B., Price, S. H., Sanders, R. L., Shivaiei, I., & Siana, B. (2017). THE MOSDEF SURVEY: AGN MULTI-WAVELENGTH IDENTIFICATION, SELECTION BIASES, AND HOST GALAXY PROPERTIES. *The Astrophysical Journal*, 835(1), 27. <https://doi.org/10.3847/1538-4357/835/1/27>
- Balogh, M. L., Pearce, F. R., Bower, R. G., & Kay, S. T. (2001). Revisiting the cosmic cooling crisis. *Monthly Notices of the Royal Astronomical Society*, 326(4), 1228–1234. <https://doi.org/10.1111/j.1365-2966.2001.04667.x>
- Barkana, R., & Loeb, A. (2001). In the beginning: The first sources of light and the reionization of the universe. *Physics Reports*, 349(2), 125–238. [https://doi.org/10.1016/S0370-1573\(01\)00019-9](https://doi.org/10.1016/S0370-1573(01)00019-9)

- Baron, D., & Netzer, H. (2019). Discovering AGN-driven winds through their infrared emission – i. general method and wind location. *Monthly Notices of the Royal Astronomical Society*, 482(3), 3915–3932. <https://doi.org/10.1093/mnras/sty2935>
- Beckmann, V., & Shrader, C. R. (2012, August 1). *Active galactic nuclei* [ADS Bibcode: 2012agn..book....B]. Retrieved May 25, 2024, from <https://ui.adsabs.harvard.edu/abs/2012agn..book....B>
- Benson, A. J., Bower, R. G., Frenk, C. S., Lacey, C. G., Baugh, C. M., & Cole, S. (2003). What shapes the luminosity function of galaxies? *The Astrophysical Journal*, 599(1), 38–49. <https://doi.org/10.1086/379160>
- Bernardi, M., Sheth, R. K., Tundo, E., & Hyde, J. B. (2007). Selection bias in the  $M_*$  - and  $M_*$  -  $L$  correlations and its consequences. *The Astrophysical Journal*, 660(1), 267–275. <https://doi.org/10.1086/512719>
- Bessiere, P. S., & Ramos Almeida, C. (2022). Spatially resolved evidence of the impact of quasar-driven outflows on recent star formation: The case of mrk 34 [ADS Bibcode: 2022MNRAS.512L..54B]. *Monthly Notices of the Royal Astronomical Society*, 512, L54–L59. <https://doi.org/10.1093/mnras/512/l54>
- B  thermin, M., Wu, H.-Y., Lagache, G., Davidzon, I., Ponthieu, N., Cousin, M., Wang, L., Dor  , O., Daddi, E., & Lapi, A. (2017). The impact of clustering and angular resolution on far-infrared and millimeter continuum observations. *Astronomy & Astrophysics*, 607, A89. <https://doi.org/10.1051/0004-6361/201730866>
- Bianchi, L., Herald, J., Efremova, B., Girardi, L., Zobot, A., Marigo, P., Conti, A., & Shiao, B. (2011). GALEX catalogs of UV sources: Statistical properties and sample science applications: Hot white dwarfs in the milky way. *Astrophysics and Space Science*, 335(1), 161–169. <https://doi.org/10.1007/s10509-010-0581-x>
- Bianchi, L., Efremova, B., Herald, J., Girardi, L., Zobot, A., Marigo, P., & Martin, C. (2011). Catalogues of hot white dwarfs in the milky way from GALEX’s ultraviolet sky surveys: Constraining stellar evolution: Hot white dwarfs: UV catalogues. *Monthly Notices of the Royal Astronomical Society*, 411(4), 2770–2791. <https://doi.org/10.1111/j.1365-2966.2010.17890.x>
- Blandford & McKee. (1982). Reverberation mapping of the emission line regions of seyfert galaxies and quasars. *The Astrophysical Journal*, 255, 419. <https://doi.org/10.1086/159843>
- Blandford, Meier, D., & Readhead, A. (2019). Relativistic jets from active galactic nuclei. *Annual Review of Astronomy and Astrophysics*, 57(1), 467–509. <https://doi.org/10.1146/annurev-astro-081817-051948>
- Boissay, R., Ricci, C., & Paltani, S. (2016). A hard x-ray view of the soft excess in AGN. *Astronomy & Astrophysics*, 588, A70. <https://doi.org/10.1051/0004-6361/201526982>
- Boquien, M., Burgarella, D., Roehlly, Y., Buat, V., Ciesla, L., Corre, D., Inoue, A. K., & Salas, H. (2019). CIGALE: A python code investigating GALaxy emission. *Astronomy & Astrophysics*, 622, A103. <https://doi.org/10.1051/0004-6361/201834156>
- Boquien, M., Calzetti, D., Aalto, S., Boselli, A., Braine, J., Buat, V., Combes, F., Israel, F., Kramer, C., Lord, S., Rela  o, M., Rosolowsky, E., Stacey, G., Tabatabaei, F., Van Der Tak, F., Van Der Werf, P., Verley, S., & Xilouris, M. (2015). Measuring star formation with resolved observations: The test case of m 33. *Astronomy & Astrophysics*, 578, A8. <https://doi.org/10.1051/0004-6361/201423518>
- Bourne, N., Dunne, L., Ivison, R. J., Maddox, S. J., Dickinson, M., & Frayer, D. T. (2011). Evolution of the far-infrared-radio correlation and infrared spectral energy distributions of massive galaxies over  $z=0-2$ : Evolution of the FRC and IR SEDs. *Monthly Notices of the Royal Astronomical Society*, 410(2), 1155–1173. <https://doi.org/10.1111/j.1365-2966.2010.17517.x>

- Bourne, N., Maddox, S. J., Dunne, L., Dye, S., Eales, S., Hoyos, C., González-Nuevo, J., Smith, D. J. B., Valiante, E., De Zotti, G., Ivison, R. J., & Rowlands, K. (2014). Colour matters: The effects of lensing on the positional offsets between optical and submillimetre galaxies in herchel -ATLAS. *Monthly Notices of the Royal Astronomical Society*, 444(2), 1884–1892. <https://doi.org/10.1093/mnras/stu1582>
- Brandt, W. N., & Alexander, D. M. (2015). Cosmic x-ray surveys of distant active galaxies: The demographics, physics, and ecology of growing supermassive black holes. *The Astronomy and Astrophysics Review*, 23(1), 1. <https://doi.org/10.1007/s00159-014-0081-z>
- Brightman, M., Baloković, M., Ballantyne, D. R., Bauer, F. E., Boorman, P., Buchner, J., Brandt, W. N., Comastri, A., Moro, A. D., Farrah, D., Gandhi, P., Harrison, F. A., Koss, M., Lanz, L., Masini, A., Ricci, C., Stern, D., Vasudevan, R., & Walton, D. J. (2017). X-ray bolometric corrections for compton-thick active galactic nuclei. *The Astrophysical Journal*, 844(1), 10. <https://doi.org/10.3847/1538-4357/aa75c9>
- Bromm, V., & Larson, R. B. (2004). The first stars. *Annual Review of Astronomy and Astrophysics*, 42(1), 79–118. <https://doi.org/10.1146/annurev.astro.42.053102.134034>
- Brüggen, M., & Scannapieco, E. (2016). THE LAUNCHING OF COLD CLOUDS BY GALAXY OUTFLOWS. II. THE ROLE OF THERMAL CONDUCTION. *The Astrophysical Journal*, 822(1), 31. <https://doi.org/10.3847/0004-637X/822/1/31>
- Brusa, M., Cresci, G., Daddi, E., Paladino, R., Perna, M., Bongiorno, A., Lusso, E., Sargent, M. T., Casasola, V., Feruglio, C., Fraternali, F., Georgiev, I., Mainieri, V., Carniani, S., Comastri, A., Duras, F., Fiore, F., Mannucci, F., Marconi, A., ... Bonaglia, M. (2018). Molecular outflow and feedback in the obscured quasar XID2028 revealed by ALMA. *Astronomy & Astrophysics*, 612, A29. <https://doi.org/10.1051/0004-6361/201731641>
- Bruzual, G., & Charlot, S. (2003). Stellar population synthesis at the resolution of 2003 [ADS Bibcode: 2003MNRAS.344.1000B]. *Monthly Notices of the Royal Astronomical Society*, 344, 1000–1028. <https://doi.org/10.1046/j.1365-8711.2003.06897.x>
- Burgarella, D., Buat, V., & Iglesias-Páramo, J. (2005). Star formation and dust attenuation properties in galaxies from a statistical ultraviolet-to-far-infrared analysis. *Monthly Notices of the Royal Astronomical Society*, 360(4), 1413–1425. <https://doi.org/10.1111/j.1365-2966.2005.09131.x>
- Calistro Rivera, G., Williams, W. L., Hardcastle, M. J., Duncan, K., Röttgering, H. J. A., Best, P. N., Brüggen, M., Chyży, K. T., Conselice, C. J., De Gasperin, F., Engels, D., Gürkan, G., Intema, H. T., Jarvis, M. J., Mahony, E. K., Miley, G. K., Morabito, L. K., Prandoni, I., Sabater, J., ... White, G. J. (2017). The LOFAR window on star-forming galaxies and AGNs – curved radio SEDs and IR–radio correlation at  $0 < z < 2.5$ . *Monthly Notices of the Royal Astronomical Society*, 469(3), 3468–3488. <https://doi.org/10.1093/mnras/stx1040>
- Calzetti, D. (2012). Star formation rate indicators. <https://doi.org/10.48550/ARXIV.1208.2997>
- Calzetti, D., Armus, L., Bohlin, R. C., Kinney, A. L., Koornneef, J., & Storchi-Bergmann, T. (2000). The dust content and opacity of actively star-forming galaxies. *The Astrophysical Journal*, 533(2), 682–695. <https://doi.org/10.1086/308692>
- Capelo, P. R., Feruglio, C., Hickox, R. C., & Tombesi, F. (2023). Black hole-galaxy co-evolution and the role of feedback. In C. Bambi & A. Santangelo (Eds.), *Handbook of x-ray and gamma-ray astrophysics* (pp. 1–50). Springer Nature Singapore. [https://doi.org/10.1007/978-981-16-4544-0\\_115-1](https://doi.org/10.1007/978-981-16-4544-0_115-1)
- Carlberg, R. G., & Couchman, H. M. P. (1989). Mergers and bias in a cold dark matter cosmology. *The Astrophysical Journal*, 340, 47. <https://doi.org/10.1086/167375>
- Carnall, A. C., McLure, R. J., Dunlop, J. S., McLeod, D. J., Wild, V., Cullen, F., Magee, D., Begley, R., Cimatti, A., Donnan, C. T., Hamadouche, M. L., Jewell, S. M., & Walker, S. (2023). A

- massive quiescent galaxy at redshift 4.658. *Nature*, 619(7971), 716–719. <https://doi.org/10.1038/s41586-023-06158-6>
- Carraro, R., Rodighiero, G., Cassata, P., Brusa, M., Shankar, F., Baronchelli, I., Daddi, E., Delvecchio, I., Franceschini, A., Griffiths, R., Gruppioni, C., López-Navas, E., Mancini, C., Marchesi, S., Negrello, M., Puglisi, A., Sani, E., & Suh, H. (2020). Coevolution of black hole accretion and star formation in galaxies up to  $z = 3.5$ . *Astronomy & Astrophysics*, 642, A65. <https://doi.org/10.1051/0004-6361/201936649>
- Casey, C. M., Chen, C.-C., Cowie, L. L., Barger, A. J., Capak, P., Ilbert, O., Koss, M., Lee, N., Le Floch, E., Sanders, D. B., & Williams, J. P. (2013). Characterization of scuba-2 450  $\mu\text{m}$  and 850  $\mu\text{m}$  selected galaxies in the COSMOS field. *Monthly Notices of the Royal Astronomical Society*, 436(3), 1919–1954. <https://doi.org/10.1093/mnras/stt1673>
- Cazzoli, S., Arribas, S., Maiolino, R., & Colina, L. (2016). Neutral gas outflows in nearby [u]LIRGs via optical NaD feature. *Astronomy & Astrophysics*, 590, A125. <https://doi.org/10.1051/0004-6361/201526788>
- Chabrier, G. (2003). Galactic stellar and substellar initial mass function [ADS Bibcode: 2003PASP..115..763C]. *Publications of the Astronomical Society of the Pacific*, 115, 763–795. <https://doi.org/10.1086/376392>
- Chapin, E. L., Chapman, S. C., Coppin, K. E., Devlin, M. J., Dunlop, J. S., Greve, T. R., Halpern, M., Hasselfield, M. F., Hughes, D. H., Ivison, R. J., Marsden, G., Moncelsi, L., Netterfield, C. B., Pascale, E., Scott, D., Smail, I., Viero, M., Walter, F., Weiss, A., & Werf, P. V. D. (2011). A joint analysis of BLAST 250-500  $\mu\text{m}$  and LABOCA 870  $\mu\text{m}$  observations in the extended chandra deep field-south: BLAST and LABOCA observations of the ECDF-s. *Monthly Notices of the Royal Astronomical Society*, 411(1), 505–549. <https://doi.org/10.1111/j.1365-2966.2010.17697.x>
- Charlot, S., & Fall, S. M. (2000). A simple model for the absorption of starlight by dust in galaxies. *The Astrophysical Journal*, 539(2), 718–731. <https://doi.org/10.1086/309250>
- Choi, E., Somerville, R. S., Ostriker, J. P., Hirschmann, M., & Naab, T. (2024). The origins of gas accreted by supermassive black holes: The importance of recycled gas. *The Astrophysical Journal*, 964(1), 54. <https://doi.org/10.3847/1538-4357/ad245a>
- Cicone, C., Brusa, M., Ramos Almeida, C., Cresci, G., Husemann, B., & Mainieri, V. (2018). The largely unconstrained multiphase nature of outflows in AGN host galaxies. *Nature Astronomy*, 2(3), 176–178. <https://doi.org/10.1038/s41550-018-0406-3>
- Cimatti, A., Fraternali, F., & Nipoti, C. (2019). Introduction to galaxy formation and evolution. from primordial gas to present-day galaxies. <https://doi.org/10.48550/ARXIV.1912.06216>
- Cole, S., Lacey, C. G., Baugh, C. M., & Frenk, C. S. (2002). Hierarchical galaxy formation: Hierarchical galaxy formation. *Monthly Notices of the Royal Astronomical Society*, 319(1), 168–204. <https://doi.org/10.1046/j.1365-8711.2000.03879.x>
- Coleman, B., Kirkpatrick, A., Cooke, K. C., Glikman, E., La Massa, S., Marchesi, S., Peca, A., Treister, E., Auge, C., Urry, C. M., Sanders, D., Turner, T. J., & Ananna, T. T. (2022). Accretion history of AGN: Estimating the host galaxy properties in x-ray luminous AGN from  $z = 0-3$ . *Monthly Notices of the Royal Astronomical Society*, 515(1), 82–98. <https://doi.org/10.1093/mnras/stac1679>
- Combes, F. (2017). AGN feedback and its quenching efficiency. *Frontiers in Astronomy and Space Sciences*, 4, 10. <https://doi.org/10.3389/fspas.2017.00010>
- Costa, T., Rosdahl, J., Sijacki, D., & Haehnelt, M. G. (2018). Driving gas shells with radiation pressure on dust in radiation-hydrodynamic simulations. *Monthly Notices of the Royal Astronomical Society*, 473(3), 4197–4219. <https://doi.org/10.1093/mnras/stx2598>

- Costa, T., Sijacki, D., & Haehnelt, M. G. (2014). Feedback from active galactic nuclei: Energy- versus momentum-driving. *Monthly Notices of the Royal Astronomical Society*, *444*(3), 2355–2376. <https://doi.org/10.1093/mnras/stu1632>
- Cowie, L. L., Songaila, A., Hu, E. M., & Cohen, J. G. (1996). New insight on galaxy formation and evolution from keck spectroscopy of the hawaii deep fields. *The Astronomical Journal*, *112*, 839. <https://doi.org/10.1086/118058>
- Cresci, G., Marconi, A., Zibetti, S., Risaliti, G., Carniani, S., Mannucci, F., Gallazzi, A., Maiolino, R., Balmaverde, B., Brusa, M., Capetti, A., Cicone, C., Feruglio, C., Bland-Hawthorn, J., Nagao, T., Oliva, E., Salvato, M., Sani, E., Tozzi, P., . . . Venturi, G. (2015). The MAGNUM survey: Positive feedback in the nuclear region of NGC 5643 suggested by MUSE [ADS Bibcode: 2015A&A...582A..63C]. *Astronomy and Astrophysics*, *582*, A63. <https://doi.org/10.1051/0004-6361/201526581>
- Croton, D. J., Springel, V., White, S. D. M., De Lucia, G., Frenk, C. S., Gao, L., Jenkins, A., Kauffmann, G., Navarro, J. F., & Yoshida, N. (2006). The many lives of active galactic nuclei: Cooling flows, black holes and the luminosities and colours of galaxies. *Monthly Notices of the Royal Astronomical Society*, *365*(1), 11–28. <https://doi.org/10.1111/j.1365-2966.2005.09675.x>
- Croton, D. J., Stevens, A. R. H., Tonini, C., Garel, T., Bernyk, M., Bibiano, A., Hodkinson, L., Mutch, S. J., Poole, G. B., & Shattow, G. M. (2016). SEMI-ANALYTIC GALAXY EVOLUTION (SAGE): MODEL CALIBRATION AND BASIC RESULTS. *The Astrophysical Journal Supplement Series*, *222*(2), 22. <https://doi.org/10.3847/0067-0049/222/2/22>
- Daddi, E., Delvecchio, I., Dimauro, P., Magnelli, B., Gomez-Guijarro, C., Coogan, R., Elbaz, D., Kalita, B. S., Le Bail, A., Rich, R. M., & Tan, Q. (2022). The bending of the star-forming main sequence traces the cold- to hot-accretion transition mass over  $0 < z < 4$ . *Astronomy & Astrophysics*, *661*, L7. <https://doi.org/10.1051/0004-6361/202243574>
- Daddi, E., Dickinson, M., Morrison, G., Chary, R., Cimatti, A., Elbaz, D., Frayer, D., Renzini, A., Pope, A., Alexander, D. M., Bauer, F. E., Giavalisco, M., Huynh, M., Kurk, J., & Mignoli, M. (2007). Multiwavelength study of massive galaxies at  $z \sim 2$ . I. star formation and galaxy growth. *The Astrophysical Journal*, *670*(1), 156–172. <https://doi.org/10.1086/521818>
- Daddi, E., Renzini, A., Pirzkal, N., Cimatti, A., Malhotra, S., Stiavelli, M., Xu, C., Pasquali, A., Rhoads, J. E., Brusa, M., Di Serego Alighieri, S., Ferguson, H. C., Koekemoer, A. M., Moustakas, L. A., Panagia, N., & Windhorst, R. A. (2005). Passively evolving early-type galaxies at  $1.4 < z < 2.5$  in the hubble ultra deep field. *The Astrophysical Journal*, *626*(2), 680–697. <https://doi.org/10.1086/430104>
- Davies, J. J., Crain, R. A., Oppenheimer, B. D., & Schaye, J. (2020). The quenching and morphological evolution of central galaxies is facilitated by the feedback-driven expulsion of circumgalactic gas. *Monthly Notices of the Royal Astronomical Society*, *491*(3), 4462–4480. <https://doi.org/10.1093/mnras/stz3201>
- Davis, B. L., Graham, A. W., & Cameron, E. (2019). Black hole mass scaling relations for spiral galaxies. I.  $m_{\text{BH}} - m_{*,\text{sph}}$ . *The Astrophysical Journal*, *873*(1), 85. <https://doi.org/10.3847/1538-4357/aaf3b8>
- Dawoodbhoy, T., Shapiro, P. R., Ocvirk, P., Aubert, D., Gillet, N., Choi, J.-H., Iliev, I. T., Teyssier, R., Yepes, G., Gottlöber, S., D’Aloisio, A., Park, H., & Hoffman, Y. (2018). Suppression of star formation in low-mass galaxies caused by the reionization of their local neighbourhood. *Monthly Notices of the Royal Astronomical Society*, *480*(2), 1740–1753. <https://doi.org/10.1093/mnras/sty1945>

- Dawson, K. S., Kneib, J.-P., Percival, W. J., Alam, S., Albareti, F. D., Anderson, S. F., Armengaud, E., Aubourg, E., Bailey, S., Bautista, J. E., Berlind, A. A., Bershad, M. A., Beutler, F., Bizyaev, D., Blanton, M. R., Blomqvist, M., Bolton, A. S., Bovy, J., Brandt, W. N., . . . Zou, H. (2016). The SDSS-IV extended baryon oscillation spectroscopic survey: Overview and early data. *The Astronomical Journal*, 151(2), 44. <https://doi.org/10.3847/0004-6256/151/2/44>
- Dawson, K. S., Schlegel, D. J., Ahn, C. P., Anderson, S. F., Aubourg, É., Bailey, S., Barkhouser, R. H., Bautista, J. E., Beifiori, A., Berlind, A. A., Bhardwaj, V., Bizyaev, D., Blake, C. H., Blanton, M. R., Blomqvist, M., Bolton, A. S., Borde, A., Bovy, J., Brandt, W. N., . . . Zheng, Z. (2013). The baryon oscillation spectroscopic survey of SDSS-III. *The Astronomical Journal*, 145(1), 10. <https://doi.org/10.1088/0004-6256/145/1/10>
- De Gasperin, F., Edler, H. W., Williams, W. L., Callingham, J. R., Asabere, B., Brügger, M., Brunetti, G., Dijkema, T. J., Hardcastle, M. J., Iacobelli, M., Offringa, A., Norden, M. J., Röttgering, H. J. A., Shimwell, T., Van Weeren, R. J., Tasse, C., Bomans, D. J., Bonafede, A., Botteon, A., . . . Zarka, P. (2023). The LOFAR LBA sky survey: II. first data release. *Astronomy & Astrophysics*, 673, A165. <https://doi.org/10.1051/0004-6361/202245389>
- De Gasperin, F., Williams, W. L., Best, P., Brügger, M., Brunetti, G., Cuciti, V., Dijkema, T. J., Hardcastle, M. J., Norden, M. J., Offringa, A., Shimwell, T., Van Weeren, R., Bomans, D., Bonafede, A., Botteon, A., Callingham, J. R., Cassano, R., Chyży, K. T., Emig, K. L., . . . Röttgering, H. (2021). The LOFAR LBA sky survey: I. survey description and preliminary data release. *Astronomy & Astrophysics*, 648, A104. <https://doi.org/10.1051/0004-6361/202140316>
- De Lucia, G., & Blaizot, J. (2007). The hierarchical formation of the brightest cluster galaxies. *Monthly Notices of the Royal Astronomical Society*, 375(1), 2–14. <https://doi.org/10.1111/j.1365-2966.2006.11287.x>
- Dekel, A., & Silk, J. (1986). The origin of dwarf galaxies, cold dark matter, and biased galaxy formation. *The Astrophysical Journal*, 303, 39. <https://doi.org/10.1086/164050>
- Delvecchio, I., Daddi, E., Shankar, F., Mullaney, J. R., Zamorani, G., Aird, J., Bernhard, E., Cimatti, A., Elbaz, D., Giavalisco, M., & Grimmitt, L. P. (2019). The galaxy’s gas content regulated by the dark matter halo mass results in a superlinear MBH– $m_*$  relation. *The Astrophysical Journal Letters*, 885(2), L36. <https://doi.org/10.3847/2041-8213/ab4e21>
- Delvecchio, I., Gruppioni, C., Pozzi, F., Berta, S., Zamorani, G., Cimatti, A., Lutz, D., Scott, D., Vignali, C., Cresci, G., Feltre, A., Cooray, A., Vaccari, M., Fritz, J., Le Floch, E., Magnelli, B., Popesso, P., Oliver, S., Bock, J., . . . Scodreggio, M. (2014). Tracing the cosmic growth of supermassive black holes to  $z \sim 3$  with herchel. *Monthly Notices of the Royal Astronomical Society*, 439(3), 2736–2754. <https://doi.org/10.1093/mnras/stu130>
- Delvecchio, I., Lutz, D., Berta, S., Rosario, D. J., Zamorani, G., Pozzi, F., Gruppioni, C., Vignali, C., Brusa, M., Cimatti, A., Clements, D. L., Cooray, A., Farrah, D., Lanzuisi, G., Oliver, S., Rodighiero, G., Santini, P., & Symeonidis, M. (2015). Mapping the average AGN accretion rate in the SFR– $m_*$  plane for herchel -selected galaxies at  $0 < z < 2.5$ . *Monthly Notices of the Royal Astronomical Society*, 449(1), 373–389. <https://doi.org/10.1093/mnras/stv213>
- Deshmukh, S., Caputi, K. I., Ashby, M. L. N., Cowley, W. I., McCracken, H. J., Fynbo, J. P. U., Fèvre, O. L., Milvang-Jensen, B., & Ilbert, O. (2018). The spitzer matching survey of the UltraVISTA ultra-deep stripes (SMUVS): The evolution of dusty and nondusty galaxies with stellar mass at  $z = 2–6$ . *The Astrophysical Journal*, 864(2), 166. <https://doi.org/10.3847/1538-4357/aad9f5>
- Di Matteo, T., Springel, V., & Hernquist, L. (2005). Energy input from quasars regulates the growth and activity of black holes and their host galaxies. *Nature*, 433(7026), 604–607. <https://doi.org/10.1038/nature03335>

- Dijkstra, M., Ferrara, A., & Mesinger, A. (2014). Feedback-regulated supermassive black hole seed formation. *Monthly Notices of the Royal Astronomical Society*, 442(3), 2036–2047. <https://doi.org/10.1093/mnras/stu1007>
- Ding, X., Treu, T., Silverman, J. D., Bhowmick, A. K., Menci, N., & Di Matteo, T. (2020). Testing the fidelity of simulations of black hole–galaxy coevolution at  $z \sim 1.5$  with observations. *The Astrophysical Journal*, 896(2), 159. <https://doi.org/10.3847/1538-4357/ab91be>
- Donnari, M., Pillepich, A., Nelson, D., Marinacci, F., Vogelsberger, M., & Hernquist, L. (2021). Quenched fractions in the IllustrisTNG simulations: Comparison with observations and other theoretical models. *Monthly Notices of the Royal Astronomical Society*, 506(4), 4760–4780. <https://doi.org/10.1093/mnras/stab1950>
- Draine, B. T., Aniano, G., Krause, O., Groves, B., Sandstrom, K., Braun, R., Leroy, A., Klaas, U., Linz, H., Rix, H.-W., Schinnerer, E., Schmiedeke, A., & Walter, F. (2014). Andromeda’s dust [ADS Bibcode: 2014ApJ...780..172D]. *The Astrophysical Journal*, 780, 172. <https://doi.org/10.1088/0004-637X/780/2/172>
- Driver, S. P., Hill, D. T., Kelvin, L. S., Robotham, A. S. G., Liske, J., Norberg, P., Baldry, I. K., Bamford, S. P., Hopkins, A. M., Loveday, J., Peacock, J. A., Andrae, E., Bland-Hawthorn, J., Brough, S., Brown, M. J. I., Cameron, E., Ching, J. H. Y., Colless, M., Conselice, C. J., ... Warren, S. J. (2011). Galaxy and mass assembly (GAMA): Survey diagnostics and core data release: GAMA. *Monthly Notices of the Royal Astronomical Society*, 413(2), 971–995. <https://doi.org/10.1111/j.1365-2966.2010.18188.x>
- Du, Lu, K.-X., Zhang, Z.-X., Huang, Y.-K., Wang, K., Hu, C., Qiu, J., Li, Y.-R., Fan, X.-L., Fang, X.-E., Bai, J.-M., Bian, W.-H., Yuan, Y.-F., Ho, L. C., Wang, J.-M., & (SEAMBH collaboration). (2016). SUPERMASSIVE BLACK HOLES WITH HIGH ACCRETION RATES IN ACTIVE GALACTIC NUCLEI. v. a NEW SIZE–LUMINOSITY SCALING RELATION FOR THE BROAD-LINE REGION. *The Astrophysical Journal*, 825(2), 126. <https://doi.org/10.3847/0004-637X/825/2/126>
- Du, M., Ho, L. C., Debattista, V. P., Pillepich, A., Nelson, D., Hernquist, L., & Weinberger, R. (2021). The evolutionary pathways of disk-, bulge-, and halo-dominated galaxies. *The Astrophysical Journal*, 919(2), 135. <https://doi.org/10.3847/1538-4357/ac0e98>
- Dunlop, J. S., McLure, R. J., Yamada, T., Kajisawa, M., Peacock, J. A., Mann, R. G., Hughes, D. H., Aretxaga, I., Muxlow, T. W. B., Richards, A. M. S., Dickinson, M., Ivison, R. J., Smith, G. P., Smail, I., Serjeant, S., Almaini, O., & Lawrence, A. (2004). Discovery of the galaxy counterpart of HDF 850.1, the brightest submillimetre source in the *Hubble Deep Field*. *Monthly Notices of the Royal Astronomical Society*, 350(3), 769–784. <https://doi.org/10.1111/j.1365-2966.2004.07700.x>
- Duras, F., Bongiorno, A., Ricci, F., Piconcelli, E., Shankar, F., Lusso, E., Bianchi, S., Fiore, F., Maiolino, R., Marconi, A., Onori, F., Sani, E., Schneider, R., Vignali, C., & La Franca, F. (2020). Universal bolometric corrections for active galactic nuclei over seven luminosity decades. *Astronomy & Astrophysics*, 636, A73. <https://doi.org/10.1051/0004-6361/201936817>
- Eales, S., Dunne, L., Clements, D., Cooray, A., De Zotti, G., Dye, S., Ivison, R., Jarvis, M., Lagache, G., Maddox, S., Negrello, M., Serjeant, S., Thompson, M. A., Van Kampen, E., Amblard, A., Andreani, P., Baes, M., Beelen, A., Bendo, G. J., ... White, G. J. (2010). The herchel ATLAS. *Publications of the Astronomical Society of the Pacific*, 122(891), 499–515. <https://doi.org/10.1086/653086>
- Elbaz, D., Daddi, E., Le Borgne, D., Dickinson, M., Alexander, D. M., Chary, R.-R., Starck, J.-L., Brandt, W. N., Kitzbichler, M., MacDonald, E., Nonino, M., Popesso, P., Stern, D., & Vanzella,

- E. (2007). The reversal of the star formation-density relation in the distant universe. *Astronomy & Astrophysics*, 468(1), 33–48. <https://doi.org/10.1051/0004-6361:20077525>
- Elbaz, D., Dickinson, M., Hwang, H. S., Díaz-Santos, T., Magdis, G., Magnelli, B., Le Borgne, D., Galliano, F., Pannella, M., Chanial, P., Armus, L., Charmandaris, V., Daddi, E., Aussel, H., Popesso, P., Kartaltepe, J., Altieri, B., Valtchanov, I., Coia, D., ... Wilson, G. (2011). GOODS–*Herschel* : An infrared main sequence for star-forming galaxies. *Astronomy & Astrophysics*, 533, A119. <https://doi.org/10.1051/0004-6361/201117239>
- Ellison, S. L., Wong, T., Sánchez, S. F., Colombo, D., Bolatto, A., Barrera-Ballesteros, J., García-Benito, R., Kalinova, V., Luo, Y., Rubio, M., & Vogel, S. N. (2021). The EDGE–CALIFA survey: Central molecular gas depletion in AGN host galaxies – a smoking gun for quenching? *Monthly Notices of the Royal Astronomical Society: Letters*, 505(1), L46–L51. <https://doi.org/10.1093/mnrasl/slab047>
- Elvis, M., Wilkes, B. J., McDowell, J. C., Green, R. F., Bechtold, J., Willner, S. P., Oey, M. S., Polomski, E., & Cutri, R. (1994). Atlas of quasar energy distributions. *The Astrophysical Journal Supplement Series*, 95, 1. <https://doi.org/10.1086/192093>
- Fabian, A. C. (2012). Observational evidence of AGN feedback. *Annual Review of Astronomy and Astrophysics*, 50(1), 455–489. <https://doi.org/10.1146/annurev-astro-081811-125521>
- Faucher-Giguère, C.-A., & Quataert, E. (2012). The physics of galactic winds driven by active galactic nuclei: AGN outflow physics. *Monthly Notices of the Royal Astronomical Society*, 425(1), 605–622. <https://doi.org/10.1111/j.1365-2966.2012.21512.x>
- Ferrarese, L., & Merritt, D. (2000). A fundamental relation between supermassive black holes and their host galaxies. *The Astrophysical Journal*, 539(1), L9–L12. <https://doi.org/10.1086/312838>
- Figueira, M., Pollo, A., Malek, K., Buat, V., Boquien, M., Pistis, F., Cassarà, L. P., Vergani, D., Hamed, M., & Salim, S. (2022). SFR estimations from  $z = 0$  to  $z = 0.9$ : A comparison of SFR calibrators for star-forming galaxies. *Astronomy & Astrophysics*, 667, A29. <https://doi.org/10.1051/0004-6361/202141701>
- Firmani, C., & Avila-Reese, V. (2010). GALAXY DOWNSIZING EVIDENCED BY HYBRID EVOLUTIONARY TRACKS. *The Astrophysical Journal*, 723(1), 755–766. <https://doi.org/10.1088/0004-637X/723/1/755>
- Fonseca Alvarez, G., Trump, J. R., Homayouni, Y., Grier, C. J., Shen, Y., Horne, K., Li, J. I.-H., Brandt, W. N., Ho, L. C., Peterson, B. M., & Schneider, D. P. (2020). The sloan digital sky survey reverberation mapping project: The  $h$  radius–luminosity relation. *The Astrophysical Journal*, 899(1), 73. <https://doi.org/10.3847/1538-4357/aba001>
- Fornasini, F. M., Elvis, M., Maksym, W. P., Fabbiano, G., Bergmann, T. S., Gandhi, P., & Whittle, M. (2022). Termination shocks and the extended x-ray emission in mrk 78. *The Astrophysical Journal*, 931(1), 65. <https://doi.org/10.3847/1538-4357/ac694d>
- Fritz, J., Franceschini, A., & Hatziminaoglou, E. (2006). Revisiting the infrared spectra of active galactic nuclei with a new torus emission model. *Monthly Notices of the Royal Astronomical Society*, 366(3), 767–786. <https://doi.org/10.1111/j.1365-2966.2006.09866.x>
- Gabuzda, D. C., Murray, É., & Cronin, P. (2004). Helical magnetic fields associated with the relativistic jets of four BL lac objects. *Monthly Notices of the Royal Astronomical Society*, 351(4), L89–L93. <https://doi.org/10.1111/j.1365-2966.2004.08037.x>
- García-Bernete, I., González-Martín, O., Ramos Almeida, C., Alonso-Herrero, A., Martínez-Paredes, M., Ward, M. J., Roche, P. F., Acosta-Pulido, J. A., López-Rodríguez, E., Rigopoulou, D., & Esparza-Arredondo, D. (2022). Torus and polar dust dependence on active galactic nucleus

- properties. *Astronomy & Astrophysics*, 667, A140. <https://doi.org/10.1051/0004-6361/202244230>
- Gawiser, E. (2005, December 15). Galaxy formation [version: 1]. <https://doi.org/10.48550/arXiv.astro-ph/0512384>
- Geach, J. E., Dunlop, J. S., Halpern, M., Smail, I., Van Der Werf, P., Alexander, D. M., Almaini, O., Aretxaga, I., Arumugam, V., Asboth, V., Banerji, M., Beanlands, J., Best, P. N., Blain, A. W., Birkinshaw, M., Chapin, E. L., Chapman, S. C., Chen, C.-C., Chrysostomou, A., ... Zemcov, M. (2017). The SCUBA-2 cosmology legacy survey: 850  $\mu\text{m}$  maps, catalogues and number counts. *Monthly Notices of the Royal Astronomical Society*, 465(2), 1789–1806. <https://doi.org/10.1093/mnras/stw2721>
- Gilli, R., Comastri, A., & Hasinger, G. (2007). The synthesis of the cosmic x-ray background in the chandra and XMM-newton era. *Astronomy & Astrophysics*, 463(1), 79–96. <https://doi.org/10.1051/0004-6361:20066334>
- Gonzalez Delgado, R. M., Heckman, T., Leitherer, C., Meurer, G., Krolik, J., Wilson, A. S., Kinney, A., & Koratkar, A. (1998). Ultraviolet-optical observations of the seyfert 2 galaxies NGC 7130, NGC 5135, and IC 3639: Implications for the starburst–active galactic nucleus connection. *The Astrophysical Journal*, 505(1), 174–198. <https://doi.org/10.1086/306154>
- González-Alfonso, E., Fischer, J., Spoon, H. W. W., Stewart, K. P., Ashby, M. L. N., Veilleux, S., Smith, H. A., Sturm, E., Farrah, D., Falstad, N., Meléndez, M., Graciá-Carpio, J., Janssen, A. W., & Lebouteiller, V. (2017). Molecular outflows in local ULIRGs: Energetics from multitransition OH analysis. *The Astrophysical Journal*, 836(1), 11. <https://doi.org/10.3847/1538-4357/836/1/11>
- Griffin, M. J., Abergel, A., Abreu, A., Ade, P. A. R., André, P., Augeres, J. .-, Babbedge, T., Bae, Y., Baillie, T., Baluteau, J. .-, Barlow, M. J., Bendo, G., Benielli, D., Bock, J. J., Bonhomme, P., Brisbin, D., Brockley-Blatt, C., Caldwell, M., Cara, C., ... Zonca, E. (2010). The herschel-SPIRE instrument and its in-flight performance [ADS Bibcode: 2010A&A...518L...3G]. *Astronomy and Astrophysics*, 518, L3. <https://doi.org/10.1051/0004-6361/201014519>
- Gunn, J. E., Siegmund, W. A., & Mannery, E. J. M. e. (2006). The 2.5 m telescope of the sloan digital sky survey. *The Astronomical Journal*, 131(4), 2332–2359. <https://doi.org/10.1086/500975>
- Gürkan, G., Hardcastle, M. J., Jarvis, M. J., Smith, D. J. B., Bourne, N., Dunne, L., Maddox, S., Ivison, R. J., & Fritz, J. (2015). *Herschel* -ATLAS: The connection between star formation and AGN activity in radio-loud and radio-quiet active galaxies. *Monthly Notices of the Royal Astronomical Society*, 452(4), 3776–3794. <https://doi.org/10.1093/mnras/stv1502>
- Habouzit, M., Genel, S., Somerville, R. S., Kocevski, D., Hirschmann, M., Dekel, A., Choi, E., Nelson, D., Pillepich, A., Torrey, P., Hernquist, L., Vogelsberger, M., Weinberger, R., & Springel, V. (2019). Linking galaxy structural properties and star formation activity to black hole activity with IllustrisTNG. *Monthly Notices of the Royal Astronomical Society*, 484(4), 4413–4443. <https://doi.org/10.1093/mnras/stz102>
- Harikane, Y., Inoue, A. K., Mawatari, K., Hashimoto, T., Yamanaka, S., Fudamoto, Y., Matsuo, H., Tamura, Y., Dayal, P., Yung, L. Y. A., Hutter, A., Pacucci, F., Sugahara, Y., & Koekemoer, A. M. (2022). A search for h-dropout lyman break galaxies at  $z = 12$ –16. *The Astrophysical Journal*, 929(1), 1. <https://doi.org/10.3847/1538-4357/ac53a9>
- Harikane, Y., Zhang, Y., Nakajima, K., Ouchi, M., Isobe, Y., Ono, Y., Hatano, S., Xu, Y., & Umeda, H. (2023). A JWST/NIRSpec first census of broad-line AGNs at  $z = 4$ –7: Detection of 10 faint AGNs with  $m_{\text{BH}} = 10^6$ – $10^8 M_{\odot}$  and their host galaxy properties. *The Astrophysical Journal*, 959(1), 39. <https://doi.org/10.3847/1538-4357/ad029e>

- Häring, N., & Rix, H.-W. (2004). On the black hole mass-bulge mass relation [ADS Bibcode: 2004ApJ...604L..89H]. *The Astrophysical Journal*, 604, L89–L92. <https://doi.org/10.1086/383567>
- Harrison, C. M., & Ramos Almeida, C. (2024). Observational tests of active galactic nuclei feedback: An overview of approaches and interpretation. *Galaxies*, 12(2), 17. <https://doi.org/10.3390/galaxies12020017>
- Hatziminaoglou, E., Farrah, D., Humphreys, E., Manrique, A., Pérez-Fournon, I., Pitchford, L. K., Salvador-Solé, E., & Wang, L. (2018). On the multiplicity of ALMA compact array counterparts of far-infrared bright quasars. *Monthly Notices of the Royal Astronomical Society*. <https://doi.org/10.1093/mnras/sty2073>
- Heavens, A., Panter, B., Jimenez, R., & Dunlop, J. (2004). The star-formation history of the universe from the stellar populations of nearby galaxies. *Nature*, 428(6983), 625–627. <https://doi.org/10.1038/nature02474>
- Heckman, T., & Best, P. (2014). The co-evolution of galaxies and supermassive black holes: Insights from surveys of the contemporary universe. *Annual Review of Astronomy and Astrophysics*, 52(1), 589–660. <https://doi.org/10.1146/annurev-astro-081913-035722>
- Helou, G., Soifer, B. T., & Rowan-Robinson, M. (1985). Thermal infrared and nonthermal radio : Remarkable correlation in disks of galaxies. [ADS Bibcode: 1985ApJ...298L...7H]. *The Astrophysical Journal*, 298, L7–L11. <https://doi.org/10.1086/184556>
- Henriques, B. M. B., White, S. D. M., Lilly, S. J., Bell, E. F., Bluck, A. F. L., & Terrazas, B. A. (2019). The origin of the mass scales for maximal star formation efficiency and quenching: The critical role of supernovae. *Monthly Notices of the Royal Astronomical Society*, 485(3), 3446–3456. <https://doi.org/10.1093/mnras/stz577>
- Hewitt, A., & Burbidge, G. (1993). A revised and updated catalog of quasi-stellar objects. *The Astrophysical Journal Supplement Series*, 87, 451. <https://doi.org/10.1086/191811>
- Heywood, I., Jarvis, M. J., Hale, C. L., Whittam, I. H., Bester, H. L., Hugo, B., Kenyon, J. S., Prescott, M., Smirnov, O. M., Tasse, C., Afonso, J. M., Best, P. N., Collier, J. D., Deane, R. P., Frank, B. S., Hardcastle, M. J., Knowles, K., Maddox, N., Murphy, E. J., ... Thorat, K. (2022). MIGHTEE: Total intensity radio continuum imaging and the COSMOS/XMM-LSS early science fields [ADS Bibcode: 2022MNRAS.509.2150H]. *Monthly Notices of the Royal Astronomical Society*, 509, 2150–2168. <https://doi.org/10.1093/mnras/stab3021>
- Heywood, I., Murphy, E. J., Jiménez-Andrade, E. F., Armus, L., Cotton, W. D., DeCoursey, C., Dickinson, M., Lazio, T. J. W., Momjian, E., Penner, K., Smail, I., & Smirnov, O. M. (2021). The VLA frontier fields survey: Deep, high-resolution radio imaging of the MACS lensing clusters at 3 and 6 GHz. *The Astrophysical Journal*, 910(2), 105. <https://doi.org/10.3847/1538-4357/abdf61>
- Hill, G. J., Gebhardt, K., Komatsu, E., Drory, N., MacQueen, P. J., Adams, J., Blanc, G. A., Koehler, R., Rafal, M., Roth, M. M., Kelz, A., Gronwall, C., Ciardullo, R., & Schneider, D. P. (2008, June 1). The hobby-eblerly telescope dark energy experiment (HETDEX): Description and early pilot survey results. <https://doi.org/10.48550/arXiv.0806.0183>
- Hiroi, K., Ueda, Y., Akiyama, M., & Watson, M. G. (2012). COMOVING SPACE DENSITY AND OBSCURED FRACTION OF HIGH-REDSHIFT ACTIVE GALACTIC NUCLEI IN THE SUBARU/ XMM-NEWTON DEEP SURVEY. *The Astrophysical Journal*, 758(1), 49. <https://doi.org/10.1088/0004-637X/758/1/49>
- Hirschmann, M., Khochfar, S., Burkert, A., Naab, T., Genel, S., & Somerville, R. S. (2010). On the evolution of the intrinsic scatter in black hole versus galaxy mass relations: Scatter evolution of massive black holes. *Monthly Notices of the Royal Astronomical Society*, 407(2), 1016–1032. <https://doi.org/10.1111/j.1365-2966.2010.17006.x>

- Hodge, J. A., Becker, R. H., White, R. L., Richards, G. T., & Zeimann, G. R. (2011). HIGH-RESOLUTION VERY LARGE ARRAY IMAGING OF SLOAN DIGITAL SKY SURVEY STRIPE 82 AT 1.4 GHz. *The Astronomical Journal*, *142*(1), 3. <https://doi.org/10.1088/0004-6256/142/1/3>
- Holland, W. S., Robson, E. I., Gear, W. K., Cunningham, C. R., Lightfoot, J. F., Jenness, T., Ivison, R. J., Stevens, J. A., Ade, P. A. R., Griffin, M. J., Duncan, W. D., Murphy, J. A., & Naylor, D. A. (1999). SCUBA: A common-user submillimetre camera operating on the James Clerk Maxwell telescope. *Monthly Notices of the Royal Astronomical Society*, *303*(4), 659–672. <https://doi.org/10.1046/j.1365-8711.1999.02111.x>
- Homayouni, Y., Trump, J. R., Grier, C. J., Horne, K., Shen, Y., Brandt, W. N., Dawson, K. S., Alvarez, G. F., Green, P. J., Hall, P. B., Hernández Santisteban, J. V., Ho, L. C., Kinemuchi, K., Kochanek, C. S., Li, J. I.-H., Peterson, B. M., Schneider, D. P., Starkey, D. A., Bizyaev, D., ... Simmons, A. (2020). The Sloan Digital Sky Survey Reverberation Mapping Project: Mg II lag results from four years of monitoring. *The Astrophysical Journal*, *901*(1), 55. <https://doi.org/10.3847/1538-4357/ababa9>
- Hopkins, P. F., Hernquist, L., Cox, T. J., & Kereš, D. (2008). A cosmological framework for the co-evolution of quasars, supermassive black holes, and elliptical galaxies. I. Galaxy mergers and quasar activity. *The Astrophysical Journal Supplement Series*, *175*(2), 356–389. <https://doi.org/10.1086/524362>
- Hopkins, P. F., Somerville, R. S., Hernquist, L., Cox, T. J., Robertson, B., & Li, Y. (2006). The relation between quasar and merging galaxy luminosity functions and the merger-driven star formation history of the universe. *The Astrophysical Journal*, *652*(2), 864–888. <https://doi.org/10.1086/508503>
- Humphrey, A., Villar-Martín, M., Ramos Almeida, C., Tadhunter, C. N., Arribas, S., Bessiere, P. S., & Cabrera-Lavers, A. (2015). VLT FORS2 optical imaging and spectroscopy of nine luminous type 2 AGN at  $0.3 < z < 0.6$  – I. Ionized gas nebulae. *Monthly Notices of the Royal Astronomical Society*, *454*(4), 4452–4466. <https://doi.org/10.1093/mnras/stv2177>
- Hurley, P. D., Oliver, S., Betancourt, M., Clarke, C., Cowley, W. I., Duivenvoorden, S., Farrah, D., Griffin, M., Lacey, C., Le Floch, E., Papadopoulos, A., Sargent, M., Scudder, J. M., Vaccari, M., Valtchanov, I., & Wang, L. (2017). HELP: Xid+, the probabilistic de-blender for *Herschel* SPIRE maps. *Monthly Notices of the Royal Astronomical Society*, *464*(1), 885–896. <https://doi.org/10.1093/mnras/stw2375>
- Husemann, B., Jahnke, K., Sánchez, S. F., Wisotzki, L., Nugroho, D., Kupko, D., & Schramm, M. (2014). Integral field spectroscopy of nearby QSOs – I. ENLR size–luminosity relation, ongoing star formation and resolved gas-phase metallicities. *Monthly Notices of the Royal Astronomical Society*, *443*(1), 755–783. <https://doi.org/10.1093/mnras/stu1167>
- Inayoshi, K., Omukai, K., & Tasker, E. (2014). Formation of an embryonic supermassive star in the first galaxy. *Monthly Notices of the Royal Astronomical Society: Letters*, *445*(1), L109–L113. <https://doi.org/10.1093/mnrasl/slu151>
- Ito, K., Tanaka, M., Miyaji, T., Ilbert, O., Kauffmann, O. B., Koekemoer, A. M., Marchesi, S., Shuntov, M., Toft, S., Valentino, F., & Weaver, J. R. (2022). COSMOS2020: Ubiquitous AGN activity of massive quiescent galaxies at  $0 < z < 5$  revealed by x-ray and radio stacking. *The Astrophysical Journal*, *929*(1), 53. <https://doi.org/10.3847/1538-4357/ac5aaf>
- Ivison, R. J., Page, M. J., Cirasuolo, M., Harrison, C. M., Mainieri, V., Arumugam, V., & Dudzevičiūtė, U. (2019). Hyperluminous starburst gives up its secrets. *Monthly Notices of the Royal Astronomical Society*, *489*(1), 427–436. <https://doi.org/10.1093/mnras/stz2180>
- Jansen, F., Lumb, D., Altieri, B., Clavel, J., Ehle, M., Erd, C., Gabriel, C., Guainazzi, M., Gondoin, P., Much, R., Muñoz, R., Santos, M., Schartel, N., Texier, D., & Vacanti, G. (2001). XMM-

- newton observatory: I. the spacecraft and operations. *Astronomy & Astrophysics*, 365(1), L1–L6. <https://doi.org/10.1051/0004-6361:20000036>
- Jarvis, M., Taylor, R., Agudo, I., Allison, J. R., Deane, R. P., Frank, B., Gupta, N., Heywood, I., Maddox, N., McAlpine, K., Santos, M., Scaife, A. M., Vaccari, M., Zwart, J. T., Adams, E. A. K., Bacon, D. J., Baker, A. J., Bassett, B. A., Best, P. N., ... Smith, D. J. (2018). The MeerKAT international GHz tiered extragalactic exploration (MIGHTEE) survey. *Proceedings of MeerKAT Science: On the Pathway to the SKA — PoS(MeerKAT2016)*, 006. <https://doi.org/10.22323/1.277.0006>
- Jarvis, M. J., Smith, D. J. B., Bonfield, D. G., Hardcastle, M. J., Falder, J. T., Stevens, J. A., Ivison, R. J., Auld, R., Baes, M., Baldry, I. K., Bamford, S. P., Bourne, N., Buttiglione, S., Cava, A., Cooray, A., Dariush, A., De Zotti, G., Dunlop, J. S., Dunne, L., ... White, G. (2010). Herschel-ATLAS: The far-infrared-radio correlation at  $z \lesssim 0.5$ : The far-infrared-radio correlation at  $z \lesssim 0.5$ . *Monthly Notices of the Royal Astronomical Society*, 409(1), 92–101. <https://doi.org/10.1111/j.1365-2966.2010.17772.x>
- Johnson, H. L., & Morgan, W. W. (1953). Fundamental stellar photometry for standards of spectral type on the revised system of the yerkes spectral atlas. *The Astrophysical Journal*, 117, 313. <https://doi.org/10.1086/145697>
- Just, D. W., Brandt, W. N., Shemmer, O., Steffen, A. T., Schneider, D. P., Chartas, G., & Garmire, G. P. (2007). The x-ray properties of the most luminous quasars from the sloan digital sky survey. *The Astrophysical Journal*, 665(2), 1004. <https://doi.org/10.1086/519990>
- Kakimoto, T., Tanaka, M., Onodera, M., Shimakawa, R., Wu, P.-F., Gould, K. M. L., Ito, K., Jin, S., Kubo, M., Suzuki, T. L., Toft, S., Valentino, F., & Yabe, K. (2024). A massive quiescent galaxy in a group environment at  $z = 4.53$ . *The Astrophysical Journal*, 963(1), 49. <https://doi.org/10.3847/1538-4357/ad1ff1>
- Kalfountzou, E., Stevens, J. A., Jarvis, M. J., Hardcastle, M. J., Smith, D. J. B., Bourne, N., Dunne, L., Ibar, E., Eales, S., Ivison, R. J., Maddox, S., Smith, M. W. L., Valiante, E., & De Zotti, G. (2014). Herschel-ATLAS : Far-infrared properties of radio-loud and radio-quiet quasars. *Monthly Notices of the Royal Astronomical Society*, 442(2), 1181–1196. <https://doi.org/10.1093/mnras/stu782>
- Kalfountzou, E., Stevens, J. A., Jarvis, M. J., Hardcastle, M. J., Wilner, D., Elvis, M., Page, M. J., Trichas, M., & Smith, D. J. B. (2017). Observational evidence that positive and negative AGN feedback depends on galaxy mass and jet power. *Monthly Notices of the Royal Astronomical Society*, 471(1), 28–58. <https://doi.org/10.1093/mnras/stx1333>
- Kalita, B. S., Daddi, E., Bournaud, F., Rich, R. M., Valentino, F., Gómez-Guijarro, C., Codis, S., Delvecchio, I., Elbaz, D., Strazzullo, V., De Souza Magalhaes, V., Pety, J., & Tan, Q. (2022). Bulge formation inside quiescent lopsided stellar disks: Connecting accretion, star formation, and morphological transformation in a  $z \sim 3$  galaxy group. *Astronomy & Astrophysics*, 666, A44. <https://doi.org/10.1051/0004-6361/202243100>
- Kauffmann, G., White, S. D. M., & Guiderdoni, B. (1993). The formation and evolution of galaxies within merging dark matter haloes\*. *Monthly Notices of the Royal Astronomical Society*, 264(1), 201–218. <https://doi.org/10.1093/mnras/264.1.201>
- Kawaguchi, T., Yutani, N., & Wada, K. (2020). Mass accretion toward black holes in the final phase of galaxy mergers. *The Astrophysical Journal*, 890(2), 125. <https://doi.org/10.3847/1538-4357/ab655a>
- Kellermann, K. I., Condon, J. J., Kimball, A. E., Perley, R. A., & Ivezić, Ž. (2016). RADIO-LOUD AND RADIO-QUIET QSOs. *The Astrophysical Journal*, 831(2), 168. <https://doi.org/10.3847/0004-637X/831/2/168>

- Kennicutt. (1983). The rate of star formation in normal disk galaxies. *The Astrophysical Journal*, 272, 54. <https://doi.org/10.1086/161261>
- Kennicutt. (1998). Star formation in galaxies along the hubble sequence [ADS Bibcode: 1998ARA&A..36..189K]. *Annual Review of Astronomy and Astrophysics*, 36, 189–232. <https://doi.org/10.1146/annurev.astro.36.1.189>
- Kennicutt & Evans, N. J. (2012). Star formation in the milky way and nearby galaxies. *Annual Review of Astronomy and Astrophysics*, 50(1), 531–608. <https://doi.org/10.1146/annurev-astro-081811-125610>
- Kennicutt, R. C., Hao, C.-N., Calzetti, D., Moustakas, J., Dale, D. A., Bendo, G., Engelbracht, C. W., Johnson, B. D., & Lee, J. C. (2009). DUST-CORRECTED STAR FORMATION RATES OF GALAXIES. i. COMBINATIONS OF h AND INFRARED TRACERS. *The Astrophysical Journal*, 703(2), 1672–1695. <https://doi.org/10.1088/0004-637X/703/2/1672>
- Kim, D., & Im, M. (2018). What makes red quasars red?: Observational evidence for dust extinction from line ratio analysis. *Astronomy & Astrophysics*, 610, A31. <https://doi.org/10.1051/0004-6361/201731963>
- Kim, D., Im, M., Glikman, E., Woo, J.-H., & Urrutia, T. (2015). ACCRETION RATES OF RED QUASARS FROM THE HYDROGEN  $\rho$  LINE. *The Astrophysical Journal*, 812(1), 66. <https://doi.org/10.1088/0004-637X/812/1/66>
- King, A. R., & Pounds, K. A. (2003). Black hole winds. *Monthly Notices of the Royal Astronomical Society*, 345(2), 657–659. <https://doi.org/10.1046/j.1365-8711.2003.06980.x>
- Kirkpatrick, A., Urry, C. M., Brewster, J., Cooke, K. C., Estrada, M., Glikman, E., Hamblin, K., Ananna, T. T., Carlile, C., Coleman, B., Johnson, J., Kartaltepe, J. S., LaMassa, S. M., Marchesi, S., Powell, M., Sanders, D., Treister, E., & Jan Turner, T. (2020). The accretion history of AGN: A newly defined population of cold quasars. *The Astrophysical Journal*, 900(1), 5. <https://doi.org/10.3847/1538-4357/aba358>
- Klessen, R. S., & Glover, S. C. O. (2016). Physical processes in the interstellar medium [ADS Bibcode: 2016SAAS...43...85K]. *Saas-Fee Advanced Course*, 43, 85. [https://doi.org/10.1007/978-3-662-47890-5\\_2](https://doi.org/10.1007/978-3-662-47890-5_2)
- Kokorev, V., Fujimoto, S., Labbe, I., Greene, J. E., Bezanson, R., Dayal, P., Nelson, E. J., Atek, H., Brammer, G., Caputi, K. I., Chemerynska, I., Cutler, S. E., Feldmann, R., Fudamoto, Y., Furtak, L. J., Goulding, A. D., De Graaff, A., Leja, J., Marchesini, D., ... Zitrin, A. (2023). UNCOVER: A NIRSpect identification of a broad-line AGN at  $z = 8.50$ . *The Astrophysical Journal Letters*, 957(1), L7. <https://doi.org/10.3847/2041-8213/ad037a>
- Kormendy, J., & Ho, L. C. (2013). Coevolution (or not) of supermassive black holes and host galaxies. *Annual Review of Astronomy and Astrophysics*, 51(1), 511–653. <https://doi.org/10.1146/annurev-astro-082708-101811>
- Kouroumpatzakis, K., Zezas, A., Sell, P., Kovelakas, K., Bonfini, P., Willner, S. P., Ashby, M. L. N., Maragkoudakis, A., & Jarrett, T. H. (2020). Sub-galactic scaling relations between x-ray luminosity, star formation rate, and stellar mass. *Monthly Notices of the Royal Astronomical Society*, 494(4), 5967–5984. <https://doi.org/10.1093/mnras/staa1063>
- Krolik, J. H., & Begelman, M. C. (1988). Molecular tori in seyfert galaxies - feeding the monster and hiding it. *The Astrophysical Journal*, 329, 702. <https://doi.org/10.1086/166414>
- Kuźmicz, A., Sethi, S., & Jamrozy, M. (2021). Giant radio quasars: Composite optical spectra. *The Astrophysical Journal*, 922(1), 52. <https://doi.org/10.3847/1538-4357/ac27ad>
- La Plante, P., & Trac, H. (2016). HELIUM REIONIZATION SIMULATIONS. i. MODELING QUASARS AS RADIATION SOURCES. *The Astrophysical Journal*, 828(2), 90. <https://doi.org/10.3847/0004-637X/828/2/90>

- Larson, K. L., Sanders, D. B., Barnes, J. E., Ishida, C. M., Evans, A. S., U, V., Mazzarella, J. M., Kim, D.-C., Privon, G. C., Mirabel, I. F., & Flewelling, H. A. (2016). MORPHOLOGY AND MOLECULAR GAS FRACTIONS OF LOCAL LUMINOUS INFRARED GALAXIES AS a FUNCTION OF INFRARED LUMINOSITY AND MERGER STAGE. *The Astrophysical Journal*, 825(2), 128. <https://doi.org/10.3847/0004-637X/825/2/128>
- Le Floch, E., Papovich, C., Dole, H., Bell, E. F., Lagache, G., Rieke, G. H., Egami, E., Perez-Gonzalez, P. G., Alonso-Herrero, A., Rieke, M. J., Blaylock, M., Engelbracht, C. W., Gordon, K. D., Hines, D. C., Misselt, K. A., Morrison, J. E., & Mould, J. (2005). Infrared luminosity functions from the chandra deep field–south: The *Spitzer* view on the history of dusty star formation at  $0 < z < 1$ . *The Astrophysical Journal*, 632(1), 169–190. <https://doi.org/10.1086/432789>
- Lee, Ogle, P. M., Canizares, C. R., Marshall, H. L., Schulz, N. S., Morales, R., Fabian, A. C., & Iwasawa, K. (2001). Revealing the dusty warm absorber in MCG 6-30-15 with the [ITAL]chandra[ITAL] high-energy transmission grating. *The Astrophysical Journal*, 554(1), L13–L17. <https://doi.org/10.1086/320912>
- Lee, Sanders, D. B., Casey, C. M., Toft, S., Scoville, N. Z., Hung, C.-L., Le Floch, E., Ilbert, O., Zahid, H. J., Aussel, H., Capak, P., Kartaltepe, J. S., Kewley, L. J., Li, Y., Schawinski, K., Sheth, K., & Xiao, Q. (2015). A TURNOVER IN THE GALAXY MAIN SEQUENCE OF STAR FORMATION AT  $M_* > 10^{10} M_\odot$  FOR REDSHIFTS  $z < 1.3$ . *The Astrophysical Journal*, 801(2), 80. <https://doi.org/10.1088/0004-637X/801/2/80>
- Leitherer, C., Li, I.-H., Calzetti, D., & Heckman, T. M. (2002). Global far-ultraviolet (912–1800 Å) properties of star-forming galaxies. *The Astrophysical Journal Supplement Series*, 140(2), 303–329. <https://doi.org/10.1086/342486>
- Li, Shen, Y., Ho, L. C., Brandt, W. N., Grier, C. J., Hall, P. B., Homayouni, Y., Koekemoer, A. M., Schneider, D. P., & Trump, J. R. (2023). The sloan digital sky survey reverberation mapping project: The black hole mass–stellar mass relations at  $0.2 < z < 0.8$ . *The Astrophysical Journal*, 954(2), 173. <https://doi.org/10.3847/1538-4357/acddda>
- Li, Silverman, J. D., Ding, X., Strauss, M. A., Goulding, A., Birrer, S., Yesuf, H. M., Xue, Y., Kawinwanichakij, L., Matsuoka, Y., Toba, Y., Nagao, T., Schramm, M., & Inayoshi, K. (2021). The sizes of quasar host galaxies in the hyper supprime-cam subaru strategic program. *The Astrophysical Journal*, 918(1), 22. <https://doi.org/10.3847/1538-4357/ac06a8>
- Li, Zimmerman, E. R., Narayan, R., & McClintock, J. E. (2005). Multitemperature blackbody spectrum of a thin accretion disk around a kerr black hole: Model computations and comparison with observations. *The Astrophysical Journal Supplement Series*, 157(2), 335–370. <https://doi.org/10.1086/428089>
- Liu, Gebhardt, K., Cooper, E. M., Davis, D., Schneider, D. P., Ciardullo, R., Farrow, D. J., Finkelstein, S. L., Gronwall, C., Guo, Y., Hill, G. J., House, L., Jeong, D., Jogee, S., Kollatschny, W., Krumpke, M., Landriau, M., Chavez Ortiz, O. A., Zhang, Y., & (The HETDEX Collaboration). (2022). The active galactic nuclei in the hobby–eberly telescope dark energy experiment survey (HETDEX). i. sample selection. *The Astrophysical Journal Supplement Series*, 261(2), 24. <https://doi.org/10.3847/1538-4365/ac6ba6>
- Liu, Zakamska, N. L., Greene, J. E., Nesvadba, N. P. H., & Liu, X. (2013). Observations of feedback from radio-quiet quasars – II. kinematics of ionized gas nebulae. *Monthly Notices of the Royal Astronomical Society*, 436(3), 2576–2597. <https://doi.org/10.1093/mnras/stt1755>
- Lu, N., Bendo, G. J., Boselli, A., Baes, M., Wu, H., Madden, S. C., Looze, I. D., Rémy-Ruyer, A., Boquien, M., Wilson, C. D., Galametz, M., Lam, M. I., Cooray, A., Spinoglio, L., & Zhao, Y. (2014). QUANTIFYING THE HEATING SOURCES FOR MID-INFRARED DUST

- EMISSIONS IN GALAXIES: THE CASE OF m 81\*. *The Astrophysical Journal*, 797(2), 129. <https://doi.org/10.1088/0004-637X/797/2/129>
- Lusso, E., Comastri, A., Simmons, B. D., Mignoli, M., Zamorani, G., Vignali, C., Brusa, M., Shankar, F., Lutz, D., Trump, J. R., Maiolino, R., Gilli, R., Bolzonella, M., Puccetti, S., Salvato, M., Impey, C. D., Civano, F., Elvis, M., Mainieri, V., ... Riguccini, L. (2012). Bolometric luminosities and eddington ratios of x-ray selected active galactic nuclei in the XMM-COSMOS survey: Bolometric luminosities and eddington ratios of AGN. *Monthly Notices of the Royal Astronomical Society*, 425(1), 623–640. <https://doi.org/10.1111/j.1365-2966.2012.21513.x>
- Lusso, E., & Risaliti, G. (2017). Quasars as standard candles: I. the physical relation between disc and coronal emission. *Astronomy & Astrophysics*, 602, A79. <https://doi.org/10.1051/0004-6361/201630079>
- Lyke, B. W., Higley, A. N., McLane, J. N., Schurhammer, D. P., Myers, A. D., Ross, A. J., Dawson, K., Chabanier, S., Martini, P., Busca, N. G., Bourboux, H. d. M. d., Salvato, M., Streblyanska, A., Zarrouk, P., Burtin, E., Anderson, S. F., Bautista, J., Bizyaev, D., Brandt, W. N., ... Weaver, B. A. (2020). The sloan digital sky survey quasar catalog: Sixteenth data release. *The Astrophysical Journal Supplement Series*, 250(1), 8. <https://doi.org/10.3847/1538-4365/aba623>
- Ma, W., Liu, K., Guo, H., Cui, W., Jones, M. G., Wang, J., Zhang, L., & Davé, R. (2022). Effects of active galactic nucleus feedback on cold gas depletion and quenching of central galaxies. *The Astrophysical Journal*, 941(2), 205. <https://doi.org/10.3847/1538-4357/aca326>
- Machacek, M., Nulsen, P. E. J., Jones, C., & Forman, W. R. (2006). Chandra observations of nuclear outflows in the elliptical galaxy NGC 4552 in the virgo cluster. *The Astrophysical Journal*, 648(2), 947–955. <https://doi.org/10.1086/505963>
- Madau, P., & Dickinson, M. (2014). Cosmic star formation history. *Annual Review of Astronomy and Astrophysics*, 52(1), 415–486. <https://doi.org/10.1146/annurev-astro-081811-125615>
- Madau, P., Haardt, F., & Dotti, M. (2014). SUPER-CRITICAL GROWTH OF MASSIVE BLACK HOLES FROM STELLAR-MASS SEEDS. *The Astrophysical Journal*, 784(2), L38. <https://doi.org/10.1088/2041-8205/784/2/L38>
- Magnelli, B., Popesso, P., Berta, S., Pozzi, F., Elbaz, D., Lutz, D., Dickinson, M., Altieri, B., Andreani, P., Aussel, H., Béthermin, M., Bongiovanni, A., Cepa, J., Charmandaris, V., Chary, R.-R., Cimatti, A., Daddi, E., Förster Schreiber, N. M., Genzel, R., ... Valtchanov, I. (2013). The deepest Herschel-PACS far-infrared survey: Number counts and infrared luminosity functions from combined PEP/GOODS-h observations. *Astronomy & Astrophysics*, 553, A132. <https://doi.org/10.1051/0004-6361/201321371>
- Maiolino, R., & Mannucci, F. (2019). De re metallica: The cosmic chemical evolution of galaxies. *The Astronomy and Astrophysics Review*, 27(1), 3. <https://doi.org/10.1007/s00159-018-0112-2>
- Maiolino, R., Russell, H. R., Fabian, A. C., Carniani, S., Gallagher, R., Cazzoli, S., Arribas, S., Belfiore, F., Bellocchi, E., Colina, L., Cresci, G., Ishibashi, W., Marconi, A., Mannucci, F., Oliva, E., & Sturm, E. (2017). Star formation inside a galactic outflow. *Nature*, 544(7649), 202–206. <https://doi.org/10.1038/nature21677>
- Maiolino, R., Scholtz, J., Curtis-Lake, E., Carniani, S., Baker, W., de Graaff, A., Tacchella, S., Übler, H., D'Eugenio, F., Witstok, J., Curti, M., Arribas, S., Bunker, A. J., Charlot, S., Chevallard, J., Eisenstein, D. J., Egami, E., Ji, Z., Jones, G. C., ... Willott, C. (2023). JADES. the diverse population of infant black holes at 4. <https://doi.org/10.48550/ARXIV.2308.01230>
- Malizia, A., Molina, M., Bassani, L., Stephen, J. B., Bazzano, A., Ubertini, P., & Bird, A. J. (2014). THE INTEGRAL HIGH-ENERGY CUT-OFF DISTRIBUTION OF TYPE 1 ACTIVE GALACTIC NUCLEI. *The Astrophysical Journal*, 782(2), L25. <https://doi.org/10.1088/2041-8205/782/2/L25>

- Malkan, M. A., & Sargent, W. L. W. (1982). The ultraviolet excess of seyfert 1 galaxies and quasars. *The Astrophysical Journal*, 254, 22. <https://doi.org/10.1086/159701>
- Malkan, M. A., Gorjian, V., & Tam, R. (1998). A hubble space telescope imaging survey of nearby active galactic nuclei [ADS Bibcode: 1998ApJS..117...25M]. *The Astrophysical Journal Supplement Series*, 117, 25–88. <https://doi.org/10.1086/313110>
- Marconi, A., & Hunt, L. K. (2003). The relation between black hole mass, bulge mass, and near-infrared luminosity. *The Astrophysical Journal*, 589(1), L21–L24. <https://doi.org/10.1086/375804>
- Martin, D. C., Fanson, J., Schiminovich, D., Morrissey, P., Friedman, P. G., Barlow, T. A., Conrow, T., Grange, R., Jelinsky, P. N., Milliard, B., Siegmund, O. H. W., Bianchi, L., Byun, Y.-I., Donas, J., Forster, K., Heckman, T. M., Lee, Y.-W., Madore, B. F., Malina, R. F., ... Wyder, T. K. (2005). The *Galaxy Evolution Explorer* : A space ultraviolet survey mission. *The Astrophysical Journal*, 619(1), L1–L6. <https://doi.org/10.1086/426387>
- McConnell, N. J., & Ma, C.-P. (2013). REVISITING THE SCALING RELATIONS OF BLACK HOLE MASSES AND HOST GALAXY PROPERTIES. *The Astrophysical Journal*, 764(2), 184. <https://doi.org/10.1088/0004-637X/764/2/184>
- McNamara, B. R., & Nulsen, P. E. J. (2012). Mechanical feedback from active galactic nuclei in galaxies, groups and clusters. *New Journal of Physics*, 14(5), 055023. <https://doi.org/10.1088/1367-2630/14/5/055023>
- Mendez, A. J., Coil, A. L., Aird, J., Diamond-Stanic, A. M., Moustakas, J., Blanton, M. R., Cool, R. J., Eisenstein, D. J., Wong, K. C., & Zhu, G. (2013). PRIMUS: INFRARED AND x-RAY AGN SELECTION TECHNIQUES AT  $0.2 < z < 1.2$ . *The Astrophysical Journal*, 770(1), 40. <https://doi.org/10.1088/0004-637X/770/1/40>
- Michiyama, T., Iono, D., Nakanishi, K., Ueda, J., Saito, T., Ando, M., Kaneko, H., Yamashita, T., Matsuda, Y., Hatsukade, B., Kikuchi, K., Komugi, S., & Muto, T. (2016). Investigating the relation between CO (3–2) and far-infrared luminosities for nearby merging galaxies using ASTE. *Publications of the Astronomical Society of Japan*, 68(6), 96. <https://doi.org/10.1093/pasj/psw087>
- Mintz, S., Coleman, B., & Kirkpatrick, A. (2024). Cold quasar investigation: Comparing star formation rates to black hole growth. *Monthly Notices of the Royal Astronomical Society*, 528(4), 7376–7382. <https://doi.org/10.1093/mnras/stae465>
- Miyazaki, S., Komiyama, Y., Kawanomoto, S., Doi, Y., Furusawa, H., Hamana, T., Hayashi, Y., Ikeda, H., Kamata, Y., Karoji, H., Koike, M., Kurakami, T., Miyama, S., Morokuma, T., Nakata, F., Namikawa, K., Nakaya, H., Nariai, K., Obuchi, Y., ... Yokota, H. (2018). Hyper supprimecam: System design and verification of image quality [ADS Bibcode: 2018PASJ...70S...1M]. *Publications of the Astronomical Society of Japan*, 70, S1. <https://doi.org/10.1093/pasj/psx063>
- Molnár, D. C., Sargent, M. T., Delhaize, J., Delvecchio, I., Smolčić, V., Novak, M., Schinnerer, E., Zamorani, G., Bondi, M., Herrera-Ruiz, N., Murphy, E. J., Vardoulaki, E., Karim, A., Leslie, S., Magnelli, B., Carollo, C. M., & Middelberg, E. (2018). The infrared–radio correlation of spheroid- and disc-dominated star-forming galaxies to  $z \sim 1.5$  in the COSMOS field. *Monthly Notices of the Royal Astronomical Society*, 475(1), 827–838. <https://doi.org/10.1093/mnras/stx3234>
- Morganti, R. (2017). The many routes to AGN feedback. *Frontiers in Astronomy and Space Sciences*, 4, 42. <https://doi.org/10.3389/fspas.2017.00042>
- Morrissey, P., Conrow, T., Barlow, T. A., Small, T., Seibert, M., Wyder, T. K., Budavari, T., Arnouts, S., Friedman, P. G., Forster, K., Martin, D. C., Neff, S. G., Schiminovich, D., Bianchi, L., Donas, J., Heckman, T. M., Lee, Y.-W., Madore, B. F., Milliard, B., ... Yi, S. K. (2007).

- The calibration and data products of *GALEX*. *The Astrophysical Journal Supplement Series*, 173(2), 682–697. <https://doi.org/10.1086/520512>
- Mortlock, A., Conselice, C. J., Bluck, A. F. L., Bauer, A. E., Grützbauch, R., Buitrago, F., & Ownsworth, J. (2011). A deep probe of the galaxy stellar mass functions at  $z \sim 1-3$  with the GOODS NICMOS survey: Galaxy stellar mass functions in the GNS. *Monthly Notices of the Royal Astronomical Society*, 413(4), 2845–2859. <https://doi.org/10.1111/j.1365-2966.2011.18357.x>
- Mullaney, J. R., Alexander, D. M., Goulding, A. D., & Hickox, R. C. (2011). Defining the intrinsic AGN infrared spectral energy distribution and measuring its contribution to the infrared output of composite galaxies: The infrared SEDs of AGNs. *Monthly Notices of the Royal Astronomical Society*, 414(2), 1082–1110. <https://doi.org/10.1111/j.1365-2966.2011.18448.x>
- Mutch, S. J., Croton, D. J., & Poole, G. B. (2013). The simplest model of galaxy formation – i. a formation history model of galaxy stellar mass growth. *Monthly Notices of the Royal Astronomical Society*, 435(3), 2445–2459. <https://doi.org/10.1093/mnras/stt1453>
- Neistein, E., Van Den Bosch, F. C., & Dekel, A. (2006). Natural downsizing in hierarchical galaxy formation. *Monthly Notices of the Royal Astronomical Society*, 372(2), 933–948. <https://doi.org/10.1111/j.1365-2966.2006.10918.x>
- Netzer, H. (2019). Bolometric correction factors for active galactic nuclei. *Monthly Notices of the Royal Astronomical Society*, 488(4), 5185–5191. <https://doi.org/10.1093/mnras/stz2016>
- Ni, Q., Brandt, W. N., Yang, G., Leja, J., Chen, C.-T. J., Luo, B., Matharu, J., Sun, M., Vito, F., Xue, Y. Q., & Zhang, K. (2020). Revealing the relation between black hole growth and host-galaxy compactness among star-forming galaxies. *Monthly Notices of the Royal Astronomical Society*, 500(4), 4989–5008. <https://doi.org/10.1093/mnras/staa3514>
- Noll, S., Burgarella, D., Giovannoli, E., Buat, V., Marcillac, D., & Muñoz-Mateos, J. C. (2009). Analysis of galaxy spectral energy distributions from far-UV to far-IR with CIGALE: Studying a SINGS test sample [ADS Bibcode: 2009A&A...507.1793N]. *Astronomy and Astrophysics*, 507, 1793–1813. <https://doi.org/10.1051/0004-6361/200912497>
- Nulsen, P., Jones, C., Forman, W., Churazov, E., McNamara, B., David, L., Murray, S., Heinz, S., & Wilcots, E. (2009). Radio mode outbursts in giant elliptical galaxies, 198–201. <https://doi.org/10.1063/1.3293033>
- Oliver, S., Rowan-Robinson, M., Alexander, D. M., Almaini, O., Balcells, M., Baker, A. C., Barcons, X., Barden, M., Bellas-Velidis, I., Cabrera-Guerra, F., Carballo, R., Cesarsky, C. J., Ciliegi, P., Clements, D. L., Crockett, H., Danese, L., Dapergolas, A., Drolías, B., Eaton, N., ... Willott, C. J. (2000). The european large area ISO survey – i. goals, definition and observations. *Monthly Notices of the Royal Astronomical Society*, 316(4), 749–767. <https://doi.org/10.1046/j.1365-8711.2000.03550.x>
- Omukai, K. (2001). Primordial star formation under far-ultraviolet radiation. *The Astrophysical Journal*, 546(2), 635–651. <https://doi.org/10.1086/318296>
- Pacucci, F., & Loeb, A. (2024). The redshift evolution of the  $m_{\bullet} - m_{*}$  relation for JWST’s supermassive black holes at  $z \lesssim 4$ . *The Astrophysical Journal*, 964(2), 154. <https://doi.org/10.3847/1538-4357/ad3044>
- Peng. (2007). How mergers may affect the mass scaling relation between gravitationally bound systems. *The Astrophysical Journal*, 671(2), 1098–1107. <https://doi.org/10.1086/522774>
- Peng, Lilly, S. J., Kovač, K., Bolzonella, M., Pozzetti, L., Renzini, A., Zamorani, G., Ilbert, O., Knobel, C., Iovino, A., Maier, C., Cucciati, O., Tasca, L., Carollo, C. M., Silverman, J., Kampczyk, P., De Ravel, L., Sanders, D., Scoville, N., ... Scaramella, R. (2010). MASS AND ENVIRONMENT AS DRIVERS OF GALAXY EVOLUTION IN SDSS AND zCOSMOS AND THE

- ORIGIN OF THE SCHECHTER FUNCTION. *The Astrophysical Journal*, 721(1), 193–221. <https://doi.org/10.1088/0004-637X/721/1/193>
- Peterson, B. M., Denney, K. D., De Rosa, G., Grier, C. J., Pogge, R. W., Bentz, M. C., Kochanek, C. S., Vestergaard, M., Kileci-Eser, E., Dalla Bontà, E., & Cioi, S. (2013). THE SIZE OF THE NARROW-LINE-EMITTING REGION IN THE SEYFERT 1 GALAXY NGC 5548 FROM EMISSION-LINE VARIABILITY. *The Astrophysical Journal*, 779(2), 109. <https://doi.org/10.1088/0004-637X/779/2/109>
- Pezzulli, E., Valiante, R., & Schneider, R. (2016). Super-eddington growth of the first black holes. *Monthly Notices of the Royal Astronomical Society*, 458(3), 3047–3059. <https://doi.org/10.1093/mnras/stw505>
- Pilbratt, G. L., Riedinger, J. R., Passvogel, T., Crone, G., Doyle, D., Gageur, U., Heras, A. M., Jewell, C., Metcalfe, L., Ott, S., & Schmidt, M. (2010). *Herschel* space observatory: An ESA facility for far-infrared and submillimetre astronomy. *Astronomy and Astrophysics*, 518, L1. <https://doi.org/10.1051/0004-6361/201014759>
- Pillepich, A., Madau, P., & Mayer, L. (2015). BUILDING LATE-TYPE SPIRAL GALAXIES BY IN-SITU AND EX-SITU STAR FORMATION. *The Astrophysical Journal*, 799(2), 184. <https://doi.org/10.1088/0004-637X/799/2/184>
- Poglitsch, A., Waelkens, C., Geis, N., Feuchtgruber, H., Vandenbussche, B., Rodriguez, L., Krause, O., Renotte, E., Hoof, C. v., Saraceno, P., Cepa, J., Kerschbaum, F., Agnèse, P., Ali, B., Altieri, B., Andreani, P., Augeres, J.-L., Balog, Z., Barl, L., . . . Wiezorrek, E. (2010). The photodetector array camera and spectrometer (PACS) on the *herchel* space observatory. *Astronomy & Astrophysics*, 518, L2. <https://doi.org/10.1051/0004-6361/201014535>
- Pontzen, A., Tremmel, M., Roth, N., Peiris, H. V., Saintonge, A., Volonteri, M., Quinn, T., & Governato, F. (2017). How to quench a galaxy. *Monthly Notices of the Royal Astronomical Society*, 465(1), 547–558. <https://doi.org/10.1093/mnras/stw2627>
- Popesso, P., Concas, A., Cresci, G., Belli, S., Rodighiero, G., Inami, H., Dickinson, M., Ilbert, O., Pannella, M., & Elbaz, D. (2022). The main sequence of star-forming galaxies across cosmic times. *Monthly Notices of the Royal Astronomical Society*, 519(1), 1526–1544. <https://doi.org/10.1093/mnras/stac3214>
- Poudel, A., Heinämäki, P., Tempel, E., Einasto, M., Lietzen, H., & Nurmi, P. (2017). The effect of cosmic web filaments on the properties of groups and their central galaxies. *Astronomy & Astrophysics*, 597, A86. <https://doi.org/10.1051/0004-6361/201629639>
- Predehl, P., Andritschke, R., Arefiev, V., Babyshkin, V., Batanov, O., Becker, W., Böhringer, H., Bogomolov, A., Boller, T., Borm, K., Bornemann, W., Bräuninger, H., Brüggem, M., Brunner, H., Brusa, M., Bulbul, E., Buntov, M., Burwitz, V., Burkert, W., . . . Yaroshenko, V. (2021). The eROSITA x-ray telescope on SRG. *Astronomy & Astrophysics*, 647, A1. <https://doi.org/10.1051/0004-6361/202039313>
- Qu, Y., Helly, J. C., Bower, R. G., Theuns, T., Crain, R. A., Frenk, C. S., Furlong, M., McAlpine, S., Schaller, M., Schaye, J., & White, S. D. M. (2017). A chronicle of galaxy mass assembly in the EAGLE simulation. *Monthly Notices of the Royal Astronomical Society*, 464(2), 1659–1675. <https://doi.org/10.1093/mnras/stw2437>
- Raga, A. C., Noriega-Crespo, A., & Velázquez, P. F. (2002). The x-ray luminosities of herbig-haro objects. *The Astrophysical Journal*, 576(2), L149–L152. <https://doi.org/10.1086/343760>
- Ratcliffe, J. (1956). The formation of the ionospheric layers f-1 and f-2. *Journal of Atmospheric and Terrestrial Physics*, 8(4), 260–269. [https://doi.org/10.1016/0021-9169\(56\)90131-3](https://doi.org/10.1016/0021-9169(56)90131-3)
- Read, S. C., Smith, D. J. B., Gürkan, G., Hardcastle, M. J., Williams, W. L., Best, P. N., Brinks, E., Calistro-Rivera, G., Chyży, K. T., Duncan, K., Dunne, L., Jarvis, M. J., Morabito, L. K., Pran-

- doni, I., Röttgering, H. J. A., Sabater, J., & Viaene, S. (2018). The far-infrared radio correlation at low radio frequency with LOFAR/h-ATLAS [ADS Bibcode: 2018MNRAS.480.5625R]. *Monthly Notices of the Royal Astronomical Society*, 480, 5625–5644. <https://doi.org/10.1093/mnras/sty2198>
- Reddick, R. M., Wechsler, R. H., Tinker, J. L., & Behroozi, P. S. (2013). THE CONNECTION BETWEEN GALAXIES AND DARK MATTER STRUCTURES IN THE LOCAL UNIVERSE. *The Astrophysical Journal*, 771(1), 30. <https://doi.org/10.1088/0004-637X/771/1/30>
- Reines, A. E., & Volonteri, M. (2015). RELATIONS BETWEEN CENTRAL BLACK HOLE MASS AND TOTAL GALAXY STELLAR MASS IN THE LOCAL UNIVERSE. *The Astrophysical Journal*, 813(2), 82. <https://doi.org/10.1088/0004-637X/813/2/82>
- Revalski, M., Dashtamirova, D., Crenshaw, D. M., Kraemer, S. B., Fischer, T. C., Schmitt, H. R., Gnilka, C. L., Schmidt, J., Elvis, M., Fabbiano, G., Storchi-Bergmann, T., Maksym, W. P., & Gandhi, P. (2018). Quantifying feedback from narrow line region outflows in nearby active galaxies. II. spatially resolved mass outflow rates for the QSO2 markarian 34\* †. *The Astrophysical Journal*, 867(2), 88. <https://doi.org/10.3847/1538-4357/aae3e6>
- Ricci, C., Assef, R. J., Stern, D., Nikutta, R., Alexander, D. M., Asmus, D., Ballantyne, D. R., Bauer, F. E., Blain, A. W., Boggs, S., Boorman, P. G., Brandt, W. N., Brightman, M., Chang, C. S., Chen, C.-T. J., Christensen, F. E., Comastri, A., Craig, W. W., Díaz-Santos, T., ... Zhang, W. W. (2017). NuSTAR OBSERVATIONS OF WISE j1036+0449, a GALAXY AT  $z \approx 1$  OBSCURED BY HOT DUST. *The Astrophysical Journal*, 835(1), 105. <https://doi.org/10.3847/1538-4357/835/1/105>
- Richards, G. T., Strauss, M. A., Fan, X., Hall, P. B., Jester, S., Schneider, D. P., Vanden Berk, D. E., Stoughton, C., Anderson, S. F., Brunner, R. J., Gray, J., Gunn, J. E., Ivezić, Ž., Kirkland, M. K., Knapp, G. R., Loveday, J., Meiksin, A., Pope, A., Szalay, A. S., ... Snedden, S. A. (2006). The sloan digital sky survey quasar survey: Quasar luminosity function from data release 3. *The Astronomical Journal*, 131(6), 2766–2787. <https://doi.org/10.1086/503559>
- Richings, A. J., & Faucher-Giguère, C.-A. (2018). The origin of fast molecular outflows in quasars: Molecule formation in AGN-driven galactic winds. *Monthly Notices of the Royal Astronomical Society*, 474(3), 3673–3699. <https://doi.org/10.1093/mnras/stx3014>
- Rieke, G. H., Young, E. T., Engelbracht, C. W., Kelly, D. M., Low, F. J., Haller, E. E., Beeman, J. W., Gordon, K. D., Stansberry, J. A., Misselt, K. A., Cadien, J., Morrison, J. E., Rivlis, G., Latter, W. B., Noriega-Crespo, A., Padgett, D. L., Stapelfeldt, K. R., Hines, D. C., Egami, E., ... Richards, P. L. (2004). The multiband imaging photometer for spitzer (MIPS) [ADS Bibcode: 2004ApJS..154...25R]. *The Astrophysical Journal Supplement Series*, 154, 25–29. <https://doi.org/10.1086/422717>
- Riffel, R., Dahmer-Hahn, L. G., Vazdekis, A., Davies, R., Rosario, D., Almeida, C. R., Audibert, A., Martín-Navarro, I., Martins, L. P., Rodríguez-Ardila, A., Riffel, R. A., Storchi-Bergmann, T., Bertoldo-Coelho, M., Trevisan, M., Hicks, E., Müller, A. S., Marinho, L. N., & Veilleux, S. (2024). Observational constraints on the stellar recycled gas in active galactic nuclei feeding. *Monthly Notices of the Royal Astronomical Society*, 531(1), 554–574. <https://doi.org/10.1093/mnras/stae1192>
- Rinaldi, P., Caputi, K. I., Van Mierlo, S. E., Ashby, M. L. N., Caminha, G. B., & Iani, E. (2022). The galaxy starburst/main-sequence bimodality over five decades in stellar mass at  $z \approx 3$ –6.5. *The Astrophysical Journal*, 930(2), 128. <https://doi.org/10.3847/1538-4357/ac5d39>
- Rodighiero, G., Brusa, M., Daddi, E., Negrello, M., Mullaney, J. R., Delvecchio, I., Lutz, D., Renzini, A., Franceschini, A., Baronchelli, I., Pozzi, F., Gruppioni, C., Strazzullo, V., Cimatti, A., & Silverman, J. (2015). RELATIONSHIP BETWEEN STAR FORMATION RATE AND

- BLACK HOLE ACCRETION AT  $z = 2$ : THE DIFFERENT CONTRIBUTIONS IN QUI-ESCENT, NORMAL, AND STARBURST GALAXIES. *The Astrophysical Journal*, 800(1), L10. <https://doi.org/10.1088/2041-8205/800/1/L10>
- Rodríguez Montero, F., Davé, R., Wild, V., Anglés-Alcázar, D., & Narayanan, D. (2019). Mergers, starbursts, and quenching in the simba simulation. *Monthly Notices of the Royal Astronomical Society*, 490(2), 2139–2154. <https://doi.org/10.1093/mnras/stz2580>
- Roebuck, E., Sajina, A., Hayward, C. C., Pope, A., Kirkpatrick, A., Hernquist, L., & Yan, L. (2016). THE ROLE OF STAR FORMATION AND AGN IN DUST HEATING OF  $z = 0.3$ – $2.8$  galaxies. II. INFORMING IR AGN FRACTION ESTIMATES THROUGH SIMULATIONS. *The Astrophysical Journal*, 833(1), 60. <https://doi.org/10.3847/1538-4357/833/1/60>
- Runnoe, J. C., Brotherton, M. S., & Shang, Z. (2012). Updating quasar bolometric luminosity corrections - II. infrared bolometric corrections: Infrared bolometric corrections. *Monthly Notices of the Royal Astronomical Society*, 426(4), 2677–2688. <https://doi.org/10.1111/j.1365-2966.2012.21644.x>
- Saintonge, A., Tacconi, L. J., Fabello, S., Wang, J., Catinella, B., Genzel, R., Graciá-Carpio, J., Kramer, C., Moran, S., Heckman, T. M., Schiminovich, D., Schuster, K., & Wuyts, S. (2012). THE IMPACT OF INTERACTIONS, BARS, BULGES, AND ACTIVE GALACTIC NUCLEI ON STAR FORMATION EFFICIENCY IN LOCAL MASSIVE GALAXIES. *The Astrophysical Journal*, 758(2), 73. <https://doi.org/10.1088/0004-637X/758/2/73>
- Salim, S., & Narayanan, D. (2020). The dust attenuation law in galaxies. *Annual Review of Astronomy and Astrophysics*, 58(1), 529–575. <https://doi.org/10.1146/annurev-astro-032620-021933>
- Sanders, D. B., & Mirabel, I. F. (1996). LUMINOUS INFRARED GALAXIES. *Annual Review of Astronomy and Astrophysics*, 34(1), 749–792. <https://doi.org/10.1146/annurev.astro.34.1.749>
- Sassano, F., Schneider, R., Valiante, R., Inayoshi, K., Chon, S., Omukai, K., Mayer, L., & Capelo, P. R. (2021). Light, medium-weight, or heavy? the nature of the first supermassive black hole seeds. *Monthly Notices of the Royal Astronomical Society*, 506(1), 613–632. <https://doi.org/10.1093/mnras/stab1737>
- Saunders, W., Rowan-Robinson, M., Lawrence, A., Efstathiou, G., Kaiser, N., Ellis, R. S., & Frenk, C. S. (1990). The 60- and far-infrared luminosity functions of IRAS galaxies. *Monthly Notices of the Royal Astronomical Society*, 242(3), 318–337. <https://doi.org/10.1093/mnras/242.3.318>
- Scharré, L., Sorini, D., & Davé, R. (2024, April 10). The effects of stellar and AGN feedback on the cosmic star formation history in the simba simulations. Retrieved May 14, 2024, from <http://arxiv.org/abs/2404.07252>
- Schneider, D. P., Richards, G. T., Hall, P. B., Strauss, M. A., Anderson, S. F., Boroson, T. A., Ross, N. P., Shen, Y., Brandt, W. N., Fan, X., Inada, N., Jester, S., Knapp, G. R., Krawczyk, C. M., Thakar, A. R., Berk, D. E. V., Voges, W., Yanny, B., York, D. G., . . . Weinberg, D. H. (2010). The sloan digital sky survey quasar catalog v. seventh data release. *The Astronomical Journal*, 139(6), 2360–2373. <https://doi.org/10.1088/0004-6256/139/6/2360>
- Scudder, J. M., Oliver, S., Hurley, P. D., Griffin, M., Sargent, M. T., Scott, D., Wang, L., & Wardlow, J. L. (2016). The multiplicity of 250- $\mu\text{m}$  *Herschel* sources in the COSMOS field. *Monthly Notices of the Royal Astronomical Society*, 460(1), 1119–1130. <https://doi.org/10.1093/mnras/stw1044>
- Shankar, F., Allevato, V., Bernardi, M., Marsden, C., Lapi, A., Menci, N., Grylls, P. J., Krumpke, M., Zanisi, L., Ricci, F., La Franca, F., Baldi, R. D., Moreno, J., & Sheth, R. K. (2019). Constraining black hole–galaxy scaling relations and radiative efficiency from galaxy clustering. *Nature Astronomy*, 4(3), 282–291. <https://doi.org/10.1038/s41550-019-0949-y>

- Shankar, F., Weinberg, D. H., & Miralda-Escudé, J. (2009). SELF-CONSISTENT MODELS OF THE AGN AND BLACK HOLE POPULATIONS: DUTY CYCLES, ACCRETION RATES, AND THE MEAN RADIATIVE EFFICIENCY. *The Astrophysical Journal*, 690(1), 20–41. <https://doi.org/10.1088/0004-637X/690/1/20>
- Shen, Y. (2013). The mass of quasars [ADS Bibcode: 2013BASI...41...61S]. *Bulletin of the Astronomical Society of India*, 41, 61–115. <https://doi.org/10.48550/arXiv.1302.2643>
- Shen, Y., Richards, G. T., Strauss, M. A., Hall, P. B., Schneider, D. P., Snedden, S., Bizyaev, D., Brewington, H., Malanushenko, V., Malanushenko, E., Oravetz, D., Pan, K., & Simmons, A. (2011). A catalog of quasar properties from sloan digital sky survey data release 7 [ADS Bibcode: 2011ApJS..194...45S]. *The Astrophysical Journal Supplement Series*, 194, 45. <https://doi.org/10.1088/0067-0049/194/2/45>
- Sheth, J. V. (2004). Morphology of mock SDSS catalogues. *Monthly Notices of the Royal Astronomical Society*, 354(2), 332–342. <https://doi.org/10.1111/j.1365-2966.2004.08191.x>
- Shimizu, T. T., Davies, R. I., Lutz, D., Burtscher, L., Lin, M., Baron, D., Davies, R. L., Genzel, R., Hicks, E. K. S., Koss, M., Maciejewski, W., Müller-Sánchez, F., Orban de Xivry, G., Price, S. H., Ricci, C., Riffel, R., Riffel, R. A., Rosario, D., Schartmann, M., ... Veilleux, S. (2019). The multiphase gas structure and kinematics in the circumnuclear region of NGC 5728. *Monthly Notices of the Royal Astronomical Society*, 490(4), 5860–5887. <https://doi.org/10.1093/mnras/stz2802>
- Shimwell, T. W., Röttgering, H. J. A., Best, P. N., Williams, W. L., Dijkema, T. J., De Gasperin, F., Hardcastle, M. J., Heald, G. H., Hoang, D. N., Horneffer, A., Intema, H., Mahony, E. K., Mandal, S., Mechev, A. P., Morabito, L., Oonk, J. B. R., Rafferty, D., Retana-Montenegro, E., Sabater, J., ... Zwart, J. T. L. (2017). The LOFAR two-metre sky survey: I. survey description and preliminary data release\*. *Astronomy & Astrophysics*, 598, A104. <https://doi.org/10.1051/0004-6361/201629313>
- Shimwell, T. W., Tasse, C., Hardcastle, M. J., Mechev, A. P., Williams, W. L., Best, P. N., Röttgering, H. J. A., Callingham, J. R., Dijkema, T. J., De Gasperin, F., Hoang, D. N., Hugo, B., Mirmont, M., Oonk, J. B. R., Prandoni, I., Rafferty, D., Sabater, J., Smirnov, O., Van Weeren, R. J., ... Wilber, A. (2019). The LOFAR two-metre sky survey: II. first data release. *Astronomy & Astrophysics*, 622, A1. <https://doi.org/10.1051/0004-6361/201833559>
- Shin, J., Woo, J.-H., Chung, A., Baek, J., Cho, K., Kang, D., & Bae, H.-J. (2019). Positive and negative feedback of AGN outflows in NGC 5728. *The Astrophysical Journal*, 881(2), 147. <https://doi.org/10.3847/1538-4357/ab2e72>
- Shirley, R., Duncan, K., Varillas, M. C. C., Hurley, P. D., Malek, K., Roehly, Y., Smith, M. W. L., Aussel, H., Bakx, T., Buat, V., Burgarella, D., Christopher, N., Duivenvoorden, S., Eales, S., Efstathiou, A., Solares, E. A. G., Griffin, M., Jarvis, M., Faro, B. L., ... Oliver, S. J. (2021). HELP: The herschel extragalactic legacy project. *Monthly Notices of the Royal Astronomical Society*, 507(1), 129–155. <https://doi.org/10.1093/mnras/stab1526>
- Silk, J. (2013). UNLEASHING POSITIVE FEEDBACK: LINKING THE RATES OF STAR FORMATION, SUPERMASSIVE BLACK HOLE ACCRETION, AND OUTFLOWS IN DISTANT GALAXIES. *The Astrophysical Journal*, 772(2), 112. <https://doi.org/10.1088/0004-637X/772/2/112>
- Silk J., Di Cintio A., & Dvorkin I. (2014). Galaxy formation. *Proceedings of the International School of Physics & Enrico Fermi*; 186, 137–187. <https://doi.org/10.3254/978-1-61499-476-3-137>
- Silverman, J. D., Green, P. J., Barkhouse, W. A., Cameron, R. A., Foltz, C., Jannuzi, B. T., Kim, D.-W., Kim, M., Mossman, A., Tananbaum, H., Wilkes, B. J., Smith, M. G., Smith, R. C.,

- & Smith, P. S. (2005). Comoving space density of x-ray-selected active galactic nuclei. *The Astrophysical Journal*, 624(2), 630–637. <https://doi.org/10.1086/429361>
- Small, T. A., & Blandford, R. D. (1992). Quasar evolution and the growth of black holes. *Monthly Notices of the Royal Astronomical Society*, 259(4), 725–737. <https://doi.org/10.1093/mnras/259.4.725>
- Smee, S., Gunn, J. E., Uomoto, A., Roe, N., Schlegel, D., Rockosi, C. M., Carr, M. A., Leger, F., Dawson, K. S., Olmstead, M. D., Brinkmann, J., Owen, R., Barkhouser, R. H., Honscheid, K., Harding, P., Long, D., Lupton, R. H., Loomis, C., Anderson, L., ... York, D. G. (2013). The multi-object, fiber-fed spectrographs for SDSS and the baryon oscillation spectroscopic survey. *The Astronomical Journal*, 146(2), 32. <https://doi.org/10.1088/0004-6256/146/2/32>
- Smirnov, O. M., & Tasse, C. (2015). Radio interferometric gain calibration as a complex optimization problem. *Monthly Notices of the Royal Astronomical Society*, 449(3), 2668–2684. <https://doi.org/10.1093/mnras/stv418>
- Smith, D. J. B., Dunne, L., Maddox, S. J., Eales, S., Bonfield, D. G., Jarvis, M. J., Sutherland, W., Fleuren, S., Rigby, E. E., Thompson, M. A., Baldry, I. K., Bamford, S., Buttiglione, S., Cava, A., Clements, D. L., Cooray, A., Croom, S., Dariush, A., De Zotti, G., ... Van Kampen, E. (2011). Herschel-ATLAS: Counterparts from the ultraviolet-near-infrared in the science demonstration phase catalogue : Herschel-ATLAS: Counterparts. *Monthly Notices of the Royal Astronomical Society*, 416(2), 857–872. <https://doi.org/10.1111/j.1365-2966.2011.18827.x>
- Smolčić, V., Novak, M., Bondi, M., Ciliegi, P., Mooley, K. P., Schinnerer, E., Zamorani, G., Navarrete, F., Bourke, S., Karim, A., Vardoulaki, E., Leslie, S., Delhaize, J., Carilli, C. L., Myers, S. T., Baran, N., Delvecchio, I., Miettinen, O., Banfield, J., ... Sheth, K. (2017). The VLA-COSMOS 3 GHz large project: Continuum data and source catalog release. *Astronomy & Astrophysics*, 602, A1. <https://doi.org/10.1051/0004-6361/201628704>
- Soltan, A. (1982). Masses of quasars. *Monthly Notices of the Royal Astronomical Society*, 200(1), 115–122. <https://doi.org/10.1093/mnras/200.1.115>
- Son, V., De Mink, S. E., Chruślińska, M., Conroy, C., Pakmor, R., & Hernquist, L. (2023). The locations of features in the mass distribution of merging binary black holes are robust against uncertainties in the metallicity-dependent cosmic star formation history. *The Astrophysical Journal*, 948(2), 105. <https://doi.org/10.3847/1538-4357/acbf51>
- Speagle, J. S., Steinhardt, C. L., Capak, P. L., & Silverman, J. D. (2014). A highly consistent framework for the evolution of the star-forming "main sequence" from  $z \sim 0-6$  [ADS Bibcode: 2014ApJS..214...15S]. *The Astrophysical Journal Supplement Series*, 214, 15. <https://doi.org/10.1088/0067-0049/214/2/15>
- Spilker, J. S., Suess, K. A., Setton, D. J., Bezanson, R., Feldmann, R., Greene, J. E., Kriek, M., Lower, S., Narayanan, D., & Verrico, M. (2022). Star formation suppression by tidal removal of cold molecular gas from an intermediate-redshift massive post-starburst galaxy. *The Astrophysical Journal Letters*, 936(1), L11. <https://doi.org/10.3847/2041-8213/ac75ea>
- Spinoglio, L., Fernández-Ontiveros, J. A., & Malkan, M. A. (2022). The high-ionization IR fine structure lines as bolometric indicators of the AGN power: Study of the complete 12  $\mu\text{m}$  AGN sample. *The Astrophysical Journal*, 941(1), 46. <https://doi.org/10.3847/1538-4357/ac9da2>
- Stacey, G. J., Hailey-Dunsheath, S., Ferkinhoff, C., Nikola, T., Parshley, S. C., Benford, D. J., Staguhn, J. G., & Fiolet, N. (2010). A 158  $\mu\text{m}$  [c II] LINE SURVEY OF GALAXIES AT  $z \sim 1-2$ : AN INDICATOR OF STAR FORMATION IN THE EARLY UNIVERSE. *The Astrophysical Journal*, 724(2), 957–974. <https://doi.org/10.1088/0004-637X/724/2/957>

- Stacy, A., Bromm, V., & Lee, A. T. (2016). Building up the population III initial mass function from cosmological initial conditions. *Monthly Notices of the Royal Astronomical Society*, *462*(2), 1307–1328. <https://doi.org/10.1093/mnras/stw1728>
- Stalevski, M., Ricci, C., Ueda, Y., Lira, P., Fritz, J., & Baes, M. (2016). The dust covering factor in active galactic nuclei. *Monthly Notices of the Royal Astronomical Society*, *458*(3), 2288–2302. <https://doi.org/10.1093/mnras/stw444>
- Steffen, A. T., Strateva, I., Brandt, W. N., Alexander, D. M., Koekemoer, A. M., Lehmer, B. D., Schneider, D. P., & Vignali, C. (2006). The x-ray-to-optical properties of optically selected active galaxies over wide luminosity and redshift ranges [ADS Bibcode: 2006AJ....131.2826S]. *The Astronomical Journal*, *131*, 2826–2842. <https://doi.org/10.1086/503627>
- Stemo, A., Comerford, J. M., Barrows, R. S., Stern, D., Assef, R. J., & Griffith, R. L. (2020). A catalog of AGN host galaxies observed with HST/ACS: Correlations between star formation and AGN activity. *The Astrophysical Journal*, *888*(2), 78. <https://doi.org/10.3847/1538-4357/ab5f66>
- Stern, J., & Laor, A. (2012). Type 1 AGN at low  $z$  - II. the relative strength of narrow lines and the nature of intermediate type AGN: Type 1 low- $z$  AGN. II. NLR relative luminosity. *Monthly Notices of the Royal Astronomical Society*, *426*(4), 2703–2718. <https://doi.org/10.1111/j.1365-2966.2012.21772.x>
- Stone, M., Veilleux, S., Meléndez, M., Sturm, E., Graciá-Carpio, J., & González-Alfonso, E. (2016). THE SEARCH FOR MOLECULAR OUTFLOWS IN LOCAL VOLUME AGNs WITH HERSCHEL-PACS\*. *The Astrophysical Journal*, *826*(2), 111. <https://doi.org/10.3847/0004-637X/826/2/111>
- Strazzullo, V., Daddi, E., Gobat, R., Valentino, F., Pannella, M., Dickinson, M., Renzini, A., Brammer, G., Onodera, M., Finoguenov, A., Cimatti, A., Carollo, C. M., & Arimoto, N. (2016). THE RED SEQUENCE AT BIRTH IN THE GALAXY CLUSTER cl j1449+0856 AT  $z = 2$ . *The Astrophysical Journal Letters*, *833*(2), L20. <https://doi.org/10.3847/2041-8213/833/2/L20>
- Suganuma, M., Yoshii, Y., Kobayashi, Y., Minezaki, T., Enya, K., Tomita, H., Aoki, T., Koshida, S., & Peterson, B. A. (2006). Reverberation measurements of the inner radius of the dust torus in nearby seyfert 1 galaxies. *The Astrophysical Journal*, *639*(1), 46–63. <https://doi.org/10.1086/499326>
- Tanaka, T. L., & Li, M. (2014). The formation of massive black holes in  $z \sim 30$  dark matter haloes with large baryonic streaming velocities. *Monthly Notices of the Royal Astronomical Society*, *439*(1), 1092–1100. <https://doi.org/10.1093/mnras/stu042>
- Tasnim Ananna, T., Treister, E., Megan Urry, C., Ricci, C., Kirkpatrick, A., LaMassa, S., Buchner, J., Civano, F., Tremmel, M., & Marchesi, S. (2019). The accretion history of AGNs. i. supermassive black hole population synthesis model. *The Astrophysical Journal*, *871*(2), 240. <https://doi.org/10.3847/1538-4357/aafb77>
- Tasse, C., Hugo, B., Mirmont, M., Smirnov, O., Atemkeng, M., Bester, L., Hardcastle, M. J., Lakhoo, R., Perkins, S., & Shimwell, T. (2018). Faceting for direction-dependent spectral deconvolution. *Astronomy & Astrophysics*, *611*, A87. <https://doi.org/10.1051/0004-6361/201731474>
- Taylor, M. B. (2005). TOPCAT & STIL: Starlink table/VOTable processing software [ADS Bibcode: 2005ASPC..347...29T], *347*, 29. Retrieved November 23, 2023, from <https://ui.adsabs.harvard.edu/abs/2005ASPC..347...29T>
- Teklu, A., Kudritzki, R.-P., Dolag, K., Remus, R.-S., & Kimmig, L. (2023). On the decline of star formation during the evolution of galaxies. *The Astrophysical Journal*, *954*(2), 182. <https://doi.org/10.3847/1538-4357/ace900>
- Thomas, R., Le Fèvre, O., Zamorani, G., Lemaux, B. C., Hibon, P., Koekemoer, A., Hathi, N., Maccagni, D., Cassata, P., Cassarà, L. P., Bardelli, S., Talia, M., & Zucca, E. (2019). The

- most massive, passive, and oldest galaxies at  $0.5 < z < 2.1$ : Downsizing signature from galaxies selected from  $mg_{UV}$  index. *Astronomy & Astrophysics*, 630, A145. <https://doi.org/10.1051/0004-6361/201935813>
- Thompson, T. A., Quataert, E., Zhang, D., & Weinberg, D. H. (2016). An origin for multiphase gas in galactic winds and haloes. *Monthly Notices of the Royal Astronomical Society*, 455(2), 1830–1844. <https://doi.org/10.1093/mnras/stv2428>
- Torbaniuk, O., Paolillo, M., D’Abrusco, R., Vignali, C., Georgakakis, A., Carrera, F. J., & Civano, F. (2023). Probing supermassive black hole growth and its dependence on stellar mass and star formation rate in low-redshift galaxies. *Monthly Notices of the Royal Astronomical Society*, 527(4), 12091–12108. <https://doi.org/10.1093/mnras/stad3965>
- Trakhtenbrot, B., Lira, P., Netzer, H., Cicone, C., Maiolino, R., & Shemmer, O. (2017). ALMA observations show major mergers among the host galaxies of fast-growing, high-redshift, supermassive black holes. *The Astrophysical Journal*, 836(1), 8. <https://doi.org/10.3847/1538-4357/836/1/8>
- Tsai, C.-W., Eisenhardt, P. R. M., Wu, J., Stern, D., Assef, R. J., Blain, A. W., Bridge, C. R., Benford, D. J., Cutri, R. M., Griffith, R. L., Jarrett, T. H., Lonsdale, C. J., Masci, F. J., Moustakas, L. A., Petty, S. M., Sayers, J., Stanford, S. A., Wright, E. L., Yan, L., ... Juneau, S. (2015). The most luminous galaxies discovered by WISE [ADS Bibcode: 2015ApJ...805...90T]. *The Astrophysical Journal*, 805, 90. <https://doi.org/10.1088/0004-637X/805/2/90>
- Übler, H., Maiolino, R., Curtis-Lake, E., Pérez-González, P. G., Curti, M., Perna, M., Arribas, S., Charlot, S., Marshall, M. A., D’Eugenio, F., Scholtz, J., Bunker, A., Carniani, S., Ferruit, P., Jakobsen, P., Rix, H.-W., Rodríguez Del Pino, B., Willott, C. J., Boeker, T., ... Rawle, T. (2023). GA-NIFS: A massive black hole in a low-metallicity AGN at  $z = 5.55$  revealed by JWST/NIRSpec IFS. *Astronomy & Astrophysics*, 677, A145. <https://doi.org/10.1051/0004-6361/202346137>
- Ueda, Y., Akiyama, M., Hasinger, G., Miyaji, T., & Watson, M. G. (2014). TOWARD THE STANDARD POPULATION SYNTHESIS MODEL OF THE x-RAY BACKGROUND: EVOLUTION OF x-RAY LUMINOSITY AND ABSORPTION FUNCTIONS OF ACTIVE GALACTIC NUCLEI INCLUDING COMPTON-THICK POPULATIONS. *The Astrophysical Journal*, 786(2), 104. <https://doi.org/10.1088/0004-637X/786/2/104>
- Ueda, Y., Akiyama, M., Ohta, K., & Miyaji, T. (2003). Cosmological evolution of the hard x-ray active galactic nucleus luminosity function and the origin of the hard x-ray background. *The Astrophysical Journal*, 598(2), 886–908. <https://doi.org/10.1086/378940>
- Urrutia, T., Lacy, M., Spoon, H., Glikman, E., Petric, A., & Schulz, B. (2012). SPITZER OBSERVATIONS OF YOUNG RED QUASARS. *The Astrophysical Journal*, 757(2), 125. <https://doi.org/10.1088/0004-637X/757/2/125>
- Urry, C. M., & Padovani, P. (1995). Unified schemes for radio-loud active galactic nuclei [ADS Bibcode: 1995PASP..107..803U]. *Publications of the Astronomical Society of the Pacific*, 107, 803. <https://doi.org/10.1086/133630>
- Valiante, E., Smith, M. W. L., Eales, S., Maddox, S. J., Ibar, E., Hopwood, R., Dunne, L., Cigan, P. J., Dye, S., Pascale, E., Rigby, E. E., Bourne, N., Furlanetto, C., & Ivison, R. J. (2016). The *Herschel* -ATLAS data release 1 – i. maps, catalogues and number counts. *Monthly Notices of the Royal Astronomical Society*, 462(3), 3146–3179. <https://doi.org/10.1093/mnras/stw1806>
- Van De Voort, F. (2017). The effect of galactic feedback on gas accretion and wind recycling. In A. Fox & R. Davé (Eds.), *Gas accretion onto galaxies* (pp. 301–321). Springer International Publishing. [https://doi.org/10.1007/978-3-319-52512-9\\_13](https://doi.org/10.1007/978-3-319-52512-9_13)

- Van De Voort, F., Schaye, J., Booth, C. M., & Dalla Vecchia, C. (2011). The drop in the cosmic star formation rate below redshift 2 is caused by a change in the mode of gas accretion and by active galactic nucleus feedback: The drop in the cosmic SFR below  $z = 2$ . *Monthly Notices of the Royal Astronomical Society*, 415(3), 2782–2789. <https://doi.org/10.1111/j.1365-2966.2011.18896.x>
- Van Haarlem, M. P., Wise, M. W., Gunst, A. W., Heald, G., McKean, J. P., Hessels, J. W. T., De Bruyn, A. G., Nijboer, R., Swinbank, J., Fallows, R., Brentjens, M., Nelles, A., Beck, R., Falcke, H., Fender, R., Hörandel, J., Koopmans, L. V. E., Mann, G., Miley, G., ... Van Zwieten, J. (2013). LOFAR: The LOW-frequency ARray. *Astronomy & Astrophysics*, 556, A2. <https://doi.org/10.1051/0004-6361/201220873>
- Vayner, A., Wright, S. A., Murray, N., Armus, L., Larkin, J. E., & Mieda, E. (2017). Galactic-scale feedback observed in the 3c 298 quasar host galaxy [ADS Bibcode: 2017ApJ...851..126V]. *The Astrophysical Journal*, 851, 126. <https://doi.org/10.3847/1538-4357/aa9c42>
- Vestergaard, M., & Peterson, B. M. (2006). Determining central black hole masses in distant active galaxies and quasars. II. improved optical and UV scaling relationships. *The Astrophysical Journal*, 641(2), 689–709. <https://doi.org/10.1086/500572>
- Viero, M. P., Asboth, V., Roseboom, I. G., Moncelsi, L., Marsden, G., Cooper, E. M., Zemcov, M., Addison, G., Baker, A. J., Beelen, A., Bock, J., Bridge, C., Conley, A., Devlin, M. J., Doré, O., Farrah, D., Finkelstein, S., Font-Ribera, A., Geach, J. E., ... Wechsler, R. (2014). The herchel stripe 82 survey (HerS): Maps and early catalog. *The Astrophysical Journal Supplement Series*, 210(2), 22. <https://doi.org/10.1088/0067-0049/210/2/22>
- Villar-Martín, M., Emonts, B., Rodríguez, M., Torres, M. P., & Drouart, G. (2013). SDSS j002531.46–104022.2 at  $z = 0.30$ : A candidate for the (ultra)luminous infrared galaxy to optical quasar transition. *Monthly Notices of the Royal Astronomical Society*, 432(3), 2104–2111. <https://doi.org/10.1093/mnras/stt538>
- Violino, G., Ellison, S. L., Sargent, M., Coppin, K. E. K., Scudder, J. M., Mendel, T. J., & Saintonge, A. (2018). Galaxy pairs in the SDSS – XIII. the connection between enhanced star formation and molecular gas properties in galaxy mergers. *Monthly Notices of the Royal Astronomical Society*, 476(2), 2591–2604. <https://doi.org/10.1093/mnras/sty345>
- Visbal, E., Haiman, Z., & Bryan, G. L. (2014). Direct collapse black hole formation from synchronized pairs of atomic cooling haloes. *Monthly Notices of the Royal Astronomical Society*, 445(1), 1056–1063. <https://doi.org/10.1093/mnras/stu1794>
- Wang, L., Gao, F., Best, P. N., Duncan, K., Hardcastle, M. J., Kondapally, R., Małek, K., McCheyne, I., Sabater, J., Shimwell, T., Tasse, C., Bonato, M., Bondi, M., Cochrane, R. K., Farrah, D., Gürkan, G., Haskell, P., Pearson, W. J., Prandoni, I., ... Williams, W. L. (2021). The bright end of the infrared luminosity functions and the abundance of hyperluminous infrared galaxies. *Astronomy & Astrophysics*, 648, A8. <https://doi.org/10.1051/0004-6361/202038811>
- Wang, L., Pearson, W. J., Cowley, W., Trayford, J. W., Béthermin, M., Gruppioni, C., Hurley, P., & Michałowski, M. J. (2019). Multi-wavelength de-blended *Herschel* view of the statistical properties of dusty star-forming galaxies across cosmic time. *Astronomy & Astrophysics*, 624, A98. <https://doi.org/10.1051/0004-6361/201834093>
- Webb, N. A., Coriat, M., Traulsen, I., Ballet, J., Motch, C., Carrera, F. J., Koliopanos, F., Authier, J., De La Calle, I., Ceballos, M. T., Colomo, E., Chuard, D., Freyberg, M., Garcia, T., Kolehmainen, M., Lamer, G., Lin, D., Maggi, P., Michel, L., ... Zakardjian, A. (2020). The *XMM-Newton* serendipitous survey: IX. the fourth *XMM-Newton* serendipitous source catalogue. *Astronomy & Astrophysics*, 641, A136. <https://doi.org/10.1051/0004-6361/201937353>

- Weeren, R. J. V., Williams, W. L., Hardcastle, M. J., Shimwell, T. W., Rafferty, D. A., Sabater, J., Heald, G., Sridhar, S. S., Dijkema, T. J., Brunetti, G., Brügger, M., Andrade-Santos, F., Ogorean, G. A., Röttgering, H. J. A., Dawson, W. A., Forman, W. R., Gasperin, F. D., Jones, C., Miley, G. K., ... White, G. J. (2016). LOFAR FACET CALIBRATION. *The Astrophysical Journal Supplement Series*, 223(1), 2. <https://doi.org/10.3847/0067-0049/223/1/2>
- Weygaert, R. V. D., & Bond, J. R. (2008). Clusters and the theory of the cosmic web. In M. Plionis, D. Hughes, & O. López-Cruz (Eds.). R. Beig, W. Beiglböck, W. Domcke, B.-G. Englert, U. Frisch, P. Hänggi, G. Hasinger, K. Hepp, W. Hillebrandt, D. Imboden, R. L. Jaffe, R. Lipowsky, H. V. Löhneysen, I. Ojima, D. Sornette, S. Theisen, W. Weise, J. Wess, & J. Zittartz (typereactors), *A pan-chromatic view of clusters of galaxies and the large-scale structure* (pp. 335–408). Springer Netherlands. [https://doi.org/10.1007/978-1-4020-6941-3\\_10](https://doi.org/10.1007/978-1-4020-6941-3_10)
- White, S. D. M., & Rees, M. J. (1978). Core condensation in heavy halos: A two-stage theory for galaxy formation and clustering. *Monthly Notices of the Royal Astronomical Society*, 183(3), 341–358. <https://doi.org/10.1093/mnras/183.3.341>
- Williams, W. L., Hardcastle, M. J., Best, P. N., Sabater, J., Croston, J. H., Duncan, K. J., Shimwell, T. W., Röttgering, H. J. A., Nisbet, D., Gürkan, G., Alegre, L., Cochrane, R. K., Goyal, A., Hale, C. L., Jackson, N., Jamrozy, M., Kondapally, R., Kunert-Bajraszewska, M., Mahatma, V. H., ... Van Weeren, R. J. (2019). The LOFAR two-metre sky survey: III. first data release: Optical/infrared identifications and value-added catalogue. *Astronomy & Astrophysics*, 622, A2. <https://doi.org/10.1051/0004-6361/201833564>
- Willott, C. J., Martínez-Sansigre, A., & Rawlings, S. (2007). Molecular gas observations of the reddened quasar 3c 318. *The Astronomical Journal*, 133(2), 564–567. <https://doi.org/10.1086/510291>
- Woo, J.-H., Son, D., & Rakshit, S. (2020). The correlation of outflow kinematics with star formation rate. VI. gas outflows in AGNs. *The Astrophysical Journal*, 901(1), 66. <https://doi.org/10.3847/1538-4357/abad97>
- Wootten, A., & Thompson, A. (2009). The atacama large millimeter/submillimeter array. *Proceedings of the IEEE*, 97(8), 1463–1471. <https://doi.org/10.1109/JPROC.2009.2020572>
- Wright, E. L., Eisenhardt, P. R. M., Mainzer, A. K., Ressler, M. E., Cutri, R. M., Jarrett, T., Kirkpatrick, J. D., Padgett, D., McMillan, R. S., Skrutskie, M., Stanford, S. A., Cohen, M., Walker, R. G., Mather, J. C., Leisawitz, D., Gautier, T. N., McLean, I., Benford, D., Lonsdale, C. J., ... Tsai, C.-W. (2010). THE WIDE-FIELD INFRARED SURVEY EXPLORER (WISE): MISSION DESCRIPTION AND INITIAL ON-ORBIT PERFORMANCE. *The Astronomical Journal*, 140(6), 1868–1881. <https://doi.org/10.1088/0004-6256/140/6/1868>
- Wu, Q., & Shen, Y. (2022). A catalog of quasar properties from sloan digital sky survey data release 16. *The Astrophysical Journal Supplement Series*, 263(2), 42. <https://doi.org/10.3847/1538-4365/ac9ead>
- Wylezalek, D., & Zakamska, N. L. (2016). Evidence of suppression of star formation by quasar-driven winds in gas-rich host galaxies at  $z \lesssim 1$ ? *Monthly Notices of the Royal Astronomical Society*, 461(4), 3724–3739. <https://doi.org/10.1093/mnras/stw1557>
- Yang, G., Boquien, M., Buat, V., Burgarella, D., Ciesla, L., Duras, F., Stalevski, M., Brandt, W. N., & Papovich, C. (2020). X-CIGALE: Fitting AGN/galaxy SEDs from x-ray to infrared [ADS Bibcode: 2020MNRAS.491..740Y]. *Monthly Notices of the Royal Astronomical Society*, 491, 740–757. <https://doi.org/10.1093/mnras/stz3001>
- Yang, G., Brandt, W. N., Alexander, D. M., Chen, C. -. J., Ni, Q., Vito, F., & Zhu, F. -. (2019). Evident black hole-bulge coevolution in the distant universe [ADS Bibcode: 2019MNRAS.485.3721Y].

- Monthly Notices of the Royal Astronomical Society*, 485, 3721–3737. <https://doi.org/10.1093/mnras/stz611>
- Yang, G., Boquien, M., Brandt, W. N., Buat, V., Burgarella, D., Ciesla, L., Lehmer, B. D., Małek, K., Mountrichas, G., Papovich, C., Pons, E., Stalevski, M., Theulé, P., & Zhu, S. (2022). Fitting AGN/galaxy x-ray-to-radio SEDs with CIGALE and improvement of the code [ADS Bibcode: 2022ApJ...927..192Y]. *The Astrophysical Journal*, 927, 192. <https://doi.org/10.3847/1538-4357/ac4971>
- Zavala, J. A., Aretxaga, I., Geach, J. E., Hughes, D. H., Birkinshaw, M., Chapin, E., Chapman, S., Chen, C.-C., Clements, D. L., Dunlop, J. S., Farrah, D., Ivison, R. J., Jenness, T., Michałowski, M. J., Robson, E. I., Scott, D., Simpson, J., Spaans, M., & Van Der Werf, P. (2017). The SCUBA-2 cosmology legacy survey: The EGS deep field – i. deep number counts and the redshift distribution of the recovered cosmic infrared background at 450 and 850  $\mu$  m. *Monthly Notices of the Royal Astronomical Society*, 464(3), 3369–3384. <https://doi.org/10.1093/mnras/stw2630>
- Zdziarski, A. A., Johnson, W. N., Done, C., Smith, D., & McNaron-Brown, K. (1995). The average x-ray/gamma-ray spectra of seyfert galaxies from GINGA and OSSE and the origin of the cosmic x-ray background. *The Astrophysical Journal*, 438, L63. <https://doi.org/10.1086/187716>
- Zhang, D., Thompson, T. A., Quataert, E., & Murray, N. (2017). Entrainment in trouble: Cool cloud acceleration and destruction in hot supernova-driven galactic winds. *Monthly Notices of the Royal Astronomical Society*, 468(4), 4801–4814. <https://doi.org/10.1093/mnras/stx822>
- Zhang, Ouchi, M., Gebhardt, K., Liu, C., Harikane, Y., Mentuch Cooper Erin, Davis, D., J.Farrow, D., Gawiser, E., J.Hill, G., Kollatschny, W., Ono, Y., P.Schneider, D., L.Finkelstein, S., Gronwall, C., Jogee, S., & Krumpke, M. (2023). The stellar mass - black hole mass relation at z 2 down to MBH 107m determined by HETDEX. 2023, 16. <https://doi.org/https://doi.org/10.48550/arXiv.2303.02929>
- Zhuang, M.-Y., & Ho, L. C. (2020). The interplay between star formation and black hole accretion in nearby active galaxies. *The Astrophysical Journal*, 896(2), 108. <https://doi.org/10.3847/1538-4357/ab8f2e>
- Zhuang, M.-Y., Ho, L. C., & Shanguan, J. (2021). Black hole accretion correlates with star formation rate and star formation efficiency in nearby luminous type 1 active galaxies. *The Astrophysical Journal*, 906(1), 38. <https://doi.org/10.3847/1538-4357/abc94d>